Titre: Title:	Beamforming Design for Massive MIMO Systems with Deep Neural Networks
Auteur: Author:	Hamed Hojatian
Date:	2023
Type:	Mémoire ou thèse / Dissertation or Thesis
Référence: Citation:	Hojatian, H. (2023). Beamforming Design for Massive MIMO Systems with Deep Neural Networks [Thèse de doctorat, Polytechnique Montréal]. PolyPublie. https://publications.polymtl.ca/55979/

POLYTECHNIQUE MONTRÉAL
affiliée à l'Université de Montréal

Beamforming design for massive MIMO systems with deep neural networks

HAMED HOJATIAN
Département de génie électrique

Thèse présentée en vue de l'obtention du diplôme de *Philosophiæ Doctor*
Génie électrique

Octobre 2023

POLYTECHNIQUE MONTRÉAL
affiliée à l'Université de Montréal

Cette thèse intitulée :

Beamforming design for massive MIMO systems with deep neural networks

présentée par **Hamed HOJATIAN**
en vue de l'obtention du diplôme de *Philosophiæ Doctor*
a été dûment acceptée par le jury d'examen constitué de :

Chahé NERGUIZIAN, président
François LEDUC-PRIMEAU, membre et directeur de recherche
Jean-François FRIGON, membre et codirecteur de recherche
Gunes KARABULUT KURT, membre
Ioannis PSAROMILIGKOS, membre externe

DEDICATION

To my love, Andishe,
To the loving memories of my cherished mother, Soheila, and my beloved aunt, Soodabeh,
To my adored brothers, Hooman and Amirhosein, and my father, Khalil ...

ACKNOWLEDGEMENTS

I would like to express my heartfelt gratitude and acknowledgment to several individuals who have played significant roles in the completion of my thesis. First and foremost, I am immensely grateful to my supervisors, Professor François Leduc-Primeau and Jean-François Frigon, for their guidance, expertise, and invaluable insights throughout the research process. Their support, patience, and mentorship have been instrumental in shaping the direction of my thesis and fostering my intellectual growth.

I want to honor the memory of my beloved mother, aunt, and grandmother, whose unwavering love and support have been guiding forces in my life. I am forever grateful for their encouragement and belief in my abilities. I extend my deepest appreciation to my father, whose constant encouragement and sacrifices have been instrumental in shaping my academic journey. His unwavering support and belief in my potential have been a constant source of inspiration. I would like to express my sincere thanks to my brothers, for their continuous support, understanding, and encouragement throughout this challenging process.

I would also like to acknowledge the contributions of the post-doctoral fellow, Jeremy Nadal for his assistance and collaboration throughout the research process.

I am grateful to my dear friend and inspiration, Dr. Alireza Ghaffari, for his unwavering support, encouragement, and intellectual discussions. His friendship and insights have been a source of inspiration throughout my academic journey.

Last but certainly not least, I want to express my deepest gratitude to the love of my life, my wife Dr. Andishe Esmaeilzadeh. Her unwavering love, understanding, and encouragement have been my pillars of strength. Her support, patience, and belief in me have been instrumental in overcoming the challenges and achieving this milestone. I am forever grateful for her unwavering presence by my side.

RÉSUMÉ

L'avènement des communications sans-fil à très grand nombre d'entrées et de sorties (*massive multiple-input multiple-output* ou MIMO massif) a redéfini le fonctionnement systèmes de communication sans-fil, exploitant un ensemble d'antennes pour améliorer l'efficacité spectrale (SE) et la capacité du système. Les techniques de formation de faisceau jouent un rôle crucial dans les performances du MIMO massif, avec deux catégories principales : le pré-codage entièrement numérique (FDP) et la formation de faisceau hybride (HBF). Alors que le FDP offre de la flexibilité mais au détriment de la complexité matérielle, le HBF équilibre complexité et performance. Cependant, le calcul pour la formation de faisceau est difficile en raison de facteurs tels que l'information d'état de canal (CSI) imparfaite, les problèmes d'optimisation non convexes et les connexions de sous-réseau discrètes dans le HBF. Aborder ces défis est crucial pour maximiser les avantages de la formation de faisceau dans les systèmes MIMO massif. Les approches traditionnelles font face à des problèmes d'optimisation non convexes et la dépendance à l'égard d'un CSI précis. Ces inconvénients entravent leur extensibilité et leur efficacité, conduisant souvent à des performances sous-optimales. De plus, l'acquisition d'un CSI précis introduit une surcharge de signalisation substantielle. Pour surmonter ces défis, il existe un intérêt croissant à exploiter la puissance de techniques utilisant l'apprentissage profond (DL).

Dans cette thèse, nous abordons la question cruciale : «Comment l'apprentissage profond peut améliorer les performances globales des systèmes MIMO massif?» Notre travail se concentre sur le développement de solutions de formation de faisceau basées sur l'apprentissage profond qui dépassent les limites des méthodes conventionnelles. Plus précisément, nous explorons divers schémas de formation de faisceau, y compris le pré-codage entièrement numérique, la formation de faisceau hybride et le MIMO massif sans cellule (CF-mMIMO), avec différents niveaux de connaissances du CSI, couvrant les systèmes avec duplexage en fréquence (FDD) et duplexage en temps (TDD). Le premier aspect abordé dans cette recherche est l'utilisation de l'apprentissage profond pour la conception de faisceau. En utilisant des réseaux neuronaux profonds avec apprentissage non-supervisé et en utilisant la rétroaction de l'indicateur de force du signal reçu (RSSI), une nouvelle approche est proposée pour concevoir des pré-codeurs hybrides sans dépendre de l'estimation et de la rétroaction du CSI. Cette méthode réduit non seulement la complexité de calcul et la latence de manière significative, mais atteint également une efficacité spectrale près de l'optimal.

En s'appuyant sur le succès de l'apprentissage non supervisé pour les scénarios à une seule

station de base, la thèse se penche ensuite sur les systèmes de communication MIMO massifs sans cellule (CF-mMIMO). Dans les systèmes sans cellule, plusieurs points d'accès (AcP) collaborent pour desservir les utilisateurs, ce qui présente des défis pour atteindre une formation de faisceau distribuée presque optimale avec un échange limité de signalisation entre les AcP et le contrôleur de réseau. Pour relever ce défi, la thèse introduit de nouvelles architectures de réseaux neuronaux profonds non supervisés pour la formation de faisceau coordonnée décentralisée. Ces architectures permettent une mise en œuvre efficace et évolutive en réduisant la complexité computationnelle et la surcharge de signalisation tout en atteignant une SE presque optimale. Cette proposition améliore considérablement l'efficacité spectrale des systèmes CF-mMIMO. De plus, la thèse explore la formation de faisceau HBF sans dictionnaire de codes (codebook) de sous-réseau, visant à réduire la consommation d'énergie en optimisant les connexions entre les chaînes radio (RF) et les antennes. Cependant, la nature discrète des connexions de sous-réseau et des quantités de déphasage pose un problème complexe d'optimisation. Pour y remédier, une approche d'apprentissage non supervisé est proposée, éliminant la nécessité d'un codebook de formation de faisceau. Le réseau de neurones profond est formé pour prendre en compte la quantification des déphaseurs et le CSI bruité, ce qui permet d'améliorer la SE par rapport aux méthodes existantes. Cette contribution favorise des solutions de formation de faisceau écoénergétiques dans les systèmes MIMO massifs. Enfin, la thèse étudie la conception d'architecture et la sélection d'antennes adaptatives à l'aide de l'apprentissage profond non supervisé. En abordant le problème complexe d'optimisation de la sélection du sous-ensemble d'antennes optimal et de la conception de l'architecture de formation de faisceau, une approche d'apprentissage non supervisé est proposée pour optimiser ces paramètres de manière adaptative. Le modèle d'apprentissage en profondeur est formé pour maximiser les performances du système tout en tenant compte de l'efficacité énergétique, de l'efficacité spectrale et du nombre d'utilisateurs actifs. Cette proposition offre des informations précieuses sur la conception d'architectures de formation de faisceaux efficaces et intelligentes dans les systèmes MIMO massifs.

ABSTRACT

The emergence of massive multiple-input multiple-output (mMIMO) technology has reshaped wireless communication systems, leveraging an array of antennas to enhance spectral efficiency (SE) and network performance. Beamforming techniques play a pivotal role in mMIMO's performance, with two primary categories: fully digital precoding (FDP) and hybrid beamforming (HBF). While FDP offers flexibility but at the cost of hardware complexity, HBF balances complexity, and performance. However, beamforming is challenging due to factors like imperfect Channel State Information (CSI), non-convex optimization problems, and discrete sub-array connections in HBF. Addressing these challenges is crucial for maximizing the benefits of beamforming in mMIMO systems. Traditional approaches to beamforming in mMIMO systems grapple with non-convex optimization problems and the reliance on accurate CSI. These drawbacks hinder their scalability and efficiency, often leading to suboptimal performance. Additionally, the acquisition of precise CSI introduces substantial signaling overhead. To overcome these challenges, there is a growing interest in leveraging the power of deep learning (DL) techniques.

In this thesis, we address the pivotal question: "How can deep learning improve the overall performance of massive MIMO systems?" Our work focuses on developing DL-based beamforming solutions that surpass the limitations of conventional methods. Specifically, we explore various beamforming schemes, including Full Digital Precoding, Hybrid Beamforming, and cell-free massive MIMO (CF-mMIMO), under different levels of CSI knowledge, spanning frequency division duplexing (FDD) and time division duplexing (TDD) systems. The first aspect addressed in this research is using deep learning for beamforming design. By employing deep neural networks and utilizing received signal strength indicator (RSSI) feedback, a novel approach is proposed to design hybrid precoders without relying on complex CSI estimation and feedback. This method not only significantly reduces computational complexity and latency but also achieves near-optimal SE, thus enhancing the spectral efficiency of massive MIMO systems.

Building upon the success of unsupervised learning for single base station scenarios, the thesis then explores cell-free mMIMO (CF-mMIMO) communication systems. In cell-free systems, multiple access points (AcPs) collaborate to serve users, presenting challenges in achieving near-optimal SE beamforming with limited signaling exchange between AcPs and the network controller. To tackle this challenge, the thesis introduces novel unsupervised deep neural network architectures for decentralized coordinated beamforming. These archi-

tectures enable efficient and scalable implementation by reducing computational complexity and signaling overhead while achieving near-optimal SE. This research significantly enhances the spectral efficiency of CF-mMIMO systems. Furthermore, the thesis explores sub-array codebook-free HBF, aiming to reduce power consumption by optimizing the connections between radio frequency (RF) chains and antennas. However, the discrete nature of sub-array connections and phase-shift amounts poses a complex optimization problem. To address this, an unsupervised learning approach is proposed, eliminating the need for a beamforming codebook. The deep neural network is trained to consider phase-shifter quantization and noisy CSI, resulting in higher SE compared to existing methods. This contribution promotes energy-efficient beamforming solutions in massive MIMO systems. Finally, the thesis investigates architecture design and adaptive antenna selection using unsupervised deep learning. By addressing the intricate optimization problem of selecting the optimal antenna subset and designing the beamforming architecture, an unsupervised learning approach is proposed to adaptively optimize these parameters. The deep learning model is trained to maximize system performance while considering energy efficiency, spectral efficiency, and the number of active users. This research offers valuable insights into designing efficient and intelligent beamforming architectures in massive MIMO systems.

TABLE OF CONTENTS

DEDICATION iii

ACKNOWLEDGEMENTS iv

RÉSUMÉ v

ABSTRACT vii

TABLE OF CONTENTS ix

LIST OF TABLES xiii

LIST OF FIGURES xiv

LIST OF SYMBOLS AND ABBREVIATIONS xvii

CHAPTER 1 INTRODUCTION 1
1.1 Motivation 1
1.2 Background and Concept Definition 2
1.2.1 Massive multiple-inputs multiple-outputs 2
1.2.2 Massive MIMO Beamforming 5
1.2.3 Deep Neural Networks 6
1.2.4 Deep Learning Applied to Wireless Communications 8
1.3 Problem Statement 9
1.4 Research Objectives 11
1.5 General Organization of the Thesis 12
1.6 Claimed Contributions 13

CHAPTER 2 LITERATURE REVIEW 16
2.1 Introduction 16
2.2 Massive MIMO Beamforming Techniques 17
2.2.1 Fully Digital Precoder 17
2.2.2 Analog-only Beamforming 20
2.2.3 Hybrid Beamforming 21
2.2.4 Coordinated Beamforming 25
2.3 Deep Learning-based Massive MIMO Beamforming 28

2.3.1 Different Beamforming Scheme with Deep Learning 28
2.3.2 Different Learning Approaches for Massive MIMO Beamforming Design 33
2.4 Summary 37

CHAPTER 3 ARTICLE 1: UNSUPERVISED DEEP LEARNING FOR MASSIVE MIMO HYBRID BEAMFORMING 38
3.1 Abstract 38
3.2 Introduction 38
3.3 System Model 41
3.3.1 Step 1: SS Bursts Transmission 42
3.3.2 Step 2: RSSI Feedback 42
3.3.3 Step 3: Downlink Data Transmission 43
3.4 Dataset Generation for DNN 44
3.4.1 Channel Model 44
3.4.2 Dataset Generation Method 45
3.4.3 Fully Digital Precoder Design 45
3.4.4 Hybrid Beamforming Design 47
3.5 Synchronization Signal and Codebook design 48
3.5.1 Proposed SS Burst Design 48
3.5.2 Proposed Codebook Design 49
3.6 RSSI-Based Hybrid Beamforming with Deep Neural Network 51
3.6.1 Deep Neural Network Architecture 51
3.6.2 Unsupervised Training 53
3.6.3 Evaluation Phase 56
3.7 Numerical Evaluation 56
3.7.1 Spectral Efficiency Evaluation for All Areas 59
3.7.2 Impact of The RSSI Length and Quantization 61
3.7.3 Impact of The Number of Users and Antennas 61
3.7.4 Computational Complexity Comparison 63
3.8 Conclusion 68

CHAPTER 4 ARTICLE 2: DECENTRALIZED BEAMFORMING FOR CELL-FREE MASSIVE MIMO WITH UNSUPERVISED LEARNING 69
4.1 Abstract 69
4.2 Introduction 69
4.3 System Description 70
4.3.1 Baseline CF-mMIMO Beamforming With Perfect CSI 71

4.3.2 Beam Training . . . 72
4.3.3 Codebook Design for Hybrid Beamforming . . . 73
4.4 Distributed DNNs for Cell-Free Beamforming . . . 73
4.4.1 Fully Decentralized Beamforming . . . 73
4.4.2 Partially Decentralized Beamforming . . . 74
4.4.3 Training Mode (Offline Phase) . . . 75
4.4.4 Testing Mode (Online Phase) . . . 75
4.5 Simulation Results . . . 76
4.6 Conclusion . . . 79

CHAPTER 5 ARTICLE 3: LEARNING ENERGY-EFFICIENT TRANSMITTER CONFIGURATIONS FOR MASSIVE MIMO BEAMFORMING . . . 81
5.1 Abstract . . . 81
5.2 Introduction . . . 82
5.2.1 Related Works . . . 83
5.2.2 Contributions . . . 84
5.2.3 Paper Organization and Notation . . . 85
5.3 System Model and Baselines . . . 85
5.3.1 Conventional Beamforming Structures . . . 86
5.3.2 Problem Definition . . . 90
5.3.3 Channel Model . . . 91
5.4 Energy Model . . . 91
5.4.1 General Beamforming Structure . . . 91
5.4.2 Energy Consumption Analysis . . . 93
5.5 Energy-Efficient Beamforming Driven By Deep Unsupervised Learning . . . 96
5.5.1 Deep Neural Network Architecture . . . 97
5.5.2 Training Phase: Unsupervised Learning . . . 99
5.5.3 Online Phase: Transmitting Data . . . 103
5.6 Performance Evaluation . . . 104
5.6.1 Spectral Efficiency and Power Consumption Analysis . . . 104
5.6.2 Varying the Number of Users . . . 109
5.6.3 Training with Imperfect CSI . . . 110
5.6.4 Computational Complexity Analysis . . . 112
5.7 Conclusion . . . 115

CHAPTER 6 GENERAL DISCUSSION . . . 116

CHAPTER 7 CONCLUSION AND RECOMMENDATIONS 120
7.1 Summary of Works and Contributions 120
7.2 Future Research 121
7.3 Publications 123

REFERENCES 124

LIST OF TABLES

Table 3.1 Parameter selection for the deepMIMO channel model 46
Table 3.2 Multi-tasking DNN Hyper-Parameters 57
Table 3.3 Number of Parameters in DNN-Based HBF 66
Table 3.4 Complexity comparison of Proposed method and state-of-the-art . . 67
Table 4.1 Comparison of Beamforming Type, Signaling Exchange, and Complexity ($N_{\mathsf{T}} = 64$, $N_{\mathsf{RF}} = 8$, $N_{\mathsf{U}} = 4$, $K = 16$, $M = 4$) 76
Table 5.1 Energy Model Notations and Parameters 93
Table 5.2 Hardware Complexity Comparison 93
Table 5.3 Passive Phase Shifter IL Comparison 95
Table 5.4 Parameter selection for the deepMIMO channel model 106
Table 5.5 Proposed DNN hyper-parameters 106
Table 5.6 Simulation parameters for the energy model 107
Table 5.7 Computational Complexity Comparison 114

LIST OF FIGURES

Figure 1.1 Downlink operation of a massive MIMO link [4] 3
Figure 1.2 Downlink operation of a point-to-point massive MIMO link [4] . . 4
Figure 1.3 Deep neural network (DNN) architecture [28] 7
Figure 2.1 Massive MIMO Fully digital precoder architecture [50] 18
Figure 2.2 Massive MIMO analog beamforming architecture [53] 20
Figure 2.3 Massive MIMO hybrid beamforming architecture [55] 21
Figure 2.4 Different types of HBF architecture, a) Fully connected HBF [64], b) Fixed subarray HBF [64], c) Dynamic subarray HBF [65] . . . 22
Figure 2.5 Different possible antenna configurations for a massive MIMO base station [14] 26
Figure 2.6 Cell-free massive MIMO system [10] 27
Figure 3.1 System architecture of the hybrid RF beamforming in mmWave massive MIMO with three steps beam training 43
Figure 3.2 Steps to generate the core and DNN datasets 46
Figure 3.3 Proposed multi-tasking DNN architecture to design the HBF . . . 51
Figure 3.4 The diagram for the unsupervised training in offline mode and the prediction mode of the proposed DNN in online mode 54
Figure 3.5 Illustration of each type of area covered for the deepMIMO channel model 56
Figure 3.6 Spectral efficiency performance of Hybrid beamforming design in "AFP-Net" and "HBF-Net" in three scenarios: a) Extended Area b) Crossroad Area c) Limited Area ($N_{\mathsf{U}} = 4, N_{\mathsf{RF}} = 8, N_{\mathsf{T}} = 64, K = 32$) 58
Figure 3.7 Spectral efficiency performance of FDP design in "AFP-Net" in three scenarios: a) Extended Area b) Crossroad Area c) Limited Area ($N_{\mathsf{U}} = 4, N_{\mathsf{RF}} = 8, N_{\mathsf{T}} = 64, K = 32$) 60
Figure 3.8 Spectral efficiency performance of HBF design in AFP-Net in different number of RSSI (K) ($N_{\mathsf{U}} = 4, N_{\mathsf{RF}} = 8, N_{\mathsf{T}} = 64$) 62
Figure 3.9 Spectral efficiency performance of HBF design in "AFP-Net" in different number of quantization bits (N_b) ($N_{\mathsf{U}} = 4, N_{\mathsf{RF}} = 8, N_{\mathsf{T}} = 64, K = 32$) 62
Figure 3.10 Spectral efficiency performance of HBF design in "AFP-Net" and "HBF-Net" versus different number of user (N_{U}) in "Extended area" ($\sigma^2 = -130$ dBW, $K = 32$, $N_{\mathsf{T}} = 64$, and $N_{\mathsf{RF}} = 8$) 64

Figure 3.11 Spectral efficiency performance of HBF design in "AFP-Net" and "HBF-Net" versus different number of antenna in BS (N_{T}) in "Extended area" ($\sigma^2 = -130$ dBW, $K = 32, N_{\mathsf{U}} = 4$, and $N_{\mathsf{RF}} = 8$) . . 64
Figure 3.12 Spectral efficiency performance of HBF design in "AFP-Net" versus different number of antenna in BS (N_{T}) in "Extended area" for different number of RSSI (K) ($\sigma^2 = -130$ dBW, $N_{\mathsf{U}} = 4$, and $N_{\mathsf{RF}} = 8$) 65
Figure 4.1 a) Fully distributed DNN "FullDeC-HBF" or "FullDeC-FDP", b) Partially distributed DNN "PartDeC-HBF" or "PartDeC-FDP" . 74
Figure 4.2 Achievable spectral efficiency (b/s/Hz) performance (a) FDP, (b) HBF 78
Figure 4.3 CDFs of the per-user spectral efficiency ($\sigma^2 = -130$ dBW, $M = 4$, $N_{\mathsf{T}} = 64$) 78
Figure 4.4 Spectral efficiency versus N_{U} ($\sigma^2 = -120$ dBW, $M = 4$, $N_{\mathsf{T}} = 64$) 79
Figure 5.1 Massive MIMO system model structure with one transmitter BS employing HBF to serve a set of users 86
Figure 5.2 Example of connection matrices ($\mathbf{\Omega}_{\mathsf{HB}}$) of some conventional HBF structures. Each green square indicates a connection. Top: FC-HBF. Middle: FSA-HBF. Bottom: DSA-HBF 88
Figure 5.3 General beamforming structure. (a) Hybrid beamforming structure. (b) Fully digital precoder structure 92
Figure 5.4 $\text{DNN}_{\mathsf{core}}$ architecture which is identical for both HBF and FDP . . 97
Figure 5.5 Proposed DNN architecture for (a) Hybrid beamforming, (b) Fully digital precoder 98
Figure 5.6 Training (left) and online (right) phases for efficient beamforming. The outputs of the DNN depend on the BF structure (HBF, FDP) 99
Figure 5.7 Illustration of the selected covered area from deepMIMO channel model [141] 105
Figure 5.8 Maximum spectral efficiency of E-FDP-Net and E-HBF-Net, compared to other conventional approaches. System parameters are set to: $N_{\mathsf{U}} = 4$, $N_{\mathsf{RF}} = 8$, $N_{\mathsf{T}} = 64$ 105
Figure 5.9 Power required to achieve a given SE for the various transmitter configurations. Idle P_{BF} is the power consumed by the BF structure when $P_{\mathsf{TX}} = 0$. The parameters are set to: $N_{\mathsf{U}} = 4$, $N_{\mathsf{T}} = 64$, $N_{\mathsf{RF}} = 8$, and $\sigma^2 = -130$ dBm 108

Figure 5.10 The connection matrix $\bar{\mathbf{\Omega}}_{\mathsf{FD}} = \text{diag}(\bar{\boldsymbol{\omega}})$ of E-FDP-Net for one input sample, and for different values of hyper-parameter R_{d}, where a blue square represents the value 1 and a white one represents the value 0. System parameters are set to: $N_{\mathsf{U}} = 4$, $N_{\mathsf{T}} = 64$, and $\sigma^2 = -130$ dBm 108

Figure 5.11 The average value of the connection matrix $\bar{\mathbf{\Omega}}_{\mathsf{HB}}$ of E-HBF-Net given for different values of hyper-parameter R_{d}, where the shade of each square represents the range of values from 0 (light) to 1 (dark). System parameters are set to: $N_{\mathsf{U}} = 4$, $N_{\mathsf{T}} = 64$, $N_{\mathsf{RF}} = 8$, and $\sigma^2 = -130$ dBm 109

Figure 5.12 EE versus SE for the proposed E-HBF-Net and E-FDF-Net. The parameters are set to: $N_{\mathsf{U}} = 4$, $N_{\mathsf{T}} = 64$, $N_{\mathsf{RF}} = 8$, and $\sigma^2 = -130$ dBm 110

Figure 5.13 The normalized number of active RF chains, EE, and power consumption of the proposed E-FDP-Net (left sub-plots), E-HBF-Net (right sub-plots) versus different numbers of users. System parameters are set to: $N_{\mathsf{RF}} = 8$, $N_{\mathsf{T}} = 64$, and $\sigma^2 = -130$ dBm 111

Figure 5.14 The SE comparison of the different BF solutions with different values of β. System parameters are set to: $N_{\mathsf{U}} = 4$, $N_{\mathsf{RF}} = 8$, $N_{\mathsf{T}} = 64$, $\gamma = 0$, $\sigma^2 = -130$ dBm 113

Figure 5.15 Training steps of E-FDP-Net. The parameters are set to: $N_{\mathsf{U}} = 4$, $N_{\mathsf{RF}} = 8$, $N_{\mathsf{T}} = 64$, and $R_{\mathsf{d}} = 3$ 113

LIST OF SYMBOLS AND ABBREVIATIONS

AcP	access point
AI	artificial intelligence
AoA	angle of arrival
AoD	angle of departure
AP	analog precoder
AWGN	additive white Gaussian noise
BS	base station
CB	conjugate beamforming
CEL	cross-entropy loss
CF-BF	cell-free beamforming
CF-HBF	cell-free hybrid beamforming
CF-mMIMO	cell-free massive MIMO
CL	convolutional layer
CNN	convolution neural network
CoMP	coordinated multi-point
CSI	channel state information
DAC	digital-to-analog converter
DDPG	deep deterministic policy gradient
DL	deep learning
DNN	deep neural network
DP	digital precoder
DQN	deep Q-network
DRL	deep reinforcement learning
DSA-HBF	dynamic subarray HBF
DUSA-HBF	dynamic unequally subarray HBF
EC	energy consumption
EE	energy efficiency
FC-HBF	fully-connected HBF
FDD	frequency division duplex
FDM	frequency-division multiplexing
FDP	fully digital precoder
FL	fully-connected layer
FSA-HBF	fixed subarray HBF

HBF	hybrid beamforming
HSHO	hybrid structured heuristic optimization
IA	initial access
IL	insertion loss
IoT	internet-of-things
JT	joint transmission
LO	local oscillator
LPA	linear power amplifier
LPF	low pass filter
MAC	medium access control
MIMO	multiple-input multiple-output
MISO	multiple-input single-output
ML	machine learning
mMIMO	massive MIMO
MMSE	minimum mean square error
mmWave	millimeter wave
MSE	mean square error
MU-MIMO	multi-user MIMO
NC	network controller
NLP	natural language processing
O-FDP	optimal fully digital precoder
OFDM	orthogonal frequency division multiplexing
OMP	orthogonal matching pursuit
PA	power amplifier
PS	phase-shifter
PSO	particle swarm optimization
PZF	phase zero forcing
QoS	quality of service
RF	radio frequency
RIS	reconfigurable intelligent surfaces
RL	reinforcement learning
RNN	recurrent neural network
RSSI	received signal strength indicator
SA-HBF	subarray HBF
SE	spectral efficiency
SINR	signal-to-interference plus noise ratio

SNR	signal-to-noise ratio
SS	synchronization signal
SSB	synchronization signal burst
STE	straight through estimator
SVD	singular-value decomposition
TDD	time division duplex
TDM	time-division multiplexing
UE	user equipment
URLLC	ultra-reliable low-latency communication
WMMSE	weighted minimum mean square error
ZF	zero forcing

CHAPTER 1 INTRODUCTION

1.1 Motivation

In the era of 5G and beyond, wireless communication networks are increasingly expected to deliver high data rates, low latency, and reliable connections [1, 2],. To face this challenge, massive MIMO (mMIMO) has become an essential asset in the design of future wireless networks [2]. Massive MIMO systems have been identified as a potential way to improve the spectral efficiency (SE) and system capacity through the use of beamforming techniques [3–5]. Furthermore, to improve the energy efficiency (EE) of the mMIMO systems with fully digital precoder (FDP), the use of hybrid beamforming (HBF) techniques is critical, which combine the advantages of digital and analog beamforming [6]. Hybrid beamforming allows for a trade-off between performance and complexity by utilizing a limited number of radio frequency (RF) chains with analog and digital beamforming. However, the design of HBF solutions for mMIMO systems poses significant challenges due to the non-convex and discrete nature of the problem, as well as the reliance on accurate channel state information (CSI) [6]. These limitations highlight the need for innovative approaches that can address these challenges and fully exploit the potential of beamforming in mMIMO systems.

Recently, machine learning (ML) has become instrumental in numerous fields and various domains, enabling computers to learn patterns and make predictions based on them. Deep learning (DL), a subset of ML, utilizes multi-layered artificial neural networks to extract intricate patterns from extensive datasets [7]. Deep learning has revolutionized areas like computer vision and natural language processing (NLP), showcasing its remarkable potential. Deep learning can also offer a promising avenue for innovation in wireless communication networks. Its ability to leverage vast amounts of data and extract complex patterns can significantly enhance the design and performance of wireless communication systems [8]. The abundance of large datasets has encouraged the use of DL in wireless communication networks. By leveraging the power of DL, it becomes possible to optimize beamforming schemes based on real-world channel data, taking into account dynamic variations in the wireless environment and improving adaptability to changing network conditions. This presents an exciting opportunity to broaden the boundaries of traditional beamforming techniques and unlock new levels of efficiency and effectiveness in wireless communication systems.

Taking advantage of DL technology as a promising solution to the challenges of mMIMO beamforming design, this thesis aims to incorporate DL techniques to create beamforming techniques for mMIMO systems [9]. A key advantage of exploiting the capabilities of DL is

that it enables the achievement of near-optimal SE beamforming solutions by overcoming the limitations of non-DL approaches while also reducing computational complexity. This thesis explores the application of DL in various aspects of beamforming, starting with single base station (BS) scenarios and extending to cooperative beamforming in cell-free massive MIMO (CF-mMIMO) systems [10]. It further investigates different HBF structures, and subarray HBF, all with the goal of enhancing the SE, reducing complexity, and optimizing the EE. In addition to addressing the challenges of non-convex optimization, discrete subarray designs, coordination across distributed access point (AcP), and scalability, this thesis also focuses on addressing the need for adaptive and intelligent architecture design and antenna selection in mMIMO systems. Through comprehensive evaluations and comparisons with state-of-the-art techniques, this thesis aims to provide practical solutions that improve the performance and efficiency of mMIMO beamforming while considering the challenges associated with computational complexity and robustness against imperfections in CSI acquisition in both frequency division duplex (FDD) and time division duplex (TDD) communication.

1.2 Background and Concept Definition

In this section, we will review two fundamental technologies that form the basis of this thesis: mMIMO systems and deep neural networks (DNNs). We will explore their principles, advantages, and challenges, providing a solid understanding of their relevance in the context of artificial intelligence (AI)-aided wireless communication.

1.2.1 Massive multiple-inputs multiple-outputs

The concept of multiple-input multiple-output (MIMO) was first introduced in the 1970s as a means to improve the performance of wireless communication by utilizing multiple antennas at both the transmitter and receiver [11, 12]. By taking advantage of multipath propagation, MIMO systems can achieve higher data rates, better reliability, and increased the SE compared to traditional single-antenna systems. The term "massive" refers to the deployment of a large number of antennas at the BS in modern communication networks. Unlike traditional MIMO systems that typically utilize a few antennas, mMIMO systems can employ tens or even hundreds of antennas, significantly increasing the SE and enhancing system performance [13, 14]. Massive MIMO is a revolutionary technology in wireless communication that has gained significant attention in recent years [15]. As wireless networks evolve towards 5G beyond and 6G, mMIMO is expected to play a crucial role in meeting the ever-growing demands for higher data rates and ultra-reliable low-latency communication (URLLC). The major benefit of mMIMO is that it can take advantage of spatial diversity and multiplexing

with multiple paths of propagation. Using an array of antennas, the system can create highly focused and directional beams, reducing interference and enhancing the signal-to-interference plus noise ratio (SINR) ratio. This spatial processing enables more efficient use of the available spectrum, leading to improved overall network performance. Advancement of mMIMO technology in 5G and beyond 5G not only enables improved the SE but also paves the way for new and innovative use cases, such as massive IoT connectivity, improving the EE, and high-bandwidth applications [16].

Massive MIMO finds its relevance in various applications such as millimeter wave (mmWave) frequencies and internet-of-things (IoT). In mmWave communications, which operate in high-frequency bands, i.e. above 30 GHz, mMIMO plays a crucial role in overcoming the challenges of high path loss and limited cell coverage. By deploying a large number of antennas, mMIMO can compensate for high propagation losses and achieve beamforming with narrow beams, enabling reliable and high capacity communication in mmWave bands [17,18]. In the context of IoT, mMIMO offers numerous benefits. The increasing use of IoT gadgets, which are usually low-power and small-sized, necessitates effective and reliable wireless connectivity. Massive MIMO systems can provide better coverage, increased capacity, and enhance the EE for IoT deployments. By exploiting spatial multiplexing, mMIMO can support simultaneous communications with a large number of IoT devices, enabling seamless connectivity in crowded IoT environments. Furthermore, the beamforming capabilities of mMIMO help mitigate interference and ensure reliable communication between IoT devices and network [19].

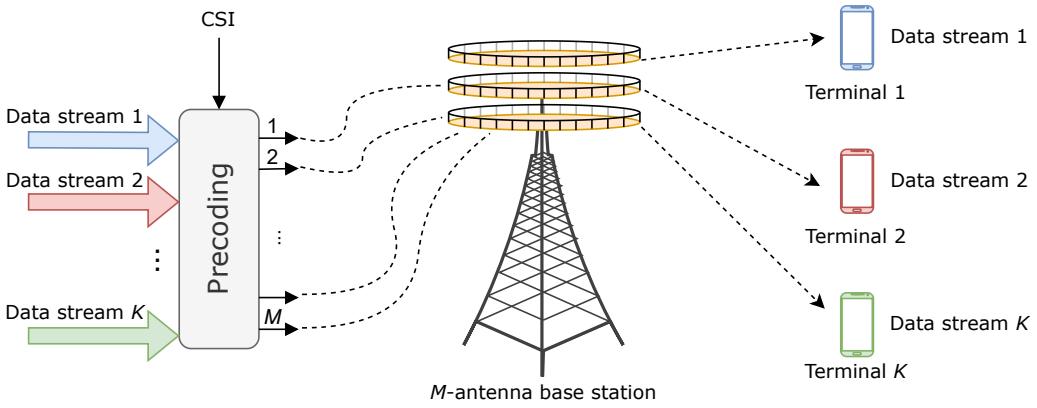

Figure 1.1: Downlink operation of a massive MIMO link [4]

Figure 1.1 shows the key characteristics of mMIMO. This diagram represents a single cell within a network of cells, or it can be seen as an isolated site within a single cell. A collection of small antennas, which are not directive in nature, are deployed to serve multiple independent

users. Typically, each terminal is equipped with a single antenna. The figure illustrates the downlink operation, where distinct data streams are transmitted to each user. The goal is to make sure that each user gets the data stream they were meant to receive without any major interference from other data streams. In contemporary systems, this multiplexing task is typically achieved by employing a combination of time-division multiplexing (TDM) (sending data streams at different times) and frequency-division multiplexing (FDM) (sending data streams over different frequencies). On the contrary, mMIMO employs spatial-division multiplexing, enabling multiple data streams to occupy the same frequencies and times. This is accomplished using an array of independently controlled antennas. When there is a direct line of sight between the antennas and users, the data streams are transmitted on focused beams. However, in environments with obstructions and multiple paths, the data streams can arrive from various directions simultaneously. In such cases, the streams can reinforce each other where desired and interfere where unwanted. To enable multiplexing, the array requires knowledge of the frequency response of the propagation channels between each antenna and the user. This information, known as CSI, is utilized in the precoding block (shown in Figure 1.1). In this block, the data streams are mapped to the signals that drive each antenna. Increasing the number of antennas allows a more precise beam to focus towards specific users [3, 4].

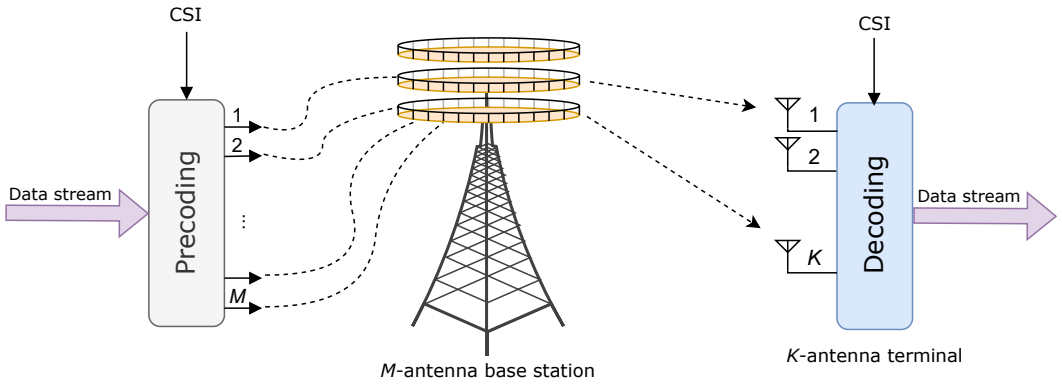

Figure 1.2: Downlink operation of a point-to-point massive MIMO link [4]

In general, there are two primary types of mMIMO: multi-user MIMO (MU-MIMO) and point-to-point MIMO. Multi-user MIMO as shown in Figure 1.1 is designed to serve multiple users simultaneously with the same time and frequency resources [3, 4]. In MU-MIMO, the BS employs a large antenna array to create independent spatial beams for each user. This enables the simultaneous transmission of multiple data streams to different users on the same frequency and time slots. Spatial beams are focused on each user, resulting in improved signal

quality and increased overall network capacity. Multi-user MIMO is particularly effective in scenarios where there are multiple users with different quality of service (QoS) requirements because it allows the system to dynamically allocate resources and tailor the transmission strategy to the specific needs of each user.

On the other hand, point-to-point MIMO as shown in Figure 1.2, also known as single-user MIMO, focuses on enhancing the communication link between a single BS and a specific user. In point-to-point MIMO, both the BS and the user device are equipped with multiple antennas [3, 4]. This allows for the creation of multiple spatial streams that are transmitted simultaneously, leveraging the spatial dimension to increase data throughput and reliability. The multiple antennas at both ends enable the system to exploit the spatial multiplexing gain, achieving higher data rates and improved link robustness for the specific user. Both MU-MIMO and point-to-point MIMO are powerful techniques that leverage the benefits of mMIMO technology. These variations of mMIMO contribute to the development of advanced wireless systems that can meet the growing demand for reliable high-speed connectivity in various communication scenarios.

In general, mMIMO technology, with its abilities, has immense potential in various applications. As wireless networks evolve towards 5G and beyond, mMIMO is expected to play a predominant role in meeting the ever-growing demands for reliable high-capacity, low-latency wireless communication services. As research and development efforts continue, we can anticipate further breakthroughs in mMIMO technology, revolutionizing wireless communication and shaping the future of mobile networks and beyond.

1.2.2 Massive MIMO Beamforming

Beamforming in mMIMO systems represents a fundamental aspect of the capabilities and benefits of this technology. Beamforming in mMIMO systems enables simultaneous communication with multiple users, each of which may experience different channel conditions [20]. By adjusting the phase and magnitude of the signals transmitted from each antenna, beamforming optimizes the signal strength for the intended user while minimizing interference for other users or unwanted directions. By enabling efficient spatial multiplexing and interference mitigation, beamforming in mMIMO enhances the network capacity and SE, allowing for the support of a large number of simultaneous users and high-demand applications [21, 22]. In addition, beamforming in mMIMO can also improve coverage, extend cell range, and improve QoS in challenging environments [23]. Another significant application of beamforming in mMIMO is in mmWave communications. With increasing interest in utilizing higher frequency bands for wireless communication, mMIMO beamforming can address the challenges

associated with mmWave propagation, such as high channel attenuation and limited cell coverage. Using a large antenna array and adaptive beamforming, mMIMO systems can steer narrow beams toward the desired user, compensating for the high propagation losses and achieving reliable communication in mmWave frequency bands [24].

Furthermore, beamforming in mMIMO systems has applications in wireless backhaul and relay systems, where it enables efficient and high-capacity data transmission between the BSs. By applying beamforming techniques, mMIMO systems can focus the energy transmitted toward the desired relay nodes or backhaul links, reducing interference and improving overall system performance [25]. Furthermore, beamforming in mMIMO has potential applications in IoT networks, where it can support the massive connectivity requirements and provide reliable communication in crowded IoT environments. By adaptively steering beams toward IoT devices, beamforming helps mitigate interference and extend coverage, thereby enabling efficient connectivity for IoT applications. In general, beamforming in mMIMO systems finds various applications and holds promise in enhancing wireless communication in terms of capacity, coverage, and QoS [26].

1.2.3 Deep Neural Networks

Artificial intelligence is a rapidly evolving field that aims to develop intelligent systems capable of performing tasks that typically require human intelligence. A prominent subset of AI is machine learning (ML), which focuses on enabling computers to learn from data and improve their performance. Machine learning algorithms extract patterns and insights from large datasets, enabling computers to make predictions, classify objects, and make informed decisions. Techniques such as supervised learning, unsupervised learning, and reinforcement learning have revolutionized various domains, including image and speech recognition, natural language processing, and data analysis. Artificial intelligence and ML have become crucial tools in numerous industries, from healthcare and finance to transportation and entertainment [27].

Deep learning (DL) is a subfield of ML that has gained great attention in recent years. Deep learning models, also known as artificial neural networks, are inspired by the structure and function of the human brain. These models are made up of multiple layers of interconnected artificial neurons that allow them to learn hierarchical representations of data autonomously. These layers, as shown in Figure 1.3, include an input layer, one or more hidden layers, and an output layer. The input layer receives raw data as input, which is then passed through the hidden layers for feature extraction and transformation. The output layer produces the final predictions or classifications based on the learned features. In a DNN, each artificial neuron

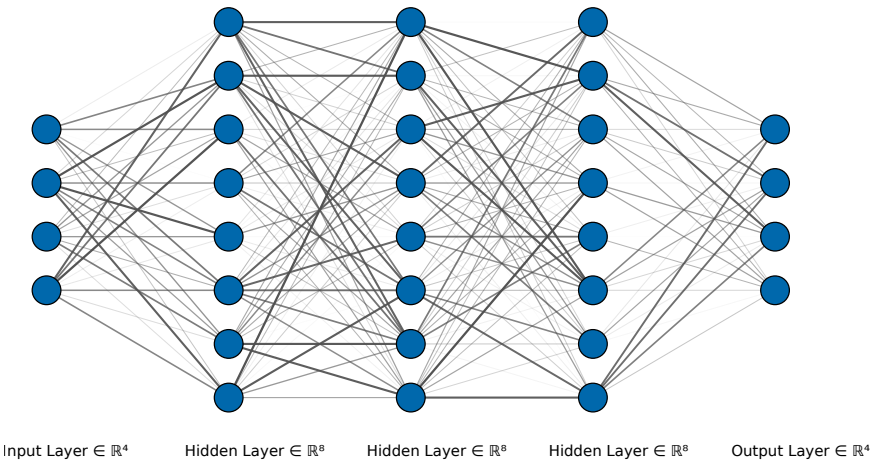

Figure 1.3: Deep neural network (DNN) architecture [28]

in the hidden layers processes its input using a set of learnable parameters, known as weights and biases. These parameters are adjusted during the training process using optimization algorithms to minimize the difference between the predicted outputs and the actual labels in the training data. This process is known as backpropagation, and it allows the DNN to iteratively update its parameters and learn to make accurate predictions [7].

Deep learning has revolutionized several domains, achieving state-of-the-art results in image and speech recognition, natural language processing, and many other tasks. The success of DL can be attributed to its ability to handle large-scale datasets and its ability to automatically learn complex features from raw data, eliminating the need for manual feature engineering. Deep learning techniques, such as convolution neural networks (CNNs) and recurrent neural networks (RNNs), have demonstrated remarkable performance in various applications [28]. Deep learning has also made significant contributions to the solution of challenging research problems. For example, DL has been applied to healthcare, where it has shown promising results in medical image analysis, disease diagnosis, and drug discovery [29]. Furthermore, the DL models have also demonstrated their potential in autonomous vehicles, allowing advanced perception systems for object detection, lane detection, and decision-making [30, 31]. The wide-ranging applications of DL have fueled its rapid adoption and have prompted extensive research and development in the field.

As DL continues to evolve, researchers are actively exploring new architectures, optimization algorithms, and regularization techniques to further enhance its capabilities. Ongoing efforts are focused on addressing challenges related to data efficiency, interpretability, and ethical implications of AI systems. Interdisciplinary collaborations between AI researchers, domain

experts, and ethicists are critical to ensure the responsible development and deployment of DL technology. The future of DL holds tremendous potential for advancing fields such as healthcare, robotics, finance, and many others, providing opportunities for innovation and transformation across diverse sectors [28].

There are several types of DL algorithms, including supervised learning, unsupervised learning, and reinforcement learning. Supervised learning is the most common type of DL. It involves training a neural network using labeled data, where the input data is paired with the corresponding output labels. The network learns to map the input data to the correct output labels by optimizing a loss function. An example of supervised learning is image classification, where a neural network is trained on a labeled image data set to correctly classify new images into different categories, such as identifying whether an image contains a cat or a dog [32]. Unsupervised learning, on the other hand, involves training a neural network on unlabeled data to discover patterns or relationships within the data. The network learns to extract meaningful features or representations from the input data without explicit supervision. Clustering is an example of unsupervised learning where the goal is to group similar data points together based on their intrinsic properties. For example, clustering can be used to segment customer data into distinct groups for targeted marketing campaigns [28]. Reinforcement learning is a type of learning in which an agent learns to interact with an environment and make decisions to maximize a cumulative reward. The agent explores the environment through trial and error and receives feedback in the form of rewards or penalties based on its actions. The goal is to learn an optimal policy that maximizes the long-term reward. An example of reinforcement learning is training an autonomous vehicle to navigate through a simulated environment. The agent learns to take actions (e.g., accelerate, brake, turn) based on the observed state of the environment (e.g., road conditions, obstacles) to reach its destination safely and efficiently [33].

1.2.4 Deep Learning Applied to Wireless Communications

Drawing upon the capabilities highlighted earlier, the application of deep learning within wireless communication emerges as a promising avenue to address evolving challenges and improve the performance of wireless communication systems [8]. Deep learning techniques leverage the power of multiple layers of artificial neural networks to automatically learn intricate patterns and relationships from large amounts of wireless data. By exploiting the inherent capabilities of DL, improvements can be achieved at various layers of the communication protocol stack [34–36].

Very recently, DL has made significant contributions to the physical layer of wireless commu-

nication systems. One area where DL has been used is in channel modeling and estimation. Traditionally, channel models are derived on the basis of assumptions about propagation environments, such as path loss, fading, and multipath characteristics. However, these models may not fully capture the complexity and variability of real-world wireless channels. Deep learning offers the potential to learn the mapping between transmitted signals and received signals directly from data, allowing for more accurate and adaptive channel modeling. Deep learning models can capture complex channel characteristics, spatial correlations, and interference patterns to estimate channel parameters and optimize equalization filters. These applications have shown promise in improving the robustness and capacity of wireless communication systems [37]. This can facilitate better channel estimation [38], adaptive modulation and coding, and efficient resource allocation based on the predicted channel conditions [39,40].

Another application of DL in the physical layer is signal detection. Traditional signal detection algorithms, such as maximum likelihood detection, can be computationally complex and may not scale well with increasing system dimensions [41]. Deep learning models, such as RNN, offer an alternative approach to performing signal detection directly from received signals. By training on large datasets of labeled signals, DL models can learn to distinguish different modulation schemes and extract the relevant features from the received signals, even in the presence of noise, interference, and fading channels. This can lead to efficient and accurate signal detection, allowing improved system performance [42].

Moreover, DL techniques have been applied to antenna array optimization in wireless communication systems. Deep learning can be used to optimize the antenna array configuration, as well as the beamforming and precoding weights. Deep learning-based techniques allow for better signal transmission, interference suppression, and user-specific spatial focusing, leading to improved overall system performance [9]. By leveraging DL techniques at the physical layer, wireless communication systems can benefit from improved channel modeling and estimation, enhanced signal detection capabilities [43], and optimized antenna array configurations. These advances have the potential to increase the SE, enhance system capacity, and improve overall performance in wireless networks. However, it is important to consider challenges such as the availability of training data, the interpretability of DL models, and real-time implementation constraints in order to fully exploit the potential of DL in the physical layer of wireless communication systems.

1.3 Problem Statement

In the rapidly evolving landscape of wireless communication networks, the ever-increasing demand for high data rates, low latency, and reliable connections has become an undeni-

able reality. The surge in wireless device usage, data-intensive applications, and emerging technologies such as IoT have created a pressing need for innovative approaches to maximize SE, increase system capacity, and optimize energy consumption. In this pursuit, mMIMO systems and advanced beamforming techniques, such as FDP and HBF, have emerged as promising strategies. These techniques leverage the inherent spatial diversity and multipath propagation characteristics of wireless channels to improve system performance.

However, while mMIMO and beamforming offer tremendous potential, their design and implementation present significant challenges [44]. Traditional non-deep learning approaches struggle to address the inherent complexity of optimizing beamforming solutions in the context of mMIMO systems. The non-convex nature of the beamforming design problem, combined with the reliance on accurate CSI, hinders the efficacy of conventional methods [45]. Conventional methods often require extensive computation and suffer from sub-optimal performance. Furthermore, the need for accurate CSI acquisition and feedback of CSI introduces significant signaling overhead, limiting the scalability and practicality of beamforming solutions.

To overcome these challenges, there is growing interest in leveraging the power of DL techniques for beamforming in mMIMO systems. Deep learning-based approaches offer several advantages over traditional methods. The problem addressed in this thesis is to explore DL-based beamforming techniques that can overcome the limitations of traditional approaches and optimize the performance of mMIMO systems. The objectives are dedicated to crafting DL-driven beamforming strategies capable of overcoming the constraints of traditional methods, thereby unlocking the full potential of mMIMO systems. This includes exploring various beamforming schemes, such as FDP, HBF, and coordinated beamforming in CF-mMIMO systems. Furthermore, the thesis aims to extend the application of DL to address challenges specific to subarray HBF structures, adaptive antenna selection, and EE in mMIMO systems. By integrating DL into these beamforming techniques, it is possible to improve the performance of the system in terms of SE and EE.

Furthermore, this thesis considers scenarios with different levels of CSI knowledge in FDD and TDD systems. In FDD systems, the uplink and downlink operate in separate frequency bands, which introduces additional complexities in CSI acquisition. Due to the large number of antennas in mMIMO systems, the channel estimation process becomes more challenging and resource-intensive. The estimation of CSI requires the transmission of pilot signals from user devices to the BS, and the subsequent estimation process introduces overhead and consumes valuable resources. In TDD systems, the uplink and downlink share the same frequency band, which simplifies the acquisition of CSI compared to FDD systems.

The key advantage of TDD systems is the ability to leverage channel reciprocity, where the uplink and downlink channels are assumed to be similar or symmetric due to the shared environment and propagation conditions. However, the challenge lies in the fact that the reciprocity assumption is not perfectly accurate in practical scenarios. Therefore, in practical scenarios, mMIMO knowledge may be limited or unavailable due to channel estimation errors, feedback limitations, or fast-changing channel conditions. Designing DL-based beamforming techniques that can adapt to different levels of CSI knowledge is crucial for ensuring robust performance in various wireless communication environments.

Moreover, the unsupervised approach extends beyond emulating conventional methods' performance; it has the capacity to discover superior solutions. However, it comes with unique challenges, particularly in the design of appropriate loss functions and achieving the proper convergence of the learning process. Unlike supervised learning, where labeled data guide the optimization process, unsupervised learning lacks predefined success criteria. This makes the task of crafting effective loss functions critical. The challenge involves aligning the loss function with beamforming objectives and translating high-level goals into quantifiable measures for the DL model to optimize. As a consequence, addressing the challenges associated with loss function design is essential to harnessing the power of unsupervised learning effectively and ensuring that the resulting beamforming solutions are both meaningful and impactful in wireless communication scenarios.

1.4 Research Objectives

In response to the challenges identified in Section 1.3, this thesis proposes a range of DL-based beamforming solutions to optimize mMIMO systems, focusing on HBF, FDP, and antenna selection in single-cell scenarios, as well as exploring CF-mMIMO cooperative beamforming. The central question driving this research is: "How can deep learning be used effectively to improve the performance of mMIMO beamforming, and what enhancements can it provide to the overall system performance?" Consequently, this thesis aims to develop and investigate DL-based beamforming techniques that can improve conventional approaches in mMIMO systems. The specific objectives are as follows.

1. We seek to maximize SE. Deep learning models have the potential to learn and optimize beamforming strategies that improve the overall SE of the system. By intelligently allocating resources and optimizing spatial and spectral utilization, DL-based beamforming methods can enhance the system's capacity to transmit and receive more data within the available bandwidth.

2. We are also interested in simultaneously reducing the computational complexity associated with beamforming in mMIMO systems. To achieve this, our objective is to leverage the power of DL to transfer the computational complexity from the online phase (during operation) to the offline phase (during training). By employing DL models to efficiently represent and parameterize the beamforming process during the training phase, we can reduce the computational burden during real-time operation. This approach has the potential to alleviate hardware requirements and reduce energy consumption, making DL-based beamforming techniques more practical and efficient for deployment in resource-constrained scenarios.

3. Another objective is to improve the robustness of beamforming solutions against imperfect CSI. The performance of traditional beamforming techniques relies on accurate CSI for optimal SE performance. However, in realistic scenarios, obtaining precise CSI can be challenging due to various factors, including channel estimation errors and feedback signaling overhead. Deep learning-based models can learn to adapt and compensate for these imperfections, making beamforming solutions more robust and reliable in real-world environments.

4. Last but not least, EE is also a crucial objective for DL-based beamforming techniques in mMIMO systems. By leveraging the learning capabilities of the DL models, it is possible to optimize the beamforming process to minimize energy consumption while maintaining or even improving SE. This objective aligns with the broader goal of developing more sustainable and environmentally friendly wireless communication systems.

1.5 General Organization of the Thesis

This thesis is written in an article-based format, where CHAPTERS 3, 4, 5 correspond to distinct journal articles each featuring specific contributions. These chapters are based on three journal articles to achieve the research objectives stated above.

CHAPTER 2 provides a comprehensive review of the existing literature in the field of DL-based beamforming techniques in MIMO systems. This chapter sets the stage of the following chapters by highlighting the current state of research, identifying gaps, and contextualizing the significance of subsequent contributions.

CHAPTER 3 focuses on the innovative application of unsupervised DL for hybrid beamforming in massive MIMO systems. The article presented in this chapter introduces a novel approach that harnesses the power of DL to design hybrid beamforming solutions that enhance the SE without relying on complex CSI estimation and feedback. The chapter discusses

the methodology, experimental setup, results, and insights garnered from this research [46].

CHAPTER 4 investigates decentralized beamforming techniques for CF-mMIMO systems. The article presented in this chapter proposes novel unsupervised DL architectures for decentralized coordinated beamforming, overcoming challenges related to excessive signaling exchange between AcPs and the network controller (NC). This chapter outlines the research approach, findings, and implications of this article [47].

CHAPTER 5, based on a journal article submitted in August 2023, contributes to the design of energy-efficient transmitter configurations using unsupervised DL in massive MIMO beamforming. The article addresses the optimization of parameters such as power allocation and antenna-radio frequency chain connections, promoting energy savings without compromising system performance. This chapter provides an overview of the research methodology, outcomes, and implications discussed in the article [48].

CHAPTER 6 serves as a general discussion that synthesizes the findings, implications, and contributions of the articles presented in CHAPTERS 3, 4, and 5. This chapter engages in a broader dialogue that contextualizes the importance of research within the larger field of DL-based beamforming in wireless communication systems.

CHAPTER 7 concludes the thesis by summarizing the key insights, implications, and contributions made throughout the research. This chapter also presents recommendations for future research directions and highlights the overall impact of this work on the advancement of the field of DL-based beamforming in massive MIMO systems.

1.6 Claimed Contributions

The claims of this thesis represent a comprehensive exploration of DL-based beamforming techniques in mMIMO systems, addressing key challenges and pushing the boundaries of beamforming performance. The first contribution focuses on the development of an innovative RSSI-based hybrid beamforming approach. By leveraging received signal strength indicator (RSSI) measurements in FDD communication, this approach improves the efficiency and reduces the signaling overhead of the HBF design, leading to enhanced wireless network performance. Based on this foundation, CHAPTER 3 presents a novel unsupervised DL method for mMIMO hybrid beamforming systems. Notably, this research marks the first attempt to apply unsupervised learning to the HBF technique. Inspired by the RSSI-based method, this research explores two alternative architectures with different throughput-complexity tradeoffs. Furthermore, the proposed method includes the design of synchronization signals (SSs) in initial access (IA) and the codebook for the analog precoder. By training the DL mod-

els on large-scale datasets, this approach achieves near-optimal beamforming solutions while considerably reducing the computational complexity and signaling overhead in FDD communication. By leveraging partial CSI feedback in FDD communication, unsupervised DL eliminates the need for labeled data or optimal values during training. This approach saves a significant amount of time and computational resources for target values as optimal SE solutions while achieving improved beamforming performance and improving the overall SE of mMIMO systems [46].

Moving to CHAPTER 4, the focus shifts to decentralized beamforming techniques within CF-mMIMO systems. The aim is to achieve near-optimal beamforming solutions while minimizing excessive signaling exchange between the AcPs and the NC. The proposed solutions enable fully distributed and partially distributed beamforming optimization, reducing complexity and signaling exchange compared to conventional approaches. It also provides an example of the trade-off between overall computational complexity and signaling overhead by designing an alternative architecture for which complexity is further reduced at the cost of increased fronthaul signaling. This research highlights the feasibility of achieving high SE, and system performance while enabling distributed and cooperative beamforming in cell-free mMIMO systems, including both FDP and HBF techniques [47]. Furthermore, it is shown that the proposed schemes can also be used to reduce the computational complexity and signaling overhead in a coordinated FDP system.

In CHAPTER 5, the contributions center around the design of energy-efficient transmitter configurations in mMIMO beamforming using unsupervised DL for both FDP and HBF. By optimizing parameters such as power allocation and antenna-radio frequency chain connections, the research achieves energy savings without compromising system performance. Due to the binary constraints of beamforming connections, our unsupervised deep learning approach makes use of the Gumbel-Sigmoid technique inspired by Gumbel-Softmax. The proposed solution is designed to be flexible by carefully designing the loss function, allowing it to adjust the power consumption in accordance with the number of active users, and to provide an optimal balance between SE and EC. This contribution further highlights the potential of DL-based techniques in enhancing EE and reducing the complexity of mMIMO beamforming systems. Furthermore, the study examines the capacity of the model to be trained solely using imperfect CSI for both the input to the deep learning model and the calculation of the loss function [48]. Training deep learning models with imperfect CSI is a practical choice for real-world wireless communication systems due to several key advantages. Imperfect CSI reflects the dynamic and complex nature of wireless networks, ensuring that models learn to operate in realistic conditions. This approach eliminates the need to obtain perfect CSI, which is difficult in practice, making it more efficient and cost-effective. Training

models with imperfect CSI makes them more realistic in real deployments.

The performance of all the above-mentioned contributions has been assessed using a realistic ray-tracing channel model. This evaluation provides insight into the real-world performance of the techniques and demonstrates their effectiveness under more practical and complex channel conditions. Together, these contributions form a comprehensive body of research that pushes the boundaries of beamforming techniques in mMIMO systems, showcasing the potential of DL to improve wireless communication networks and address their evolving demands. A patent application has been submitted for the work detailed in CHAPTER 5 in collaboration with Ericsson [49], further highlighting the practical significance and real-world applicability of the proposed DL-based beamforming techniques. These techniques contribute significantly to advancing energy-efficient transmitter configurations in mMIMO systems.

CHAPTER 2 LITERATURE REVIEW

2.1 Introduction

In this chapter, we take a look at the wide range of mMIMO beamforming techniques, exploring the various approaches that have been instrumental in the development of wireless communication systems. At the core of this exploration lies the critical role of beamforming in optimizing spectral efficiency and energy efficiency, driving the pursuit of methods that balance complexity and spectral efficiency.

We will begin with an in-depth exploration of FDP, a technique renowned for its remarkable flexibility in beamforming design. Yet, this versatility often necessitates intricate hardware configurations, challenging the implementation's feasibility and cost-effectiveness. On the other hand, within the spectrum of beamforming strategies, the analog-only approach emerges as a noteworthy contender. Using exclusively analog components, this technique navigates the complexities associated with digital processing, while retaining its potential to optimize performance. However, it grapples with the limitations of exclusively analog solutions, striving to find the sweet spot between simplicity and efficacy. As a consequence, HBF then takes center stage, offering a promising synergy between digital and analog components. This approach attempts to take advantage of the best of both techniques, maximizing efficiency while maintaining simplicity.

We then focus on coordinated beamforming in CF-mMIMO. This approach takes advantage of distributed antenna and macro-diversity in mMIMO systems, facilitating AcP to work together seamlessly in serving users with utmost efficiency. Coordinated beamforming seeks to attain near-optimal performance by orchestrating coordinated actions between AcP. However, it confronts the intricate challenge of effectively managing the exchange of signaling information between different components of the network.

We then move our exploration to the realm of deep learning after having explored the various beamforming strategies. We delve into an array of studies that investigate the integration of DNNs with various beamforming methods. The fusion of DNNs with beamforming unlocks new dimensions in performance enhancement, as the network's ability to automatically learn complex mappings between input data and optimal beamforming parameters aligns seamlessly with the intricate requirements of mMIMO systems. This chapter also looks at the various learning approaches that shape the design of beamforming strategies. From supervised learning that leverages labeled data to unsupervised learning that empowers low

complexity and flexible solutions, each approach adds a layer of innovation and advancement to the field. By probing this array of techniques, we not only gain a comprehensive understanding of the landscape but also pave the way for the subsequent chapters that showcase our contributions to the evolution of mMIMO beamforming through the prism of deep learning and innovative learning approaches.

The following chapters of this thesis are carefully constructed to broaden the examination of mMIMO beamforming techniques and delve further into the area of creative solutions enabled by deep learning approaches. They aim to address the critical challenges, push the boundaries of conventional methods discussed in this chapter, and elevate the performance of mMIMO systems to new heights.

2.2 Massive MIMO Beamforming Techniques

Massive MIMO beamforming is a cutting-edge technology that revolutionizes wireless communications by deploying an extensive array of antennas at the transmitter and receiver. This advanced technique enables unprecedented spectral and energy efficiency, enhancing the capacity and reliability of wireless networks. By using mMIMO, beamforming can direct radio signals toward specific users, optimizing the signal strength and decreasing interference, leading to higher data rates and better overall performance. In the realm of mMIMO beamforming, various transmitter configuration schemes have been explored to optimize signal transmission and reception. These schemes can be broadly categorized into three general categories, FDP, Analog-only Beamforming, and HBF. In this section, we will delve into each of these beamforming schemes, exploring their strengths, weaknesses, and applications in mMIMO systems. The subsequent sections will provide a detailed analysis of the existing studies related to each scheme, showcasing the potential of applied DL techniques, and addressing challenges in optimizing beamforming designs.

2.2.1 Fully Digital Precoder

Fully digital precoder is a beamforming technique that operates entirely in the digital domain, without the need for analog components, where each antenna at the BS is connected to one RF chain as shown in Figure 2.1. In FDP, the precoding matrix is calculated using digital signal processing algorithms, and the resulting weights are applied to the transmitted signals. The goal of FDP is to optimize the transmission of signals in a multi-antenna system, such as a mMIMO system. Fully digital precoder offers several advantages, including high flexibility design and adaptability in adjusting beamforming weights based on channel conditions and

user requirements.

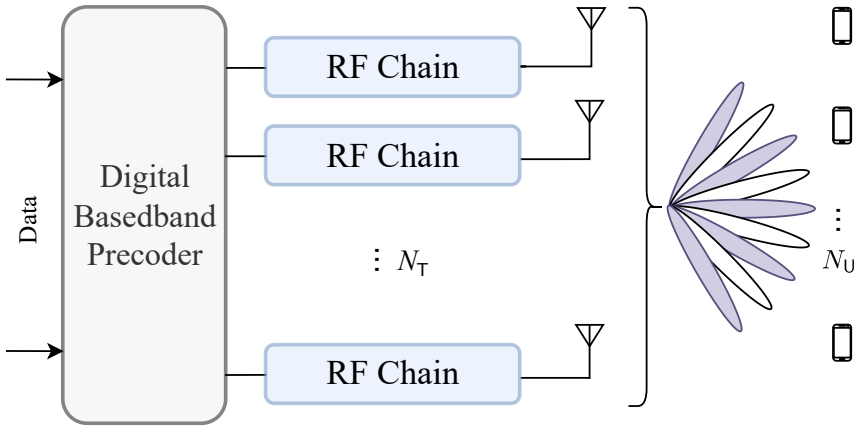

Figure 2.1: Massive MIMO Fully digital precoder architecture [50]

Fully digital precoder can be implemented using different algorithms, three of which are as

- Zero forcing (ZF) Precoding: ZF precoding aims to eliminate interference between users by projecting the transmitted signals onto orthogonal subspaces. It achieves this by inverting the channel matrix, effectively canceling the interference caused by other users. The ZF precoding matrix, denoted as $\mathbf{U}_{\text{ZF}}$, is computed as follows:

$$\mathbf{U}_{\text{ZF}} = \mathbf{H}^{\text{H}}(\mathbf{H}\mathbf{H}^{\text{H}})^{-1}, \tag{2.1}$$

  where $\mathbf{H}$ is the channel matrix. While ZF precoding provides excellent interference mitigation, it may suffer from noise amplification due to the inversion operation. As a result, ZF may not be optimal SE in scenarios with noisy channels or when the channel matrix is not well-conditioned [51].

- Minimum mean square error (MMSE) Precoding: MMSE precoding takes into account the noise and interference statistics to minimize the mean square error between the transmitted and received signals. The MMSE precoding matrix, denoted as $\mathbf{U}_{\text{MMSE}}$, is computed as follows:

$$\mathbf{U}_{\text{MMSE}} = \mathbf{H}^{\text{H}}(\mathbf{H}\mathbf{H}^{\text{H}} + \sigma^2\mathbf{I})^{-1}, \tag{2.2}$$

  where $\mathbf{H}$ is the channel matrix and σ^2 is the noise variance. MMSE precoding strikes a balance between interference cancellation and noise enhancement, leading to improved system performance. It can achieve better performance than ZF precoding, especially

in scenarios with noisy channels or when the channel matrix is ill-conditioned. However, the inclusion of noise statistics in the computation of the precoding matrix introduces a higher computational complexity compared to ZF precoding [3].

- Optimal fully digital precoder (O-FDP): Authors in [52] proposed optimal SE precoding techniques, where it is shown that the optimal FDP vector $\mathbf{u}_u$ of FDP matrix $\mathbf{U} = [\mathbf{u}_1, ..., \mathbf{u}_{N_\mathsf{U}}]$ for user u has the following analytical structure:

$$\mathbf{u}_u = \sqrt{p_u} \frac{\left(I_{N_\mathsf{U}} + \frac{1}{\sigma^2} \sum_{i=1}^{N_\mathsf{U}-1} \mathbf{h}_i \lambda_i \mathbf{h}_i^{\mathrm{H}}\right)^{-1} \mathbf{h}_u}{\left\| \left(I_{N_\mathsf{U}} + \frac{1}{\sigma^2} \sum_{i=1}^{N_\mathsf{U}-1} \mathbf{h}_i \lambda_i \mathbf{h}_i^{\mathrm{H}}\right)^{-1} \mathbf{h}_u \right\|}, \tag{2.3}$$

  where N_U corresponds to the number of users, I_{N_U} corresponds to the $N_\mathsf{U} \times N_\mathsf{U}$ identity matrix, p_u and λ_u are the unknown real-valued coefficients to be optimized, respectively corresponding to the beamforming power and Lagrange multiplier for the user u. In addition, we have $\sum_{\forall u} \lambda_u = 1$ and $\sum_{\forall u} p_u = 1$. Therefore, only $2 \times (N_\mathsf{U} - 1)$ real-valued coefficients must be evaluated to resolve the optimization problem, instead of the initial $N_\mathsf{T} \times N_\mathsf{U}$ complex coefficients. The particle swarm optimization (PSO) algorithm can then be employed to obtain the optimal λ_u coefficients. The optimal SE solutions can be obtained by assuming $p_u \approx \lambda_u$ and by evenly distributing the power over $\mathcal{K} \in \{1, ..., N_\mathsf{U}\}$ users and setting $p_u = 0$ for the remaining $N_\mathsf{U} - \mathcal{K}$ users. Therefore, $2^{N_\mathsf{U}-1}$ solutions have to be evaluated to find the near-optimal one. In this thesis, we use this technique as a baseline for the upper bound.

However, the precoding techniques mentioned above face challenges in terms of computational complexity and hardware requirements. The computation of the precoding matrix involves complex mathematical operations, which demand significant processing power. This can be particularly challenging in real-time implementations or systems with a large number of antennas, such as mMIMO systems. The computational burden increases with the number of antennas and the number of users, making it necessary to employ efficient algorithms and hardware architectures to ensure real-time operation [50]. Furthermore, in FDP, each antenna requires high-resolution Digital-to-analog converters (DACs) at the transmitter. These DACs convert digital signals into analog forms for transmission. High-resolution DACs can be costly and power-consuming, especially when dealing with a large number of antennas in mMIMO systems. Therefore, employing FDP for mMIMO system would be costly and energy inefficient. Consequently, optimizing the hardware design and considering power consumption becomes crucial for practical mMIMO beamforming implementations [50].

2.2.2 Analog-only Beamforming

Analog-only beamforming, also known as analog beamforming, is a straightforward beamforming technique that operates entirely in the analog domain without any digital signal processing, as shown in Figure 2.2. It involves adjusting the phase and amplitude of signals at each antenna element to create constructive interference towards the desired user [53]. Analog-only beamforming relies on beam selection from a pre-defined beamforming codebook. The codebook consists of a finite set of fixed beamforming vectors, each corresponding to a specific direction in the spatial domain. During beam selection, the analog-only beamforming system chooses the best beam from the codebook that aligns with the desired user's angle of arrival (AoA) or the user with the highest received signal strength.

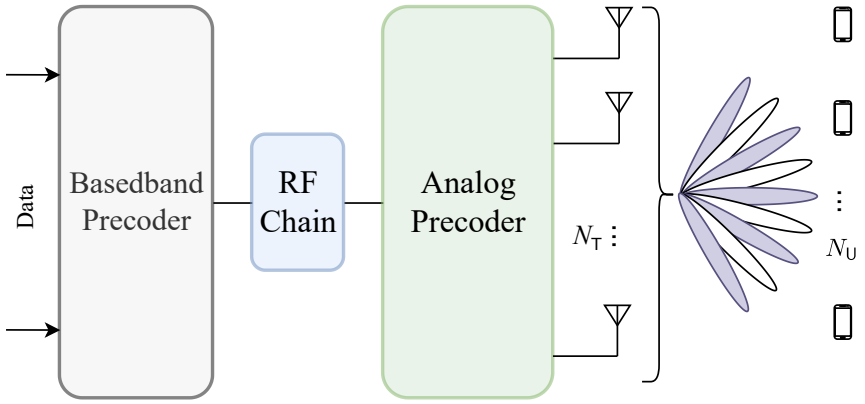

Figure 2.2: Massive MIMO analog beamforming architecture [53]

There are many studies in the context of analog-only beamforming, where the authors in [54] proposed employing beam selection from a codebook of analog beams for low-complexity analog beamforming successive interference cancellation (SIC)-based detection and compressive sensing (CS)-based channel estimation that is suitable for the BS that only has analog beamformers. While conventional studies have primarily emphasized joint BS and user equipment analog beamforming to enhance average signal-to-noise ratio (SNR) performance before baseband equalization, the authors in [53] take a different approach by focusing on optimizing the analog beamforming vectors to minimize the mean square error (MSE) of the baseband equalized signal. Such simple architecture makes analog-only beamforming particularly attractive due to its low computational complexity and hardware requirements.

However, analog-only beamforming, despite its simplicity, has some limitations that can affect its performance. One major drawback is its lack of adaptability to channel variations and interference conditions. Since the precoding weights are fixed and cannot be adjusted based on real-time channel information, the system's adaptability to changing environments

is limited. As a result, analog-only beamforming may not fully exploit the spatial diversity of the channel, leading to sub-optimal performance, especially in scenarios with severe interference or dynamic channel conditions. Moreover, analog beamforming typically provides limited spatial resolution, as it can only form a discrete set of fixed beams determined by the beamforming codebook. This limitation can lead to spatial focusing issues and reduced overall system performance, particularly in environments with dense user distributions and challenging propagation conditions.

2.2.3 Hybrid Beamforming

Hybrid beamforming offers a solution to address the challenges typically associated with FDP and analog-only beamforming. Hybrid beamforming combines the advantages of analog and digital precoding techniques and involves dividing the overall precoding task into two stages: analog precoding and digital precoding. In the analog precoding stage, a lower-dimensional precoding matrix is applied using analog components, such as phase-shifters (PSs). As shown in Figure 2.3, analog precoder (AP) reduces the number of RF chains, and therefore fewer DAC are required, which reduces implementation cost, energy consumption, and hardware requirements compared to FDP [55–58]. In the subsequent digital precoding stage, the precoding matrix is further refined using digital processing to achieve optimal SE beamforming performance. Additionally, digital precoder (DP) provides adaptability and fine-grained control over beamforming weights, enabling efficient interference management and optimization [59, 60].

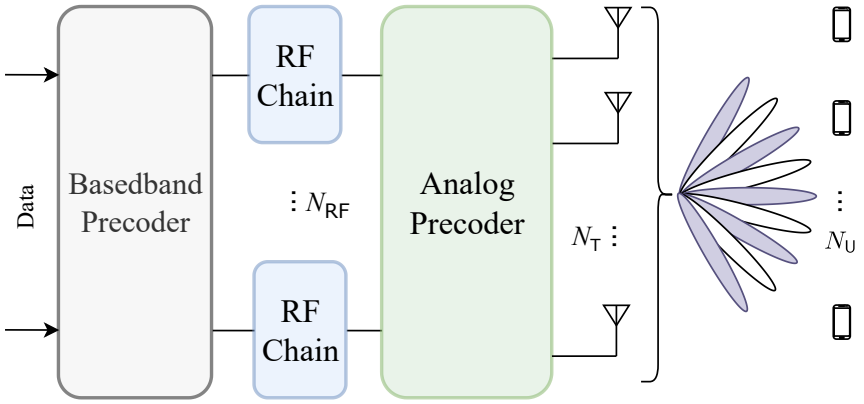

Figure 2.3: Massive MIMO hybrid beamforming architecture [55]

Hybrid beamforming presents several advantages over FDP, establishing it as a preferred choice for beamforming in mMIMO systems. Firstly, HBF strikes a balance between performance and complexity [61, 62]. With analog precoding, HBF reduces computational com-

plexity and the number of required DACs, making it feasible for real-time implementation. Secondly, HBF offers superior power efficiency compared to FDP, as it leverages analog precoding to decrease overall power consumption. This energy-saving feature is particularly crucial for mobile devices and IoT applications where extended battery life is essential. Additionally, HBF ensures improved scalability and cost-effectiveness. As the number of antennas increases in mMIMO systems, the hardware and computational demands of FDP become impractical [63]. Hybrid beamforming provides a scalable solution with analog precoding, facilitating efficient implementation in real-world scenarios. Moreover, the reduced hardware complexity of HBF leads to cost savings, making it a more economically viable option for large-scale deployments. Consequently, HBF offers a set of advantages over FDP and analog-only beamforming, including power efficiency, acceptable SE, scalability, and cost-effectiveness, making it highly favorable for beamforming in mMIMO systems [6].

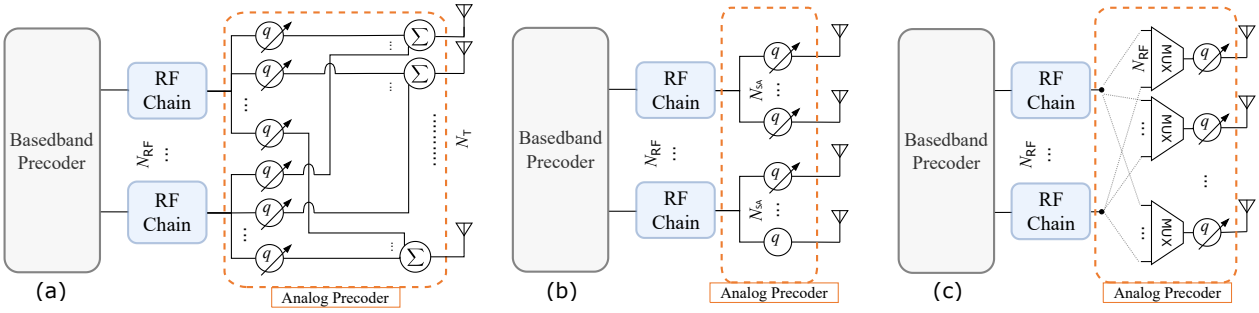

Figure 2.4: Different types of HBF architecture, a) Fully connected HBF [64], b) Fixed subarray HBF [64], c) Dynamic subarray HBF [65]

In general, there are different types of HBF configurations that can be employed based on the structure and connectivity of the antenna elements and the RF chains.

- Fully-connected HBF (FC-HBF): In FC-HBF, all antenna elements, both in the digital and analog domains, are fully connected to all RF chains through a PS and combiner as shown in Figure 2.4 (a). This means that each antenna element is connected to all digital and analog processing components. Fully connected HBF provides maximum flexibility in controlling the beamforming weights and enables adaptive beamforming optimization. However, it requires a large number of PSs and combiners, which can increase the complexity and cost of hardware [55, 58].

- Fixed subarray HBF (FSA-HBF): FSA-HBF divides the antenna array into multiple subarrays, each with its own analog and digital beamforming network as shown in Figure 2.4 (b). Each subarray operates independently with its own analog and digital

weights. This configuration reduces the number of required PS compared to a FC-HBF. However, it provides less flexibility in beamforming design, which degrades SE. The fixed subarray HBF strikes a balance between hardware complexity and SE by allowing beamforming optimization at the subarray level [64].

- Dynamic subarray HBF (DSA-HBF): DSA-HBF, also known as reconfigurable HBF, allows dynamic configuration and adaptation of analog beamforming weights. This means that analog weights can be adjusted or changed according to channel conditions, user requirements, or system constraints by switches or multiplexers as shown in Figure 2.4 (c). The dynamic subarray HBF provides flexibility in adapting to changing channel conditions and can enhance the system performance by optimizing the beamforming weights in real-time. However, DSA-HBF may introduce additional complexity in terms of control and signaling mechanisms [65].

Each type of HBF configuration offers unique advantages and considerations. The fully connected structure provides maximum flexibility but requires more hardware complexity. The fixed subarray structure strikes a balance between complexity and adaptability at the subarray level. Dynamic HBF improves the flexibility of the fixed subarray with the cost of deploying multiplexers. When choosing an HBF configuration, it is crucial to consider the specific requirements of the wireless communication system, such as the number of antennas, hardware constraints, channel conditions, and desired system performance.

Numerous studies have explored different HBF structures in mMIMO systems [58]. For the FC-HBF, the authors in [66, 67] explore the HBF architecture in large-scale MIMO systems, both at the transmitter and at the receiver. In their setup, a limited number of RF chains and finite-resolution PSs are considered. They proposed a fast heuristic algorithm for cases where the number of RF chains is either equal to or greater than the number of data streams. The results showed that this approach can improve the achievable SE. However, due to the non-convex nature of the optimization problem, the authors adopt the constant amplitude assumption on the digital beamformers and heuristically solve the analog beamforming problem with per-antenna power constraints, without conducting complexity analysis. In [68], the authors present a hybrid codebook and precoder designs considering limited feedback channels between the transmitter and the receiver. They proposed the use of the orthogonal matching pursuit (OMP) algorithm and the gradient search algorithm for the same HBF structure. The algorithms are designed to offer high-performance solutions and achieve optimization objectives. In [55], a straightforward precoding solution is proposed for a randomly selected single user in a FC-HBF system in mmWave cellular networks. The proposed solution assumes only partial channel knowledge at both the BS and user side,

represented in the form of AoA information. However, it should be noted that the proposed solution is limited to a single-cell and single-user scenario. In [69], the HBF structure is analyzed for MU-MIMO and single-user spatial multiplexing (SU-SM) with single-user analog beamforming (SU-BF) to compare coverage and rate performance. The study focused on mmWave cellular networks with perfect CSI at the transmitter and round-robin scheduling. The findings suggested that, in such scenarios, MU-MIMO using HBF is generally a more favorable option than SU-SM or SU-BF to achieve improved performance in terms of coverage and rate. A compressive sensing-assisted low-complexity optimal FDP acquisition algorithm and a beamspace hybrid precoding algorithm for a single-user mmWave MIMO system are proposed in [70]. The beamspace singular-value decomposition (SVD) algorithm is shown to reduce the complexity of hybrid precoding compared to an optimal FDP acquisition based on full-dimension SVD. Despite the significant complexity reduction, the true potential of discrete lens array beamspace remains untapped for multi-user communication systems.

In the context of subarray HBF (SA-HBF), in order to achieve diversity and multiplexing gains in mmWave systems, multiple antenna arrays are used for independent beamforming. The paper [71] introduced an HBF structure, where the transmitter and/or receiver antenna arrays are composed of multiple subarrays. Each subarray can independently perform electronic beam steering using RF phase shifters. In [72], a study presents an energy-efficient design of the hybrid precoder and combiner using a sub-array architecture. The optimization of APs and combiners is achieved through the alternating direction optimization method, allowing for easy adjustments of phase shifters with an analytical structure. Subsequently, the digital precoders and combiners are optimized to enhance the performance of MIMO communication systems. The presence of multiple RF chains within the configuration offers multiplexing capability and improves beamforming flexibility for the system [73]. The analysis of subarray architectures revealed that PS-based HBF yields better performance with narrow-band signals. On the other hand, tapping delay-based beam steering is more suitable for wideband signals but may encounter challenges related to hardware complexity. The work presented in [64] treats hybrid precoder design as a matrix factorization problem and introduces efficient alternating minimization algorithms for two HBF structures: FC-HBF and SA-HBF. The study reveals that the fully-connected structure, despite its higher complexity, may not achieve performance comparable to the fully digital precoder unless the number of RF chains slightly exceeds the number of data streams. By employing analog beamforming subarrays like phased arrays, the hybrid configuration efficiently gathers or disperses signal energy in sparse mmWave channels. In the next chapter, we adopt the method proposed in this paper as our baseline for comparison.

In the context of DSA-HBF, in [65], a dynamic subarray structure is introduced, which in-

telligently selects the subarray based on long-term channel statistics. The dynamic structure involves shifting the switching matrix towards the RF chains to enable optimal subarray selection along with phase shifters. To achieve this, a greedy algorithm with low complexity replaced exhaustive antenna partitioning, closely approaching the SE of the optimal exhaustive search solution. In [74], the author introduced a novel multi-user HBF framework designed specifically for the DSA-HBF. Unlike conventional schemes, their approach starts by selecting the multi-user set based on the analog effective channel at the BS. Then, the antenna partitioning algorithm allocates each antenna element to the RF chain based on maximizing the SINR increment. Recently, a novel energy-efficient dynamic subarray with fixed PSs architecture has been proposed for hybrid THz beamforming [75]. The proposed structure leverages fixed phase shifters but incorporates a switch network to enable dynamic connections, effectively compensating for the loss of SE caused by the fixed phase of PSs.

2.2.4 Coordinated Beamforming

Coordinated beamforming is a technique used with different beamforming schemes, including FDP, analog-only, and HBF, to improve the performance of wireless communication systems. It involves coordinating the beamforming weights across multiple BSs or AcP to jointly optimize the transmission of signals. Taking advantage of the spatial degrees of freedom offered by multiple antennas, coordinated beamforming aims to mitigate interference, improve signal quality, and enhance overall system capacity. Coordinated beamforming enables multiple BSs to work together as a virtual array, transmitting coordinated beams toward the intended users [76, 77]. By jointly optimizing the beamforming weights across the BSs, interference can be mitigated, and the desired signals can be enhanced. Coordinated beamforming can be implemented in various types of mMIMO systems as shown in Figure 2.5.

Coordinated beamforming in FDP allows efficient resource utilization, uniform SINR, and improved system performance, especially in scenarios with dense networks or high user densities [78]. Coordinated HBF combines the benefits of digital and analog beamforming techniques and coordinated beamforming. Coordinated beamforming in HBF involves optimizing the analog beamforming and digital precoding weights jointly on multiple AcPs. This coordination allows interference cancellation and enhanced signal quality, while still benefiting from the reduced hardware complexity of analog beamforming [79].

Coordinated beamforming has been applied in CF-mMIMO communication systems [10], where multiple distributed access points collaborate to serve users in a coordinated manner [80, 81]. In CF-mMIMO, as shown in Figure 2.6, the traditional concept of distinct cells is replaced by a distributed antenna system where all AcPs work together to serve users.

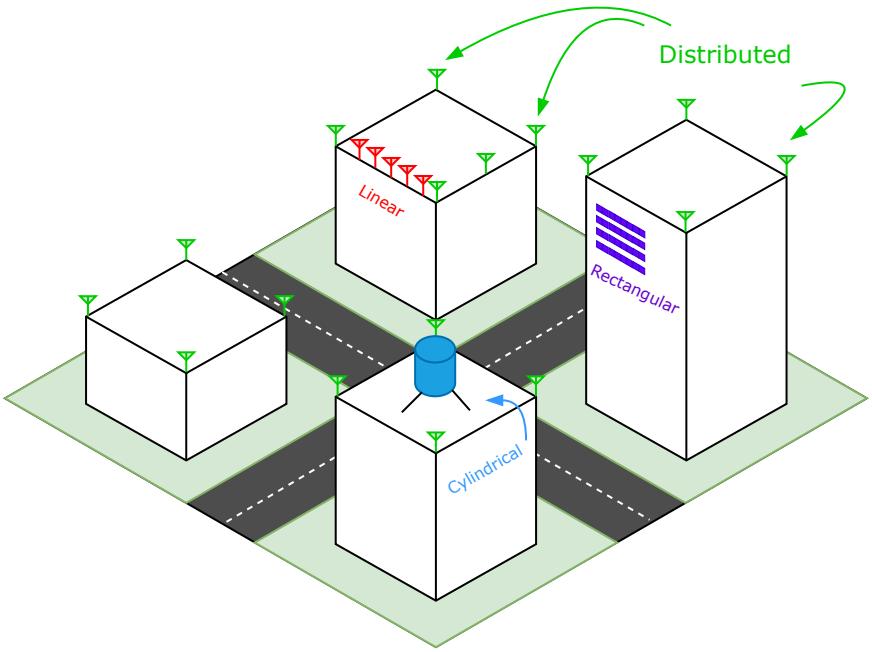

Figure 2.5: Different possible antenna configurations for a massive MIMO base station [14]

Coordinated beamforming in CF-mMIMO communication involves jointly optimizing the beamforming weights across the AcPs to maximize the quality of the signal received from the users while minimizing interference. This approach can effectively mitigate inter-cell interference and improve system capacity and coverage [82, 83]. In this thesis, we focus on CF-mMIMO systems, where multiple AcPs simultaneously serve multiple users.

There are many studies in the context of CF-mMIMO beamforming techniques. The widely used precoding technique in the literature is local conjugate beamforming (CB), primarily chosen for its low complexity and the convenience of providing closed-form expressions for downlink data rates [10]. On the contrary, a modified CB technique is introduced in [81] to enhance the channel hardening property of compact CF-mMIMO systems. The results showed that the modified CB precoding leads to a substantial improvement in achievable downlink data rates compared to conventional CB. Moreover, the achievable DL data rates using the modified CB precoding approach closely approach the data rates achieved under genie-aided system operation, where perfect channel estimates are available on the user side.

In recent studies, researchers have explored more sophisticated centralized and distributed precoding techniques to enhance the downlink performance of compact CF-mMIMO systems. However, applying centralized precoding methods requires having users' estimated channels at the NC. In [82], the authors utilized centralized ZF precoding, demonstrating that this technique significantly increases the achievable DL data rates in CF mMIMO systems. Fur-

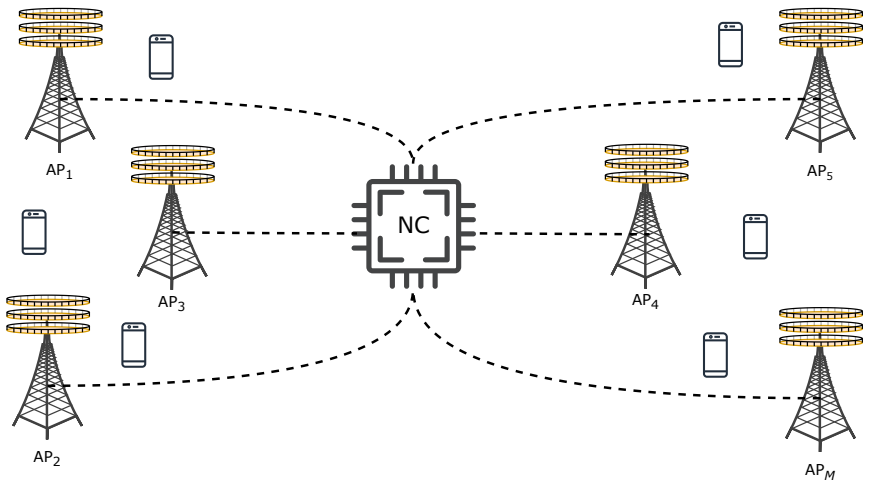

Figure 2.6: Cell-free massive MIMO system [10]

thermore, in [84], centralized MMSE precoding was employed, with DL-based precoding vectors generated based on downlink-uplink duality. They also proposed a centralized scalable partial-MMSE precoding approach, where each AcP serves a limited number of users, ensuring scalable CF-mMIMO operation.

In the context of centralized system operation, there is an increased burden on the fronthaul network as it needs to exchange users' estimated channels between AcPs and the central processing unit (CPU) or NC. To address this issue, various advanced local precoding techniques have been proposed for downlink transmission [85]. For example, the local full-pilot zero-forcing (FZF) precoding introduced in [85] has shown a significant impact on improving the achievable DL data rates. The key concept behind FZF precoding is to cancel out interference from copilot users. However, to apply this technique, a prerequisite is to have a larger number of antennas at the AcPs compared to the pilot sequence length. Therefore, its potential in enhancing DL data rates becomes less significant as the number of antennas at the AcPs decreases. To address this limitation, the authors in [85] proposed other local precoding techniques, namely, partial zero-forcing (PZF) and protective partial zero-forcing (PPZF), which can achieve high DL data rates even with a small number of antennas at the AcPs.

Both centralized and decentralized beamforming approaches have their merits and limitations in CF-mMIMO systems. Centralized beamforming offers superior performance by leveraging global information and employing sophisticated optimization algorithms. It ensures efficient resource allocation, interference mitigation, and capacity maximization. However, the heavy reliance on high-capacity fronthaul links for exchanging CSI introduces complexity, potential latency, and scalability challenges, especially as the system scales up to support a massive

number of AcPs and users. On the other hand, decentralized beamforming provides a more scalable and simple solution by reducing the fronthaul overhead. Local collaboration among neighboring AcPs enables independent beamforming decisions based on local CSI, making it less reliant on complex coordination. However, the lack of global information can lead to sub-optimal performance, especially in scenarios with dense AcP deployments, overlapping coverage areas, and significant interference.

2.3 Deep Learning-based Massive MIMO Beamforming

Recently, DL has drawn significant attention as a promising solution to tackle challenges in different beamforming schemes for mMIMO systems. Thanks to DL's excellent classification and regression capabilities, DL offers innovative approaches to optimize beamforming strategies and enhance the performance of these schemes. Although the training process can be time-consuming, the training is done in "off-line" mode. Therefore, DL techniques are a promising approach to reducing latency in cellular networks while improving the SE. Studies in this domain can be broadly categorized based on their beamforming scheme and the learning approach [86].

2.3.1 Different Beamforming Scheme with Deep Learning

Deep learning techniques offer a flexible and powerful framework for optimizing beamforming solutions across various scenarios. These schemes encompass classical methodologies such as FDP, which aims to achieve interference-free communication in mMIMO systems. DNNs can be trained to learn the optimal antenna weights that minimize interference and improve signal quality, improving the efficiency of FDP for complex real-world environments. Moreover, the application of DNNs in analog-only beamforming holds substantial potential. Analog-only beamforming, which operates exclusively at the analog level, can benefit from the ability of DNNs to optimize the phase shifts of the analog beamforming components. This enables faster adaptation to channel conditions and enhances signal reception, introducing a novel and efficient approach to enhancing analog beamforming's capabilities. Furthermore, the integration of DNNs with hybrid beamforming, such as HBF, can further amplify the capabilities of such architectures. DNNs can be harnessed to devise adaptive strategies for selecting analog and digital beamforming vectors, maximizing the benefits of both hybrid architectures and deep learning capabilities. The neural network's capacity to autonomously adjust beamforming strategies across various beamforming schemes opens new frontiers in the realm of mMIMO optimization.

Additionally, the application of DNNs in coordinated beamforming can significantly improve the collaboration among multiple BSs, mitigating interference, and enhancing overall system performance. This category of research is marked by the ability of DNNs to autonomously learn and adapt beamforming strategies to different schemes, thereby unlocking novel techniques and improved performance in mMIMO systems. The capacity of DNNs to adjust and gain knowledge from data allows for the investigation of a broad range of beamforming strategies, resulting in the discovery of new methods and improved performance in mMIMO systems.

DL-based fully digital precoder

In the context of FDP, DL-based approaches have garnered considerable attention. These techniques focus on efficiently optimizing the beamforming vectors while taking into account various constraints, such as hardware complexity and power limitations. The authors of [87], address the challenge of optimizing the ergodic sum rate in mMIMO systems by proposing a novel approach. Instead of relying on complex iterative algorithms, they leveraged a neural network to learn low-dimensional parameters characterizing the structure of the precoding vectors directly from the available CSI. In [88], the authors introduced a learning-to-compute strategy to address the challenge of reducing the computational burden associated with finding the ergodic sum rate. Their approach directly computes the complex ergodic rate function from channel covariance matrices using a DNN. By leveraging this innovative technique, they streamline the process and achieve more efficient and accurate computations of the ergodic sum rate. Using an upper limit of the ergodic rate, the authors of [89] exploited the associated Lagrangian formulation to identify key structural features of the optimal precoder. To efficiently determine Lagrange multipliers, they designed a comprehensive framework, leveraging a well-designed neural network that learns directly from CSI.

The authors in [90], introduced a robust training algorithm utilizing a DNN. The DNN is specifically designed to work with imperfect estimates and statistical information of the perfect CSI, enabling it to adapt to real-world propagation environments. In [91], the authors proposed a DL framework for optimizing downlink beamforming in multi-user MISO systems. By leveraging CNNs and expert knowledge, they constructed three beamforming neural networks (BNNs) for different optimization problems. The BNNs achieve near-optimal solutions with significantly reduced computational complexity, enabling fast realization of optimal SE beamforming in real-time scenarios. The study in [92] proposed a deep-unfolding framework called iterative algorithm induced deep-unfolding neural network (IAIDNN) to efficiently solve the sum-rate maximization problem in MU-MIMO systems. By unfolding

the iterative WMMSE algorithm, IAIDNN reduces computational complexity while achieving performance comparable to the original algorithm. The authors in [93], proposed a fast beamforming design for downlink MIMO systems. It maximizes the weighted sum rate under a total power constraint, achieving performance similar to the WMMSE algorithm with significantly reduced computational complexity. Meanwhile, in [94], the authors focused on downlink multi-user multi-antenna systems, leveraging DL techniques to optimize beamforming vectors under varying transmit power limitations at the BS. However, it is important to note that DL-based FDP approaches predominantly depend on fully digital processing, wherein each antenna element is equipped with individual DAC and ADC components. Consequently, DL models are directly optimized for the digital beamforming weights associated with each antenna element. Moreover, it is worth mentioning that the methodologies proposed in these studies cannot be easily extended to address the challenges specific to analog-only beamforming or HBF techniques.

DL-based analog-only beamforming

DL-based analog-only beamforming has emerged as a promising approach to enhance beam selection efficiency in wireless communication scenarios of multiple users. By leveraging deep learning techniques, analog beam selection solutions can be optimized and adapted dynamically to varying channel conditions, thereby overcoming the limitations of traditional methods. There are some studies for DL-based analog-only beam selection. The wide beam sweeping process is conducted in [95] using a reduced number of beams and antennas. The DNN leverages the received signals from this process to select an appropriate beam from the original set of beam candidates. In [96], the authors proposed a deep learning-based low overhead analog beam selection scheme, leveraging super-resolution technology. Specifically, DNNs are utilized to estimate beam quality based on partial beam measurements, enabling efficient and rapid beam alignment. The authors in [97], proposed a CNN-based beam selection to intelligently perform the beam selection between the transmitter-receiver pair. Drawing on the principles of ML, the authors' proposal in [98] centered around a data-driven approach for analog beam selection. Its objective is to achieve a near-optimal SE rate while keeping the complexity low. However, because of the lack of flexibility, the SE of analog-only beamforming is limited. Furthermore, the contributions of these methods are limited to analog-only beamforming.

DL-based hybrid beamforming

Deep learning-based HBFs have played a critical role in optimizing the hybrid precoding matrices. By harnessing the capabilities of DL, HBF systems can dynamically adapt to varying channel conditions and overcome the limitations of traditional methods, such as computational complexity. This adaptability allows the system to achieve optimal SE performance under different scenarios, further improving the overall efficiency and reliability of the communication system. There are numerous studies on applied DL in different HBF structures. The authors in [99], investigated multi-user multiple-antenna downlink systems. They proposed a joint antenna selection and precoding design algorithm to maximize the system sum rate subject to the power and QoS constraints. Authors in [98], proposed a data-driven approach for analog beam selection in HBF systems to optimize the uplink sum rate with reduced complexity. Using machine learning techniques and a large dataset of millimeter-wave channel samples, the method treats beam selection as a multiclass-classification problem, deriving a statistical classification model with the support vector machine algorithm. Real-time transmissions can efficiently select optimal analog beams for each user with low complexity.

In [100], a pioneering method for the AoA estimation called super-resolution, based on DL, is introduced. This method leverages a carefully designed DNN to achieve accurate results. The DNN is utilized for both offline learning and online deployment processes. When this learning mechanism is employed, the system can efficiently grasp the characteristics and spatial structures of the wireless channel. The authors in [101] developed a novel integrated ML and coordinated beamforming solution. The authors in [102] proposed an adaptive cross-entropy (ACE)-based HBF scheme. It aims to adaptively update the probability distributions of the elements in the HBF by minimizing the cross-entropy, which can generate a solution close to the optimal one with a sufficiently high probability. A novel approach utilizing a neural network to select a subset of antennas has been introduced in [103], where the primary objective is to maximize the minimum SNR ratio at the receivers. The approach involves training a neural network using extensive simulated data, where the network learns a mapping function. This function relates channel realizations to optimal antenna selection solutions. Other approaches have been proposed for the HBF design in [104], where the authors assumed that the CSI is perfectly known and tried to map the CSI to the corresponding HBF solutions.

The author in [105], proposed a CNN to design the HBF. The proposed CNN accepts the input of the channel matrix and gives the output of the analog and baseband beamformers. In [106], authors proposed an efficient beamforming design method based on DL, eliminating the need for complex operations and iterations. Initially, they established a heuristic solution structure for downlink beamforming by leveraging the virtual equivalent uplink channel

and an optimum MMSE receiver. This structure divides the problem into power allocation and virtual uplink beamforming (VUB) design. Another CNN approach has been proposed in [107], where they assume an imperfect channel matrix as input and produce the AP and the combiners as output. The solution consists of two main stages. Firstly, they devised an exhaustive search algorithm that selects the analog precoder and combiners from a predefined codebook to maximize the achievable SE. Subsequently, these selected precoders and combiners serve as output labels during the training phase of CNN-MIMO, where the input-output pairs are obtained. In [108], the authors present a formulation where antenna selection and HBF design are treated as a classification/prediction problem for CNNs. In their approach, the CNN takes the channel matrix as input and generates a subarray that maximizes SE for antenna selection.

A for subarray HBF has been proposed in [109], where the authors investigated a CNN-based SA-HBF. They also proposed a constraint-relaxation alternating minimization (CR Alt-Min) algorithm to create the target for training the CNN. By leveraging the ResNet architecture for feature extraction from channel matrices, the authors of [110] introduce two distinct neural networks: the antenna selection network (ASNet) and the hybrid beamforming network (BFNet). ASNet focuses on dynamic antenna selection, while BFNet is dedicated to HBF design. Taking advantage of the property that a complex matrix can be expressed as a scaled sum of two matrices with unit-modulus entries, the authors in [111] introduced a novel analog deep neural network (ADNN) structure. This structure is designed to be compatible with commonly used RF components, allowing for practical implementation. Building upon this ADNN structure, they further integrate it into an extended hybrid analog-digital deep neural network (HDNN) architecture. The authors in [112] proposed a deep unfolding framework that decomposes the optimal FDP into analog and digital components, resulting in two equivalent least squares (LS) problems. They solved for the DP using a closed-form LS solution, while the AP is obtained through ManNet. Furthermore, they demonstrate that ManNet can also be applied to SC-HBF designs by establishing the connections between the radio frequency chain and antennas.

DL-based cell-free beamforming

DL-based CF-mMIMO beamforming is an emerging research area focusing on utilizing deep learning techniques to optimize beamforming strategies for CF-mMIMO systems. Conventional CF-mMIMO beamforming methods often rely on iterative algorithms and exhaustive searches, leading to high computational complexity and unsuitability for real-time implementation in dynamic wireless networks. Moreover, both centralized and decentralized beam-

forming approaches in CF-mMIMO face their respective challenges, such as sub-optimal performance and significant signaling overhead.

The adoption of deep learning in CF-mMIMO beamforming offers promising solutions to overcome these challenges. By leveraging DNNs, DL-based beamforming strategies can efficiently learn from large datasets and approximate the optimal mapping between input data and beamforming solutions. This capability enables more accurate and efficient beamforming, contributing to improved system performance and reduced computational complexity. There are some studies in this regard, where the authors of [113] proposed a DNN for beamforming optimization in TDD-based sub-6GHz networks. The DNN combines low time complexity with near-optimal results, achieving accurate beamforming solutions. It takes long-term fading information as input and provides power allocation for each antenna element to each user as output. The authors of [114], proposed a DNN to optimize user power allocations for maximizing the minimum user rate. Their approach does not require known optimal power allocations during model training, making it simpler and more flexible. The scheme proposed in [115], called distributed learning for uplink cell-free massive MIMO Beamforming (DLCB), reduces communication burden in the fronthaul by applying receive beamforming to compress vector signals into scalar ones before centralized processing. It achieves multi-AcP cooperation without explicit estimation of their CSI, using a distributed learning approach inspired by the back-propagation algorithm. In [116], the authors investigate the uplink beamforming design for maximizing long-term EE in a cell-free network. The SINR expression is derived based on the minimum mean square error of the channel estimation and successive interference cancellation. The long-term EE is formulated as a function of the beamforming matrix. In [117], a feedforward neural network has been proposed for centralized power allocation in the downlink of cell-free wireless systems with conjugate beamforming. The method relies on large-scale channel gains and avoids the need for pre-computation of training data.

2.3.2 Different Learning Approaches for Massive MIMO Beamforming Design

This section delves into exploring various learning methods used to optimize beamforming strategies in wireless communication systems. Three primary learning approaches are considered: supervised learning, unsupervised learning, and reinforcement learning. These approaches enable DNNs to adapt and improve beamforming techniques based on different types of data and interactions with the environment. By understanding and comparing these learning methods, we gain valuable insights into their potential applications and contributions to enhancing beamforming performance in modern wireless networks. The following sequential subsections review studies related to each of these learning approaches for DL-based

beamforming design, exploring their advantages, challenges, and applications in different wireless communication scenarios.

Supervised learning approaches

Supervised learning involves training a DNN using labeled data, where the correct output (target) is known for each input sample. In the context of beamforming, the DNN learns to map the given input data, such as channel information and system parameters, to the desired beamforming solution [89–91, 95–97]. The advantage of supervised learning lies in its ability to achieve accurate and deterministic results. By learning from a large dataset with known optimal SE beamforming solutions, the DNN can approximate the optimal mapping, leading to high-performance beamforming strategies [100–105]. Moreover, supervised learning-based beamforming can be applied to a wide range of communication scenarios, including FDP, HBF, and CF-mMIMO. The versatility of this approach makes it suitable for different network architectures and configurations, enabling seamless deployment across various wireless systems [107–109, 111].

However, supervised learning does have limitations. The maximum performance gain achieved by supervised learning is often limited by the quality and completeness of the labeled data. Although supervised methods can provide near-optimal beamforming solutions based on the available labels, they may not be able to surpass these near-optimal values without additional information or data. The reliance on labeled data can also pose challenges in real-world implementations, as obtaining a sufficiently large and diverse dataset with accurate labels may be resource-intensive and impractical in certain scenarios. Furthermore, supervised learning is susceptible to overfitting, where the DNN memorizes the training data instead of learning the underlying patterns. This can lead to poor generalization of unseen data, making the supervised method less robust and reliable in dynamic and changing wireless environments. As a result, the performance of supervised learning-based beamforming may degrade in scenarios where the channel conditions and system parameters vary significantly.

Unsupervised learning approaches

Unsupervised learning, on the other hand, deals with unlabeled data, where DNN must identify hidden patterns or structures in input data without explicit guidance. In beamforming, unsupervised learning can reveal inherent patterns in channel conditions and user distributions, enabling the DNN to design efficient beamforming solutions without prior knowledge of optimal outcomes [106, 114]. The strength of unsupervised learning lies in its ability to discover latent features and adapt to diverse and dynamic channel conditions. Moreover,

unsupervised learning approaches can provide a better generalization to unseen scenarios and adapt to changing channel conditions. By learning from the inherent structure of the data without the constraints of predefined labels, these methods can achieve more robust and scalable beamforming solutions, crucial for dynamic and time-varying wireless environments.

However, unsupervised learning in beamforming also presents its own set of challenges. Lack of explicit supervision means that the network may converge to local optima or struggle to reach true optimal solutions for specific objectives. The training process can be more sensitive to hyper-parameter settings and initialization, requiring careful tuning to achieve desirable performance. Furthermore, unsupervised learning methods might require a larger amount of training data to effectively learn complex beamforming patterns. Obtaining sufficient data for training might be challenging in certain scenarios, especially when considering dynamic and rare channel conditions.

Moreover, in supervised learning, the loss functions are typically well-defined and conventional, commonly used to measure the discrepancy between the predicted output and the true target labels. However, in unsupervised learning, the absence of labeled data requires a more tailored approach to designing loss functions [7]. Since unsupervised learning aims to uncover the underlying patterns and structures within the data without explicit guidance, the loss function needs to be customized according to the specific problem at hand. Designing an effective unsupervised loss function is crucial to ensure that the learning process captures meaningful representations and effectively optimizes the desired objectives. This customization of loss functions in unsupervised learning allows for more flexibility and adaptability to the complexities of the data, enabling the neural network to learn without relying on ground-truth labels, and ultimately leading to improved performance in various tasks.

Deep reinforcement learning approaches

Deep reinforcement learning (DRL) is a unique approach in which the DNN learns by interacting with the environment and receiving feedback in the form of rewards or penalties based on its actions. In the context of beamforming, the DNN dynamically adjusts its beamforming strategy based on feedback from the channel performance, aiming to maximize long-term cumulative rewards, such as system throughput or energy efficiency. Deep reinforcement learning can handle uncertainties and non-stationary environments, making it suitable for adaptive beamforming in dynamic wireless scenarios. For beamforming, DRL algorithms aim to maximize long-term rewards, such as system throughput or SINR, by dynamically adapting beamforming strategies to changing channel conditions [118]. Reinforcement learning offers the advantage of adaptability and scalability, allowing beamformers to optimize per-

formance in complex and dynamic wireless environments without relying on extensive prior knowledge. It can handle continuous action spaces, making it suitable for optimizing HBF with a mix of analog and digital components [119–121].

One popular DRL algorithm for continuous action spaces is the deep deterministic policy gradient (DDPG) algorithm [122]. DDPG extends traditional DRL methods to handle continuous actions, making it suitable for beamforming and HBF with continuous beamforming vectors. However, DDPG has challenges related to hyper-parameter tuning and exploration-exploitation trade-offs. Finding appropriate hyper-parameters can be time-consuming and may affect the stability and convergence of the learning process. Moreover, exploring the action space effectively to discover optimal beamforming strategies while avoiding sub-optimal choices is a challenge, particularly in large and complex environments [123].

Despite the advantages, DRL for beamforming also faces challenges. One major challenge is the high computational complexity and time-consuming nature of DRL algorithms. Training DRL agents requires numerous interactions with the environment, which can be resource-intensive, especially for large-scale systems [124]. Furthermore, DRL algorithms typically require a large number of training episodes to achieve good performance, which may not be practical in real-time wireless networks with limited training data availability. In some cases, training a DRL-based beamforming model might require more computation and time compared to supervised or unsupervised learning [125, 126].

In conclusion, the literature underscores that DL-based HBF approaches, regardless of the chosen learning paradigm, grapple with challenges when operating under the assumption of perfect CSI. These challenges arise from various aspects of the learning process. Acquiring impeccable CSI in real-world scenarios presents a formidable challenge due to multiple factors such as channel estimation inaccuracies, aging effects, and delays in feedback. These deviations from perfect CSI can lead to performance degradation and sub-optimal beamforming outcomes. Since DL-based techniques can be based on accurate training data, the use of imperfect CSI in the training process can introduce biases and inaccuracies that undermine the overall efficacy of the learning process. This can subsequently result in sub-optimal beamforming solutions and a decline in system performance. Furthermore, the reliance on perfect CSI assumes a level of accuracy that might not be sustainable in dynamic real-world scenarios. As channel conditions evolve over time, the efficacy of DL-based models might diminish, necessitating frequent model updates to sustain optimal performance. This continual adaptation incurs computational costs and demands timely access to fresh data, which may not always be readily available. Thus, the challenges stemming from the assumption of perfect CSI reverberate across the various learning paradigms used in DL-based HBF, prompting a

need for innovative solutions that can operate effectively in the face of imperfect CSI.

2.4 Summary

Massive MIMO is a promising technology that utilizes a large number of antennas to improve the performance of wireless communication systems. It offers significant gains in SE, capacity, and interference mitigation. The concept of mMIMO has found relevance in various applications, including millimeter-wave communications and IoT networks. Beamforming plays a vital role in realizing the benefits of mMIMO by optimizing signal transmission and reception. It involves adjusting the phase and amplitude of the signals at each antenna to create constructive interference toward the desired users and suppress interference toward other users or unwanted directions.

The beamforming techniques in mMIMO can be categorized into FDP and HBF. FDP operates entirely in the digital domain, allowing for flexible beamforming weight adjustment, but at the expense of increased complexity and hardware requirements. HBF combines analog and digital precoding stages, providing a trade-off between complexity and performance. Coordinated beamforming further enhances performance by coordinating beamforming weights across multiple BSs or access points.

Artificial intelligence and ML, particularly deep learning, have emerged as valuable tools in wireless communication. Deep learning techniques leverage neural networks with multiple layers to extract complex patterns and relationships from wireless data. When applied to beamforming, deep learning can optimize beamforming parameters and improve performance. However, supervised learning-based HBF approaches face challenges due to imperfect channel state information and the need for a significant amount of labeled training data. These challenges can lead to sub-optimal beamforming solutions and pose practical constraints on deployment and scalability.

Overall, deep learning-based beamforming holds promise for improving wireless communication systems, but addressing challenges related to imperfect CSI and obtaining a large dataset with accurately labeled for supervised learning is essential for achieving practical solutions.

CHAPTER 3 ARTICLE 1: UNSUPERVISED DEEP LEARNING FOR MASSIVE MIMO HYBRID BEAMFORMING

This chapter is a reproduction of an article published in IEEE Transactions on Wireless Communications on 24 May 2021.

- H. Hojatian, J. Nadal, J. -F. Frigon and F. Leduc-Primeau, "Unsupervised Deep Learning for Massive MIMO Hybrid Beamforming," in IEEE Transactions on Wireless Communications, vol. 20, no. 11, pp. 7086-7099, 24 May 2021.

Revised edition: Equation (3.1) and (3.2) should be revised to $r_u^{(k)} = \mathbf{h}_u^{(k)\mathrm{H}} \mathbf{A}_{\mathsf{SS}}^{(k)} s^{(k)} + \eta_u^{(k)}$ and $\alpha_u^{(k)} = |\mathbf{h}_u^{(k)\mathrm{H}} \mathbf{A}_{\mathsf{SS}}^{(k)} s^{(k)}|^2 + \sigma^2$.

3.1 Abstract

Hybrid beamforming is a promising technique to reduce the complexity and cost of mMIMO systems while providing a high data rate. However, the hybrid precoder design is a challenging task requiring CSI feedback and solving a complex optimization problem. This paper proposes a novel RSSI-based unsupervised deep learning method to design hybrid beamforming in mMIMO systems. Furthermore, we propose i) a method to design the SS in IA; and ii) a method to design the codebook for the analog precoder. We also evaluate the system performance through a realistic channel model in various scenarios. We show that the proposed method not only greatly increases the spectral efficiency especially in FDD communication by using partial CSI feedback, but also has near-optimal SE and outperforms other state-of-the-art full-CSI solutions.

3.2 Introduction

New applications such as IoT and vehicular communications continuously increase the demands for higher data rates. To face this challenge, mMIMO has become an essential factor in the design of future cellular systems [16]. In mMIMO, the number of antennas in the BS scales up to serve several users and it was shown in [3] that the effects of fast fading and interference vanish when increasing the number of antenna in the BS. Higher multiplexing and diversity gain are thus obtained with mMIMO, which in turn results in higher SE and greater EE.

On the other hand, each antenna in a mMIMO array requires a RF chain. Therefore, the power consumed by RF elements such as power amplifiers renders mMIMO systems expensive and energy inefficient. To address this power consumption issue, reduce the cost-power hardware overhead, and yet provide reasonable performance, the HBF technique was introduced [6]. It consists of using a small number of analog beamformers deployed to drive multiple antennas to form a beam, each connected through a single RF chain to a digital precoder. This hybrid combination of phase-based analog and baseband digital beamformers reduces the number of transmission chains while keeping the SE to an acceptable level [66, 127]. In fact, hybrid beamforming techniques have been considered for fifth-generation cellular network technology (5G) in the mmWave bands [59,128] and recently in reconfigurable intelligent surfaces (RIS) systems [129, 130]. However, an explicit estimate of the mmWave channel is generally needed to design the hybrid beamforming matrices at the transmitter. Although several channel estimation techniques for hybrid beamforming have been proposed in the last few years [63, 131, 132], mMIMO channel estimation remains a complicated task due to the hybrid structure of the precoding and the imperfections of the RF chain. Among prior research, the authors in [67] designed hybrid beamforming by considering orthogonal frequency division multiplexing (OFDM)-based frequency-selective structures. The wideband mmWave mMIMO system was investigated in [133] to design the hybrid beamforming. In [134], the authors designed an analog beamformer based on the second-order spatial channel covariance matrix of a wideband channel. Authors in [135] assumed to have perfect knowledge of the CSI and proposed a low-complexity hybrid beamforming. All of the aforementioned methods strongly depend on full knowledge of the CSI or channel estimation by using pilots, which increases the signaling overhead and, therefore, reduces the spectral and energy efficiency of the system, especially in FDD communication where CSI acquisition and feedback is a challenging task [45]. Therefore, in this paper, we propose a system that, instead of considering the full knowledge of CSI or channel reciprocity, uses the quantized RSSI to design the hybrid beamforming precoders. Unlike CSI, RSSI is a single real value which users readily measure from the received signal. By consequence, no explicit CSI feedback is required, which reduces the signaling overhead and increases the spectral efficiency of the system.

Meanwhile, DL techniques have recently been applied widely to telecommunication systems [136] and it was demonstrated to be an outstanding tool for dealing with complex non-convex optimization problems, thanks to its excellent classification and regression capabilities. Although the training process can be time-consuming, the training is done in "off-line" mode. Therefore, DL techniques are a promising approach to reduce the latency in cellular networks. Several works have investigated the use of DNN to deal with difficult problems within the physical layer [137], including channel coding, channel estimation [40],

detection [138] and, beamforming [91,104,108,139]. In particular, the authors of [91] considered a multi-input single-output system and solved three optimization problems. By using DNN with fully-connected layer (FL) and decomposition of the channel matrix in [104], the near-optimal analog and digital precoders have been designed. In [104, 139], the authors propose a deep supervised learning-based method to estimate the hybrid beamforming by knowing the full CSI. The authors in [108] deployed a CNN to design the hybrid beamforming, by knowing the CSI. In all the mentioned literature, perfect knowledge of CSI is assumed to be available at the BS, and the DNNs are trained using supervised learning. However, supervised learning requires the optimum targets to be known, and thus requires significant additional computing resources to find these targets using conventional optimization methods. In addition, in practical situations, the knowledge of the optimum hybrid beamforming structure is hard to obtain.

Therefore, we build on the supervised deep learning system considered in [140] to introduce in this work a novel low-complexity approach with RSSI-based unsupervised learning to design the HBF in mMIMO system. To the best of the authors' knowledge, it is the first time that an unsupervised DL system has been proposed for designing hybrid beamforming precoders in the context of mMIMO systems. This approach greatly reduces the system complexity and makes it more amenable for deployment of future networks. Furthermore, we train the DNN specifically for the area where the BS is located, so that the geometrical structure of the channel model can be learned upon deployment. In this paper, this is done using a ray-tracing model [141]. The same approach could also be used to train the DNN using direct measurements of the environment. The proposed DNN architecture is a multi-tasking CNN that generates both the analog and digital parts of the hybrid beamforming, enabling to reduce the computational complexity. Furthermore, a novel loss function based on SE is proposed to train the multi-tasking DNN where the DNN is trained to jointly do classification and regression tasks. To train the model, we introduce methods to generate datasets and codebooks based on the deepMIMO channel model [141]. Particularly, in the proposed three-phase beam training method, the synchronization signals transmitted by the BS are optimized in such a way that the RSSI measurements carry the maximum information about the CSI. Three different channel models have been examined to validate the reliability and robustness of the proposed method in different scenarios. These three scenarios have been chosen to cover different environments, received signal strengths, and cell coverage. Moreover, we study the effect of RSSI quantization on the DNN's performance. The simulation results show that the SE performance of the proposed RSSI-based model outperforms other state-of-the-art full-CSI methods while the spectral efficiency, signaling overhead, training time, computational complexity, and flexibility of the system are significantly improved. In summary, the main

contributions of the paper are as follows:

- The design and evaluation of two unsupervised deep learning methods to train a multi-tasking DNN and directly design the hybrid beamforming using only quantized RSSI instead of perfect complete CSI, each achieving a different performance-complexity trade-off;
- A method to design the codebook for the phase-based AP which reduces the complexity of the DNN while providing near-optimal SE performance; and
- A method to design synchronization burst sequences in a three-phase beam training procedure for initial access maximizing the channel information carried by the RSSI.

The paper also includes the following complementary contributions:

- The description of a novel non-DL algorithm called hybrid structured heuristic optimization (HSHO) to design fully digital precoders and hybrid beamforming;
- A procedure to generate the DNN dataset for unsupervised learning; and
- The evaluation of non-DL and DL hybrid beamforming methods in a ray-tracing realistic channel model.

The rest of the paper is organized as follows. Section 3.3 describes the system model, including beam training during IA, RSSI measurement, and quantization. In Section 3.4, the channel model and dataset generation for DNN training are presented, followed by the near-optimal HBF solutions for mMIMO. The proposed method for SS planning in IA and codebook design for the analog precoder are described in Section 3.5. In Section 3.6, the DNN architecture and the unsupervised learning method are presented. Finally, in Section 3.7 the performance of the proposed HBF methods is evaluated and its complexity is compared with existing methods, and conclusions are drawn in Section 3.8.

Notation: Matrices, vectors, and scalar quantities are denoted by boldface uppercase, boldface lowercase, and normal letters, respectively. The notations $(.)^{\mathrm{H}}$, $(.)^{\mathrm{T}}$, $(.)^{\dagger}$, $|.|$, $\|.\|$, $(.)^{-1}$, $\Re[.]$ and $\Im[.]$ denote Hermitian transpose, transpose, Moore-Penrose pseudo-inverse, absolute value, ℓ^2-norm, matrix inverse, real part, and imaginary part, respectively.

3.3 System Model

The considered system model consists of a mMIMO BS in a single-cell system equipped with N_{T} antennas and N_{RF} RF chains serving N_{U} single-antenna users, where we assume

$N_{\mathsf{RF}} \ll N_{\mathsf{T}}$, as shown in Fig. 3.1. For both uplink and downlink transmission, HBF precoders are employed by the BS. We consider a fully connected architecture where each RF chain is coupled through 2-bit phase shifters to all antennas at the BS. First, to obtain the RSSI in initial access, a 3-step scenario similar to the ones described in [140] and [142] is investigated in the following sub-sections:

3.3.1 Step 1: SS Bursts Transmission

In the first step shown on the right side of Fig. 3.1, the BS transmits K, SS bursts, where each burst k uses different 2-bit phase-shift analog precoders $\mathbf{A}_{\mathsf{SS}}^{(k)} \in \{1, -1, i, -i\}^{N_{\mathsf{T}} \times 1}$. The SS $\mathbf{A}_{\mathsf{SS}}^{(k)} s^{(k)}$ are received by all users in the cell. By consequence, the received signal $r_u^{(k)}$ at the u^{th} user for the k^{th} burst can be written as

$$r_u^{(k)} = \mathbf{h}_u^{(k)\mathrm{H}} \mathbf{A}_{\mathsf{SS}}^{(k)} + \eta_u^{(k)}, \tag{3.1}$$

where $\mathbf{h}_u^{(k)} \in \mathbb{C}^{N_{\mathsf{T}} \times 1}$ stands for the channel vector from the N_{T} antennas at the BS to user u and $\eta_u^{(k)}$ is the additive white Gaussian noise (AWGN) term.

3.3.2 Step 2: RSSI Feedback

After receiving $r_u^{(k)}$, the averaged RSSI value $\alpha_u^{(k)}$ are measured by the u^{th} user for the k^{th} SS burst, which constitutes the second step. Therefore, we have

$$\alpha_u^{(k)} = |\mathbf{h}_u^{(k)\mathrm{H}} \mathbf{A}_{\mathsf{SS}}^{(k)}|^2 + \sigma^2, \tag{3.2}$$

where σ^2 is the noise power. All RSSI values of each user are then transmitted to the BS through a dedicated error-free feedback channel. These two first steps correspond to the establishment of the IA between the BS and the users.

In practical systems, due to the limited precision of the measurements and limitation in the feedback channel, the RSSIs must be quantized. Let us denote by $\boldsymbol{\alpha}_u = [\alpha_u^{(1)}, ..., \alpha_u^{(K)}]^{\mathrm{T}}/\beta$ the vector of all RSSI values obtained by the u^{th} user, re-scaled by a factor β to ensure that $\alpha_u^{(k)}/\beta \in [0, 1] \, \forall k$. Then, we define $\tilde{\boldsymbol{\alpha}}_u$ as the quantized RSSI vector of user u transmitted to the BS. Several quantization methods can be employed. We use linear quantization, given by

$$\tilde{\boldsymbol{\alpha}}_u = \frac{\lfloor \boldsymbol{\alpha}_u (2^{N_b} - 1) \rceil}{(2^{N_b} - 1)}, \tag{3.3}$$

where $\lfloor . \rceil$ is the round operator and N_b is the number of quantization bits. We study the effect of quantization on performance in Section 3.7.

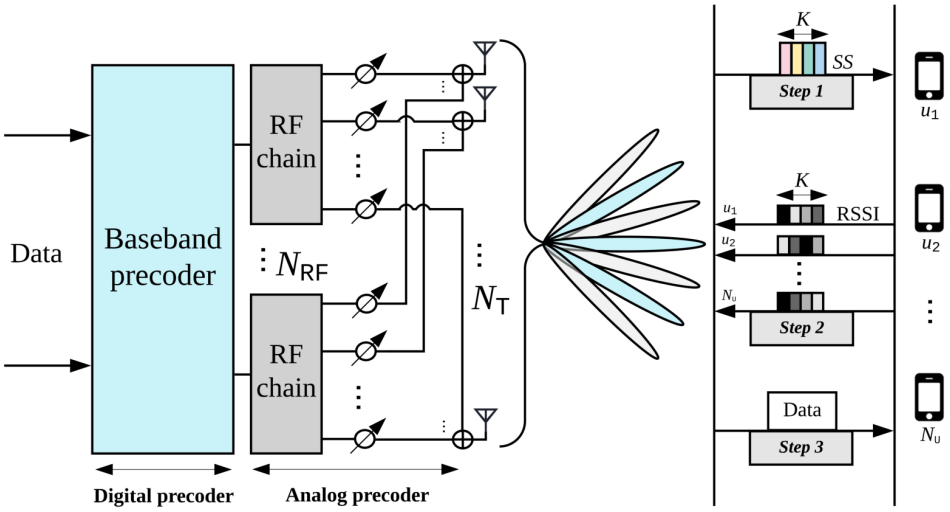

Figure 3.1: System architecture of the hybrid RF beamforming in mmWave massive MIMO with three steps beam training

3.3.3 Step 3: Downlink Data Transmission

The last step corresponds to the downlink transmission where the BS transmits data to each user. The DP matrix is $\mathbf{W} = [\mathbf{w}_1, ..., \mathbf{w}_{N_U}]$ where vector $\mathbf{w}_u \in \mathbb{C}^{N_{RF} \times 1}$ is designed to encode the data symbol of user index u. The analog precoder $\mathbf{A} \in \{1, -1, i, -i\}^{N_T \times N_{RF}}$ is designed to transfer the output of the N_{RF} RF chains to N_T antennas and applies to all users. To reduce the complexity of the HBF design, we consider that the analog precoder is chosen from a codebook $\mathcal{A}$ composed of a set of L analog beam codewords $\{\mathbf{A}_{(1)}, ..., \mathbf{A}_{(L)}\}$ where $\mathbf{A}_{(l)}$ is the l^{th} analog precoder matrix of the codebook (the codebook design is discussed in Section 3.5).

We assume that the signal received by user u can be given by

$$\mathbf{y}_u = \mathbf{h}_u^{\text{H}} \mathbf{A} \sum_{\forall u} \mathbf{w}_u x_u + \eta_u, \tag{3.4}$$

where x_u is transmit symbol for user index u, $\mathbf{h}_u \in \mathbb{C}^{N_T \times 1}$ is the channel vector between the N_T antennas at the BS and user index u, and η_u is the AWGN. The SINR of the u^{th} user received signal for a given hybrid beamformer $(\mathbf{A}, \mathbf{w}_u)$ is then expressed as

$$\text{SINR}(\mathbf{A}, \mathbf{w}_u) = \frac{\left|\mathbf{h}_u^{\text{H}} \mathbf{A} \mathbf{w}_u\right|^2}{\sum_{j \neq u} \left|\mathbf{h}_u^{\text{H}} \mathbf{A} \mathbf{w}_j\right|^2 + \sigma^2}, \tag{3.5}$$

and the spectral efficiency of the system can be obtained by evaluating the SE given by

$$R(\mathbf{A}, \mathbf{W}) = \sum_{\forall u} \log_2\Big(1 + \mathrm{SINR}(\mathbf{A}, \mathbf{w}_u)\Big). \tag{3.6}$$

Then, the HBF design consists of finding the digital precoder vectors $\mathbf{w}_u$ $\forall u$ and the analog precoder matrix $\mathbf{A}$ in the codebook $\mathcal{A}$ that maximize the SE (3.6) subject to a maximum transmission power P_{max}. More formally, the HBF design corresponds to:

$$\max_{\{\mathbf{A}\},\mathbf{w}_u} \quad R(\mathbf{A}, \mathbf{W}) = \sum_{\forall u} \log_2\Big(1 + \mathrm{SINR}(\mathbf{A}, \mathbf{w}_u)\Big). \tag{3.7a}$$

$$\text{s.t.} \quad \mathbf{A} \in \mathcal{A}, \tag{3.7b}$$

$$\sum_{\forall u} \mathbf{w}_u^{\mathrm{H}} \mathbf{A}^{\mathrm{H}} \mathbf{A} \mathbf{w}_u \leq P_{\mathsf{max}}\,. \tag{3.7c}$$

This problem is however difficult to solve as, in our case, the BS does not have direct knowledge of the channel coefficients $\mathbf{h}_u$ and the noise power σ^2. The CSI is in fact partially embedded in the received RSSIs. Therefore, we propose to employ DNN techniques to design the HBF precoders.

3.4 Dataset Generation for DNN

To train the DNNs, a dataset must be obtained beforehand. In practice, this dataset could be generated from channel measurements performed by the BS, while in this paper the channel measurements based on the system model described in Section 3.3 must be simulated. This section describes the channel model and dataset generation procedure followed by the near-optimal full-CSI solution for the HBF and FDP techniques. The HBF and FDP described in this section are used as an upper bound to evaluate the unsupervised DNN performance.

3.4.1 Channel Model

The deepMIMO [141] mmWave mMIMO dataset model is used to generate the channel coefficients $\mathbf{h}^{(k)}$ for the train and test datasets. In this model, realistic channel information is generated by applying ray-tracing methods to a three-dimensional model of an urban environment to capture the geometry-based characteristics, such as the correlation between the channels at different locations, and the dependence on the materials of the various environmental elements, among others. It provides the channel vector $\mathbf{h}$ (of length N_{T}) for each user position on a quantized grid. The considered set of channel parameters from this model is

summarized in Table 3.1. Scenario "O1" consists of several users being randomly placed in two streets surrounded by buildings. These two streets are orthogonal and intersect in the middle of the map.

A $N_{\mathsf{T}} \times N_{\mathsf{U}}$ channel matrix entry in the dataset is obtained by concatenating N_{U} channel vectors selected randomly from the available user positions of the considered area.

3.4.2 Dataset Generation Method

Two datasets are generated for training and testing the network. The first one, referred to as the *core* dataset, contains $N_{core} = 10^4$ channel realizations. This dataset is used to design the codebook $\mathcal{A}$ and the analog precoder of the SS burst $\mathbf{A}_{\mathsf{SS}}^{(k)}$ for initial access. Furthermore, near-optimal FDP and HBF precoder solutions are computed to compare the SE performance of the DNN. It is worth mentioning that, as described in Section 3.6, the proposed DNN architecture is unsupervised, and does not exploit the near-optimal solutions during training.

The second dataset contains $N_{\text{DNN}} = 10^6$ channel realizations and their related RSSIs measured from the $\mathbf{A}_{\mathsf{SS}}^{(k)}$ burst generated from the core dataset. It is used to train and test the DNN. Note that we have $N_{core} << N_{\text{DNN}}$ as the core dataset requires resolving computationally heavy optimization problems, and we empirically found that 10^4 samples are sufficient to obtain good codebook and SS design.

Fig. 3.2 shows the steps performed to generate both datasets, and the next sections provide more details about the near-optimal design of the full digital and HBF precoders, the codebook generation and the SS bursts design.

3.4.3 Fully Digital Precoder Design

Several FDP optimization techniques have been proposed in the literature to maximize the SE. Most of these techniques are computationally heavy when applied to mMIMO cases, but the optimal FDP is needed to evaluate the performance of the DNN. The FDP design problem corresponds to solving the following optimization problem:

$$\max_{\{\mathbf{u}_u\}} \quad \sum_{\forall u} \log_2\left(1 + \text{SINR}(\mathbf{u}_u)\right) \tag{3.8a}$$

$$\text{s. t.} \quad \sum_{\forall u} \mathbf{u}_u^{\text{H}} \mathbf{u}_u \leq P_{\mathsf{max}}, \tag{3.8b}$$

Table 3.1 Parameter selection for the deepMIMO channel model

System		Antennas	
Parameter	Value	Parameter	Value
`scenario`	"O1"	`num_ant_x`	1
`bandwidth`	0.5 GHz	`num_ant_y`	8
`num_OFDM`	1024	`num_ant_z`	8
`num_paths`	10	`ant_spacing`	0.5

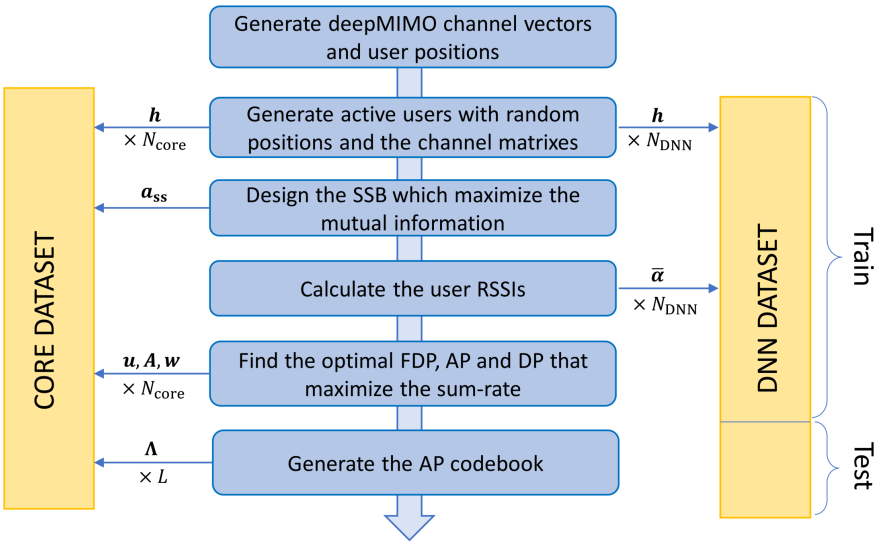

Figure 3.2: Steps to generate the core and DNN datasets

where $\mathbf{u}_u \in \mathbb{C}^{N_\mathrm{T}\times 1}$ is the fully digital precoder vector for user index u, and

$$\mathrm{SINR}(\mathbf{u}_u) = \frac{\left|\mathbf{h}_u^{\mathrm{H}}\mathbf{u}_u\right|^2}{\sum_{j\neq u}\left|\mathbf{h}_u^{\mathrm{H}}\mathbf{u}_j\right|^2 + \sigma^2}. \tag{3.9}$$

The method we employed to find the optimal FDP is based on [52], where it is demonstrated that the optimal FDP vector $\mathbf{u}_u$ of FDP matrix $\mathbf{U} = [\mathbf{u}_1, ..., \mathbf{u}_{N_\mathrm{U}}]$ for user u has the following analytical structure:

$$\mathbf{u}_u = \sqrt{p_u}\frac{\left(I_{N_\mathrm{U}} + \frac{1}{\sigma^2}\sum_{i=1}^{N_\mathrm{U}-1}\mathbf{h}_i\lambda_i\mathbf{h}_i^{\mathrm{H}}\right)^{-1}\mathbf{h}_u}{\left\|\left(I_{N_\mathrm{U}} + \frac{1}{\sigma^2}\sum_{i=1}^{N_\mathrm{U}-1}\mathbf{h}_i\lambda_i\mathbf{h}_i^{\mathrm{H}}\right)^{-1}\mathbf{h}_u\right\|}, \tag{3.10}$$

where N_{U} corresponds to the number of users, $I_{N_{\mathsf{U}}}$ corresponds to the $N_{\mathsf{U}} \times N_{\mathsf{U}}$ identity matrix, p_u and λ_u are the unknown real-valued coefficients to be optimized, respectively corresponding to the beamforming power and Lagrange multiplier for the user u. In addition, we have $\sum_{\forall u} \lambda_u = 1$ and $\sum_{\forall u} p_u = 1$.

Therefore, only $2 \times (N_{\mathsf{U}} - 1)$ real-valued coefficients must be evaluated to resolve the optimization problem, instead of the initial $N_{\mathsf{T}} \times N_{\mathsf{U}}$ complex coefficients. The PSO [143] algorithm can then be employed to obtain the optimal λ_u coefficients. However, we empirically found that near-optimal solutions can be obtained by assuming that $p_u \approx \lambda_u$ and by evenly distributing the power over $\mathcal{K} \in \{1, ..., N_{\mathsf{U}}\}$ users and setting $p_u = 0$ for the remaining $N_{\mathsf{U}} - \mathcal{K}$ users. Therefore, $2^{N_{\mathsf{U}}-1}$ solutions have to be evaluated to find the near-optimal one.

3.4.4 Hybrid Beamforming Design

When considering hybrid beamforming, (3.5) can be rewritten as

$$\mathrm{SINR}(\mathbf{A}, \mathbf{w}_u) = \frac{\left|(\mathbf{A}^{\mathrm{H}}\mathbf{h}_u)^{\mathrm{H}}\mathbf{w}_u\right|^2}{\sum_{j \neq u}\left|(\mathbf{A}^{\mathrm{H}}\mathbf{h}_u)^{\mathrm{H}}\mathbf{w}_m\right|^2 + \sigma^2}. \tag{3.11}$$

From (3.11), $\mathbf{h}' = (\mathbf{A}^{\mathrm{H}}\mathbf{h})^{\mathrm{H}}$, $\mathbf{h} = [\mathbf{h}_1, ..., \mathbf{h}_{N_{\mathsf{U}}}]$, can be seen as a virtual channel matrix with N_{RF} spatial paths. In this virtual system, $\mathbf{W} = [\mathbf{w}_1, ..., \mathbf{w}_{N_{\mathsf{U}}}]$ is the DP matrix of a transmitter with N_{RF} virtual antennas. Then, if $\mathbf{A}$ is known, the optimization method presented in 3.4.3 can be re-used to find the optimal digital precoder $\mathbf{w}$. Therefore, the analog precoder $\mathbf{A}$ must be designed first. We propose to find $\mathbf{A}$ such that the channel capacity [144] of $\mathbf{h}'$ is maximized, giving the following integer nonlinear programming problem:

$$\max_{\mathbf{A}}\left(\sum_i \max\Big(\log_2(\mu\beta_i), 0\Big)\right), \tag{3.12}$$

where β_i is the i^{th} eigenvalue of $\mathbf{h}\mathbf{h}^{\mathrm{H}}$, and μ is the water filling level chosen to satisfy the following equation:

$$\rho = \sum_i \max\Big(\mu - \frac{1}{\beta_i}, 0\Big), \tag{3.13}$$

with ρ corresponding to the SNR. To solve this problem, we used the genetic algorithm [145]. This iterative algorithm consists, for each iteration (or "generation"), of selecting, mutating, and merging solutions from a set of candidate solutions (known as a "population") that

achieve the best score with respect to the objective function (the SE in our case). At the first generation, N_c candidates are generated randomly. The process of selection consists of keeping, for the next iteration, the $\Psi < N_c$ solutions that maximize the score, referred to as *elites*. The mutation process makes small random changes in the population, excluding the elites. Finally, the merging process, called crossover, generates ζN_c new solutions by mixing solutions from the previous population, with ζ being the crossover factor. To optimize the analog precoder, we set the genetic algorithm parameters to $N_c = 200$, $\Psi = 0.05 \times N_c$, and $\zeta = 0.8$. This hybrid beamforming design will be referred to as the HSHO method.

It is worth noting that the design of the $\mathbf{A}_{\mathsf{SS}}^{(k)}$ precoders (step 1) has an impact on the amount of channel information carried by the RSSIs (step 2), which in turn affects the quality of the HBF solutions obtained by the DNN and the performance of uplink transmission in step 3. In addition, the codebook design can also greatly affect the performance of the DNN. Therefore, the codebook and SS for initial access need to be carefully planned.

3.5 Synchronization Signal and Codebook design

In this section, we address the problem of the SS burst and analog beamformer codebook design with novel methods.

3.5.1 Proposed SS Burst Design

As mentioned in Section 3.3.3, the design of the SS burst can impact the HBF SE performance because it affects the amount of information that is revealed by the RSSI measurements about the CSI. The synchronization signal burst (SSB) length also impacts the system data rate in both downlink and uplink. Therefore, it is important to design the SSB so that the measured RSSIs provide the maximum information about the CSI while minimizing the amount of data to transmit in the feedback channel.

To resolve this problem, we propose to find the SS sequences that maximize the mutual information I between the channel matrices $\mathbf{h}$ and the quantized RSSIs matrix $\tilde{\boldsymbol{\alpha}} = [\tilde{\boldsymbol{\alpha}}_1, ..., \tilde{\boldsymbol{\alpha}}_K]$ with K being the number of SS burst

$$I(\mathcal{Q}(\mathbf{h}), \tilde{\boldsymbol{\alpha}}) = \mathsf{H}(\mathcal{Q}(\mathbf{h})) + \mathsf{H}(\tilde{\boldsymbol{\alpha}}) - \mathsf{H}(\mathcal{Q}(\mathbf{h}), \tilde{\boldsymbol{\alpha}}), \tag{3.14}$$

where $\mathcal{Q}(.)$ is the quantization function defined in (3.3), and where $\mathsf{H}(x)$ corresponds to the entropy of the variable x and $\mathsf{H}(x_1, ..., x_L)$ is the joint entropy of the variables x_l, quantized

on Q_l values, defined as

$$\mathsf{H}(x_1,...,x_L) = -\sum_{k=0}^{Q_1-1}...\sum_{z=0}^{Q_L-1}\Big(\mathbb{P}(x_1=k,...,x_L=z)\times\log_2\mathbb{P}(x_1=k,...,x_L=z)\Big), \quad (3.15)$$

with $\mathbb{P}$ denoting probability. Furthermore, we have $\mathsf{H}(\tilde{\boldsymbol{\alpha}}) = \mathsf{H}(\tilde{\boldsymbol{\alpha}}_1,...,\tilde{\boldsymbol{\alpha}}_K)$. It is worth mentioning that there is no need to include more than one user in the calculation of I. In fact, user positions are selected randomly and independently, therefore knowing the RSSI of one user cannot provide any information for a second user.

A straightforward computation of (3.14) can be computationally heavy, particularly when used in an optimization loop and in the case of mMIMO. To reduce the complexity, we assumed that there exists a bijective function that links the channel matrix and the $(X_{\mathsf{U}}, Y_{\mathsf{U}})$ quantized user positions in the environment. In fact, this assumption is quite realistic due to the high channel diversity induced by mMIMO systems. Under this assumption, we have $I(\mathcal{Q}(\mathbf{h}),\tilde{\boldsymbol{\alpha}}) = I((X_{\mathsf{U}},Y_{\mathsf{U}}),\tilde{\boldsymbol{\alpha}})$. Finally, the genetic algorithm with the same parameters as described in Section 3.4.4 is used to design the SS burst sequences $\mathbf{A}_{\mathsf{SS}}^{(k)}$, by solving the following optimization problem:

$$\max_{\mathbf{A}_{\mathsf{SS}}^{(k)}\ \forall\, K} I((X_{\mathsf{U}},Y_{\mathsf{U}}),\tilde{\boldsymbol{\alpha}}). \quad (3.16)$$

Note that $\mathsf{H}(X_{\mathsf{U}},Y_{\mathsf{U}}) \geq I((X_{\mathsf{U}},Y_{\mathsf{U}}),\tilde{\boldsymbol{\alpha}})$ gives the theoretical minimum number of bits required by the feedback channel to transmit all the information about the CSI. Since the user positions are selected randomly with uniform probability on a set of P_{U} different locations, we also have $\mathsf{H}(X_{\mathsf{U}},Y_{\mathsf{U}}) = \log_2(P_{\mathsf{U}})$.

3.5.2 Proposed Codebook Design

To reduce the complexity of the AP design task for the DNN described in the next section, we propose to restrict the $4^{N_{\mathsf{T}}N_{\mathsf{RF}}}$ possible AP solutions to a subset (codebook) of N_{CB} solutions (codewords), directly chosen during the optimization phases when generating the core dataset. This is achieved through three successive steps described below.

The first step consists of generating a first codebook $\mathcal{A}$ when the near-optimal analog and digital precoder solutions presented in Section 3.4.4 are iteratively evaluated for each channel realization. Let us respectively denote $\mathbf{A}(n)$ and $\mathbf{W}(n)$ the AP and DP solutions related to the n^{th} channel matrix of the core dataset. Each of these solutions has SE $R(\mathbf{A}(n),\mathbf{W}(n))$, which can be calculated from (3.6). As a reminder, $\mathbf{A}_{(l)}$ denotes the l^{th} analog precoder in

the codebook. Then, $\mathbf{A}(n)$ is appended in the codebook if

$$R(\mathbf{A}(n), \mathbf{W}(n)) > \xi \max_{\forall l} R(\mathbf{A}_{(l)}, \mathbf{W}_{(l)}(n)), \tag{3.17}$$

where $\xi > 1$ is an arbitrary threshold value, set to 1.005 in our setup, to decide if the analog precoder will be appended to the codebook, and $\mathbf{W}_{(l)}(n)$ is the DP solution for the n^{th} channel matrix in the dataset when the analog precoder $\mathbf{A}_{(l)}$ is chosen from l^{th} codewords. Therefore, each analog precoder solution solved using the genetic algorithm is appended in the codebook if the obtained SE is higher than ξ times the best SE obtained with the APs in the current codebook. Otherwise, the obtained HBF solution is replaced by the one in the codebook having the highest SE. To avoid high computational overhead, no APs are appended to the codebook when its size reaches 1000 APs.

Since the APs are iteratively appended in the first step, it may be possible that better AP solutions are found in the later iterations. Therefore, the SE could be improved for the first channel matrices in the dataset. To address this issue, the second step aims to update the AP solutions for each channel matrix in the dataset by choosing the AP in the codebook, obtained in the first step, that maximize the SE:

$$\mathbf{A}(n) = \arg\max_{\forall \mathbf{A}_{(l)} \in \mathcal{A}} R(\mathbf{A}_{(l)}, \mathbf{W}_{(l)}(n)) \tag{3.18}$$

The final step consists of reducing the size of the codebook while keeping an acceptable level of average SE over the whole dataset. We denote $\mathcal{L}_l$ the set of AP index $n \in \{1, ..., N_{\mathsf{core}}\}$ in the core dataset that use the AP label number l ($\mathbf{A}_{(l)}$) in the current codebook as solution. To reduce the codebook size $|\mathcal{A}|$, where $|.|$ represents the cardinality operator in this context, the following operations are iteratively executed:

- The codebook is sorted in ascending order such that $|\mathcal{L}_0| \leq |\mathcal{L}_l| \; \forall \; l$,
- All the APs in the core dataset using the AP codeword $A_{(0)}$ (indexed in $\mathcal{L}_0$) are moved to other AP codewords giving the best SE:

$$\mathbf{A}(n) = \arg\max_{\mathbf{A}_{(l)}, l \neq n} R(\mathbf{A}_{(l)}, \mathbf{W}_{(l)}(n)), \forall n \in \mathcal{L}_0 \tag{3.19}$$

- The AP codeword 0 is then removed from the codebook.

Each time a codeword is removed, the average SE over the core dataset is reduced. To maintain good performance, the codebook size reduction is stopped when the average SE

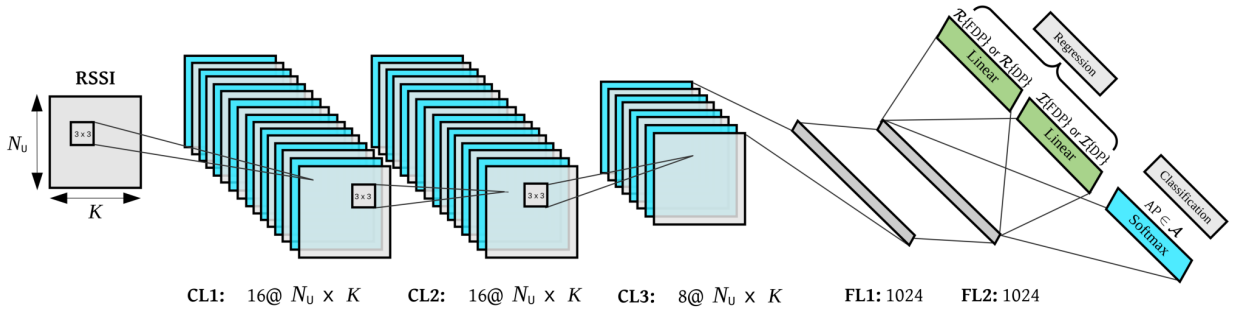

Figure 3.3: Proposed multi-tasking DNN architecture to design the HBF

reaches 99.5% of the initial SE.

3.6 RSSI-Based Hybrid Beamforming with Deep Neural Network

In this section, we propose two novel RSSI-based methods, each providing a different complexity performance trade-off, to design the HBF for mMIMO systems. The RSSI measurements by the users were explained in Section 3.3.2. The BS receives the quantized RSSI, $\tilde{\boldsymbol{\alpha}} = [\tilde{\boldsymbol{\alpha}}_1, ..., \tilde{\boldsymbol{\alpha}}_{N_U}]$ through a dedicated error-free feedback channel. Then, the BS designs the HBF matrices used to transmit data to users in the downlink step, as described in Section 3.3.3. In supervised learning, a computationally heavy optimization problem must be solved not only for each sample in the dataset but also for each BS in the cellular network because the dataset generation depends on the location of the BS. On the contrary, in unsupervised learning, the BS can be trained directly using data measured from the environment. As discussed in Section 3.7.4, this results in a significant reduction of the offline complexity.

3.6.1 Deep Neural Network Architecture

Two approaches are considered to obtain the HBF solution. In the first approach, we design a DNN, called "HBF-Net", to jointly predict the analog precoder $\mathbf{A}_{(l)} \in \mathcal{A}$ and digital precoder $\mathbf{W}$. In the second approach, referred to as "AFP-Net", the DNN predicts the analog $\mathbf{A}_{(l)}$ and fully digital precoders $\mathbf{U}$. The digital precoder $\mathbf{W}_{(l)}$ is then computed using

$$\mathbf{W}_{(l)} = \mathbf{A}_{(l)}^{\dagger}\mathbf{U}. \tag{3.20}$$

The AFP-Net approach ensures that the alignment between analog and digital precoders is maintained. In both approaches, the DNN architecture is composed of a classification task for the analog precoder prediction, and of a regression task for the digital precoder (or

fully digital precoder) prediction. To reduce the number of parameters and accordingly, the computational complexity, we design a multi-tasking DNN [146] to perform both tasks in a single DNN. The proposed DNN architecture is shown in Fig. 3.3. Referring to Fig. 3.3, the input of the DL model is the quantized RSSIs received at the BS followed by shared convolutional layer (CL), FL layers and an output layer for each task. It is worth noting that for both HBF-Net and AFP-Net, the DNN has the same architecture, except for the dimension of the output layer. Since we separate the real and imaginary parts of the output, the dimension of the output layer for DP task in HBF-Net is $2\times N_{\mathsf{U}}\times N_{\mathsf{RF}}$, and $2\times N_{\mathsf{U}}\times N_{\mathsf{T}}$ for FDP task in AFP-Net. The dimension of the AP task is the same for both approaches and it is equal to the size of the codebook ($L = N_{\mathsf{CB}}$). The CLs use the "Same" convolution operators where the dimension of the inputs and outputs are preserved. After each layer, we use batch normalization to reduce the internal covariate shift and accelerate the learning. In fact, batch normalization is a kind of regularization technique that prevents over-fitting because of its noise injection effect [147]. Since we have used the batch normalization technique, the dropout probability for all layers is selected to a very small value (0.05) to avoid the over-regularization problem. The dropout layers reduce the impact of the choice of initial weights [148]. In addition, we use the leaky ReLU activation function in each layer (except the output layers), to fix the *dying ReLU* problem after batch normalization [149]. This activation function with input X and output Y is given by

$$Y = \begin{cases} X & \text{if } X \geq 0, \\ 0.01X & \text{if } X < 0. \end{cases} \tag{3.21}$$

This function does not have a zero-slope part [149]. For the output layer of the classifier or AP task, we use a conventional "Softmax" activation function defined as

$$p_{a_{(l)}} = \frac{e^{a_l}}{\sum_{j=1}^{L} e^{a_j}}, \tag{3.22}$$

where a_l is the value of the l^{th} output of the DNN in AP task part and $p_{a_{(l)}}$ is the corresponding output of the Softmax activation function. Thus, the output vector of the classifier after the activation function is $\mathbf{p} = [p_{a_{(1)}}, ..., p_{a_{(l)}}, ..., p_{a_{(L)}}]$ where from Section 3.5.2 we consider that $L = N_{\mathsf{CB}}$. Finally, we used the "Adam" algorithm as network optimizer and "ReduceLROnPlateau" to schedule the reduction of learning rate [150].

As shown in Fig. 3.3, the output of the FDP task is separated into real and imaginary parts. Some DL frameworks only support real algebra, and therefore cannot directly support complex-valued computation. Therefore, we separately deploy the real and imaginary parts

to compute the loss function. Then, to compute the pseudo-inverse of all codewords $\mathbf{A}_{(l)}$, we use $\mathbf{A}_{(l)}^{\dagger} = (\mathbf{A}_{(l)}^{\mathsf{H}}\mathbf{A}_{(l)})^{-1}\mathbf{A}_{(l)}^{\mathsf{H}}$. To compute the $(\mathbf{A}_{(l)}^{\mathsf{H}}\mathbf{A}_{(l)})^{-1}$, we define the square matrix $\mathbf{\Phi} \triangleq \mathbf{A}_{(l)}^{\mathsf{H}}\mathbf{A}_{(l)}$ and $\mathbf{\Phi}^{-1} \triangleq \mathbf{C} + i\mathbf{D}$ where $\mathbf{C}$ and $\mathbf{D}$ are purely real. We then have the following relations based on [151]:

$$\begin{aligned} \mathbf{C} &= \left(\Re[\mathbf{\Phi}] + \Im[\mathbf{\Phi}]\Re[\mathbf{\Phi}]^{-1}\Im[\mathbf{\Phi}]\right)^{-1}, \\ \mathbf{D} &= -\Re[\mathbf{\Phi}]^{-1}\Im[\mathbf{\Phi}]\mathbf{C}\,. \end{aligned} \tag{3.23}$$

Eq. (3.23) is valid when the matrix $\Re[\mathbf{\Phi}]$ is non-singular, which holds in our case. In other cases where $\Re[\mathbf{\Phi}]$ is singular, the corresponding equations are listed in [151]. To obtain the predicted digital precoders $\mathbf{W}_{(l)}$ in (3.20), we compute

$$\begin{bmatrix} \Re[\mathbf{W}_{(l)}] & -\Im[\mathbf{W}_{(l)}] \\ \Im[\mathbf{W}_{(l)}] & \Re[\mathbf{W}_{(l)}] \end{bmatrix} = \begin{bmatrix} \Re[\mathbf{C}] & -\Im[\mathbf{D}] \\ \Im[\mathbf{D}] & \Re[\mathbf{C}] \end{bmatrix} \begin{bmatrix} \Re[\mathbf{U}] & -\Im[\mathbf{U}] \\ \Im[\mathbf{U}] & \Re[\mathbf{U}] \end{bmatrix} \tag{3.24}$$

and then, $\mathbf{W}_{(l)} = \Re[\mathbf{W}_{(l)}] + i\Im[\mathbf{W}_{(l)}]$ is formed.

3.6.2 Unsupervised Training

We propose a novel loss function to train both AP task and DP or FDP tasks without any target. Further, as shown in Fig. 3.4, the full CSI is only used in training mode to calculate the unsupervised loss function, and in evaluation mode, only the RSSI information is used at the BS and the BS does not have access to CSI.

Since we design the hybrid beamforming with two different approaches, each approach requires its own loss function for training. As a reminder, the SE achieved by the HBF is given by (3.6), and based on (3.22), we define $\mathbf{p} = [p_{a_{(1)}}, ..., p_{a_{(l)}}, ..., p_{a_{(L)}}]$ as the output vector of the AP task. We define below the unsupervised loss function for each approach.

HBF-Net

The DNN in this approach is trained to jointly design the DP and AP directly from RSSIs. For this approach, we define the unsupervised loss function as

$$\mathcal{L}_{\text{HBF}} = -\sum_{l=1}^{L} p_{a_{(l)}} R(\mathbf{A}_{(l)}, \bar{\mathbf{W}}), \tag{3.25}$$

where $\mathbf{A}_{(l)}$ is the l^{th} analog precoder of the codebook and $\bar{\mathbf{W}} = [\bar{\mathbf{w}}_1, ..., \bar{\mathbf{w}}_{N_{\text{U}}}]$ is the output of the DP task. To satisfy $||\mathbf{A}_{(l)}\bar{\mathbf{w}}_u||^2 = 1$ we further normalize $\bar{\mathbf{w}}_u$. The negative sign allows

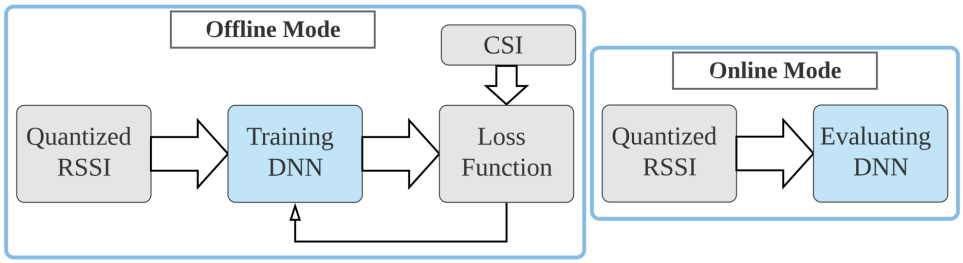

Figure 3.4: The diagram for the unsupervised training in offline mode and the prediction mode of the proposed DNN in online mode

the SE to be maximized when the DNN is trained to minimize the loss function. Algorithm 1 summarizes the steps to train the HBF-Net.

AFP-Net

The loss function in this approach is different because here we aim to design the digital precoder from the FDP and AP. To do so, we first obtain the FDP and AP, and then by using (3.20), DP can be computed. If we define

$$R(\mathbf{U}) = \sum_{\forall u} \log_2(1 + \mathrm{SINR}(\mathbf{u}_u)) \,, \tag{3.26}$$

the loss function for the FDP task can be defined as

$$\mathcal{L}_{\mathrm{FDP}} = -R(\bar{\mathbf{U}}), \tag{3.27}$$

where $\bar{\mathbf{U}} = [\bar{\mathbf{u}}_1, ..., \bar{\mathbf{u}}_{N_\mathrm{U}}]$ is the output of FDP task in AFP-Net. This loss function results in the maximization of the FDP spectral efficiency. Here again, we normalize $\bar{\mathbf{u}}_u$ to satisfying $||\bar{\mathbf{u}}_u||^2 = 1$. Now, by knowing the FDP, given AP, we compute $R(\mathbf{A}_{(l)}, \tilde{\mathbf{W}}_{(l)})$, where $\tilde{\mathbf{W}}_{(l)}$ is the DP matrix obtained from (3.20) for the l^{th} codeword in the codebook. The loss function for the AP task is defined as

$$\mathcal{L}_{\mathrm{AP}} = -\sum_{l=1}^{L} p_{a_{(l)}} R(\mathbf{A}_{(l)}, \tilde{\mathbf{W}}_{(l)}), \tag{3.28}$$

Algorithm 1: Training mode in HBF-Net

Input: $\tilde{\boldsymbol{\alpha}}$
Output Regression: DP: $\Re[\bar{\mathbf{W}}]$ and $\Im[\bar{\mathbf{W}}]$
Output Classification: AP: $\mathbf{p}$
for i ***in range(****epochs****)*** **do**
  for l ***in range(****L****)*** **do**
    Compute $R(\mathbf{A}_{(l)}, \bar{\mathbf{W}})$
  Compute $\mathcal{L}_{\text{HBF}}$ as in (3.25)
  Compute gradient over layers
  Update weights and biases with **Adam** optimizer

where unlike (3.25), this loss function is only tuning the Softmax outputs $p_{a_{(l)}}$ of the AP task. The final loss function for AFP-Net is defined as

$$\mathcal{L}_{\text{AFP}} = \mathcal{L}_{\text{FDP}} + \mathcal{L}_{\text{AP}}, \tag{3.29}$$

so that the DNN maximizes the FDP spectral efficiency while also maximizing the HBF spectral efficiency by selecting the appropriate AP from the codebook. Algorithm 2 summarizes the steps to train the AFP-Net.

Algorithm 2: Training mode in AFP-Net

Input: $\tilde{\boldsymbol{\alpha}}$
Output Regression: FDP: $\Re[\bar{\mathbf{U}}]$ and $\Im[\bar{\mathbf{U}}]$
Output Classification: AP: $\mathbf{p}$
for i ***in range(****epochs****)*** **do**
  for l ***in range(****L****)*** **do**
    Compute $\tilde{\mathbf{W}}_{(l)} = \mathbf{A}_{(l)}^{\dagger}\bar{\mathbf{U}}$ as in (3.23) and (3.24)
    Compute $R(\mathbf{A}_{(l)}, \tilde{\mathbf{W}}_{(l)})$
  Compute $\mathcal{L}_{\text{FDP}}$ as in (3.27) and $\mathcal{L}_{\text{AP}}$ as in (3.28)
  Total loss = $\mathcal{L}_{\text{FDP}} + \mathcal{L}_{\text{AP}}$
  Compute gradient over layers
  Update weights and biases with **Adam** optimizer

It can be seen that AFP-Net is more complex than HBF-Net, which directly outputs the hybrid beamforming solution. However, as shown in Section 3.7, AFP-Net achieves better SE performance by keeping the alignment between the analog and digital precoder.

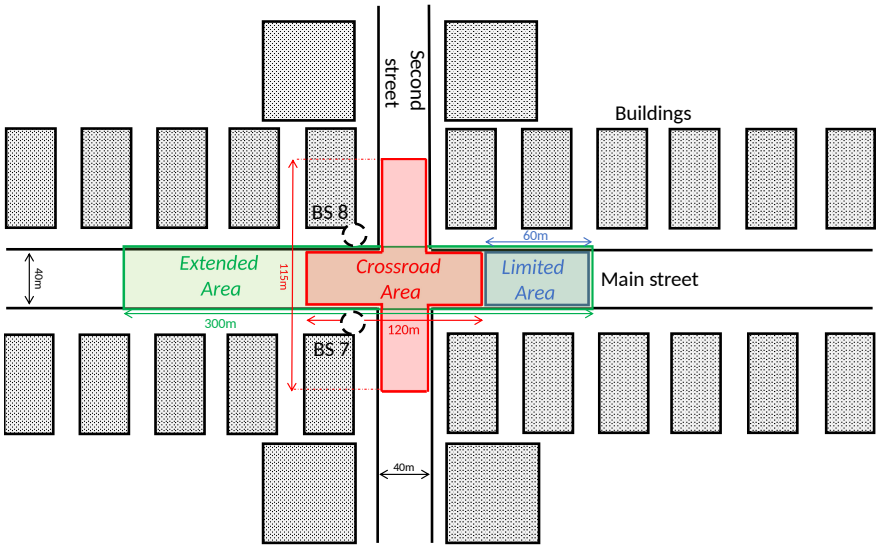

Figure 3.5: Illustration of each type of area covered for the deepMIMO channel model

3.6.3 Evaluation Phase

In the evaluation phase, a part of the DNN dataset is dedicated to testing the network, as presented in Section 3.4.2. We used the SE metric to characterize the performance. As shown in Fig. 3.4, in the online phase, only RSSI information is provided as input to the DNN. For the analog precoder, the maximum value of the "Softmax" output is selected in the classifier. So, we can compute the SE of HBF to evaluate its performance using $R(\hat{\mathbf{A}}, \hat{\mathbf{W}})$, where $\hat{\mathbf{A}}$ is the analog precoder predicted by the AP task, expressed as $\hat{\mathbf{A}} = \mathbf{A}_{(\gamma)}$, where $\mathbf{A}_{(\gamma)} \in \mathcal{A}$, $\gamma = \arg\max(\mathbf{p})$ and $\hat{\mathbf{W}} = [\hat{\mathbf{w}}_1, ..., \hat{\mathbf{w}}_{N_U}]$ is the predicted digital precoder of HBF-Net or AFP-Net obtained from (3.20). To satisfy the power constraint we normalize the $\hat{\mathbf{w}}_u$ to have $||\hat{\mathbf{A}}\hat{\mathbf{w}}_u||^2 = 1$.

Likewise, to evaluate the DNN performance for FDP spectral efficiency we compute $R(\hat{\mathbf{U}})$, where $\hat{\mathbf{U}} = [\hat{\mathbf{u}}_1, ..., \hat{\mathbf{u}}_{N_U}]$ is the predicted FDP matrix in FDP task of AFP-Net. As discussed in the next section, we evaluate the DNN using different scenarios.

3.7 Numerical Evaluation

In this section, the performance of the proposed DNN, implemented using the PyTorch DL framework, is numerically evaluated. To analyze how the DNN performance evolves with the environment, three types of datasets covering different areas are considered, as illustrated in Fig. 3.5:

Table 3.2 Multi-tasking DNN Hyper-Parameters

Parameter	Set Value
Mini-batch size	500
Initial learning rate	0.001
ReduceLROnPlateau (factor)	0.1
ReduceLROnPlateau (patience)	3
Weight decay	10^{-6}
Dropout keep probability	.95
Kernel size	3
Zero padding	1
"ϵ" in BatchNorm (1D & 2D)	10^{-5}

1. *Limited Area*: small area of 54481 possible user positions in the main street, with base station number 7 as the transmitter. The parameters "`active_user_first`" (AUF) and "`active_user_last`" (AUL) in deepMIMO are set to AUF = 1000 and AUL = 1300.

2. *Extended Area*: larger area than the limited one, with 271681 possible user positions in the main street, with AUF = 1000, AUL = 2500, and base station number 7 as the transmitter.

3. *Crossroad Area*: area located at the intersection of the two streets, with users coming from every direction (280102 positions). Three deepMIMO channel environments have been generated and concatenated to obtain this last dataset. The first environment uses AUF = 1300, AUL = 1900, the second uses AUF = 3700, AUL = 3852 and the third uses AUF = 3853, AUL = 4300. For all these models, the base station number 8 corresponds to the transmitter.

The size of the DNN dataset is set to 10^6 samples for each scenario, with 85% of the samples used for training as a training set and the remaining ones are used to evaluate the performance as the test set. It is worth noting that we evaluate the DNN performance using samples from the same scenario it is trained for. Table 3.2 shows the chosen hyper-parameters which have been used for the proposed multi-tasking DNN.

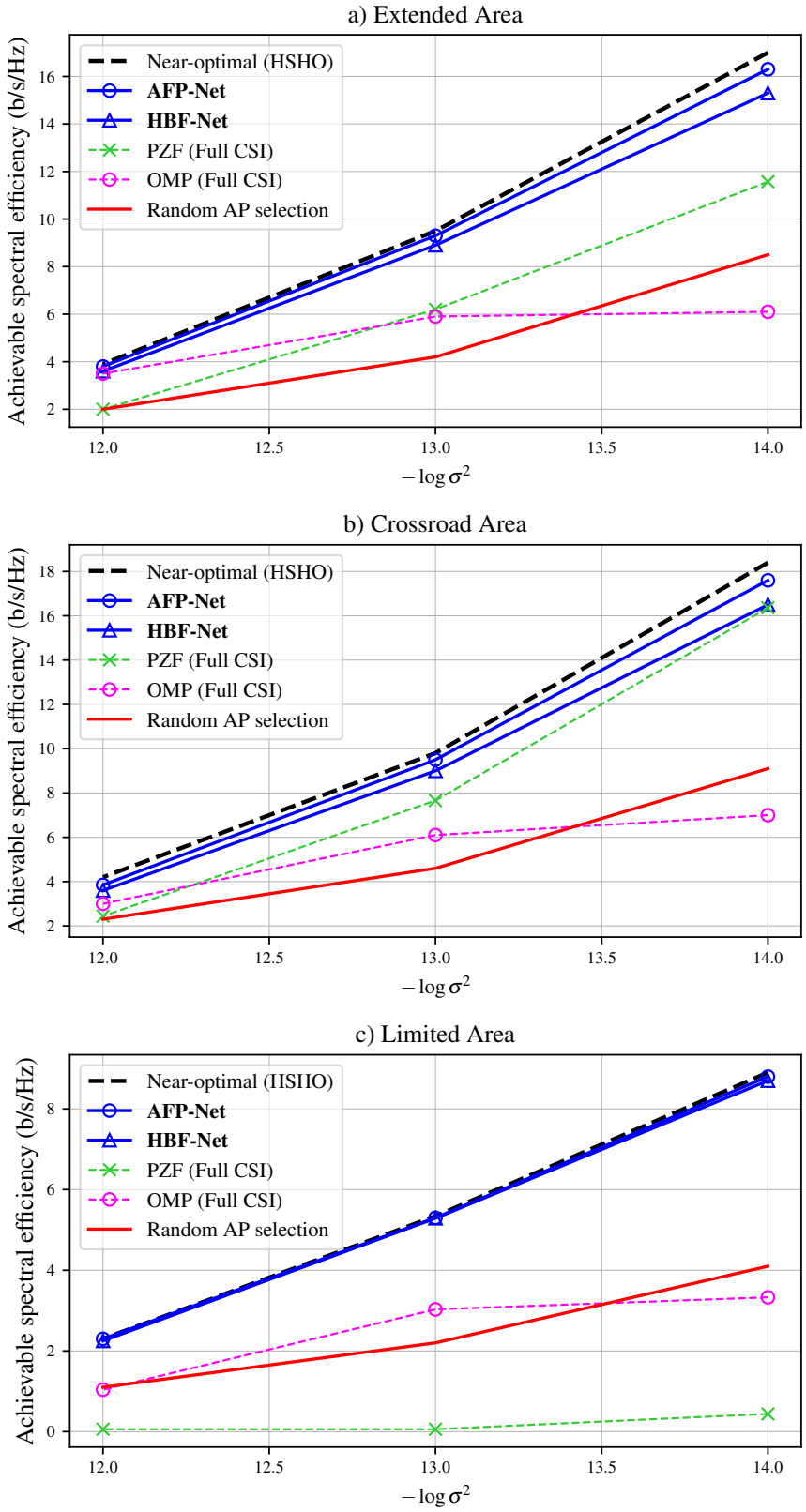

Figure 3.6: Spectral efficiency performance of Hybrid beamforming design in "AFP-Net" and "HBF-Net" in three scenarios: a) Extended Area b) Crossroad Area c) Limited Area ($N_{\mathsf{U}} = 4, N_{\mathsf{RF}} = 8, N_{\mathsf{T}} = 64, K = 32$)

3.7.1 Spectral Efficiency Evaluation for All Areas

We consider a fully connected hybrid beamforming system where each RF chain is connected to all antennas, 4 users communicating with a BS equipped with 64 antennas, 8 RF chains, and $K = 32$ full precision RSSIs are fed back to the BS. Fig. 3.6 shows the achievable SE for each considered area when considering different noise power values σ^2 ranging from -120 dBW to -140 dBW. When considering the channel attenuation, the average SNRs for $\sigma^2 \in \{-120, -130, -140\}$ dBW in Extended Area are 10.8 dB, 20.8 dB and 30.8 dB, in Crossroad Area are 10.6 dB, 20.6 dB and 30.6 dB, and in Limited Area are 4.35 dB, 14.35 dB and 24.35 dB, respectively. It can be seen that the AFP-Net has better performance when compared to the HBF-Net. It is owing to the fact that in the AFP-Net, the digital precoder is extracted from the predicted FDP and HBF based on (3.20). Therefore, the alignment between analog and digital precoder is preserved. In fact, the SE performance of the AFP-Net is very close to the upper bound obtained by using the full-CSI HBF design method presented in Section 3.4.4.

Furthermore, as shown in Fig. 3.6 the two proposed unsupervised HBF design methods presented in Section 3.6 have better SE performance, for all three areas when compared with the phase zero forcing (PZF) [135] and the OMP [127] full CSI techniques. The OMP technique uses as inputs the optimal fully digital precoder and the same AP codebook used by the DNN and designed according to the method proposed in Section 3.5. In fact, the PZF has very poor performance for the Limited Area, which is located far from BS, and therefore suffers at low SNR level. Unlike PZF which has good performance in high SNR, OMP achieves a better SE in low SNR. However, our proposed near-optimal HSHO solution and unsupervised learning DNN methods have stable performance in all SNRs. For instance, with $\sigma^2 = -130$ dBW, our proposed method in AFP-Net is better than PZF by 50%, 25%, and 8733% for scenario (a), (b), and (c), respectively, and better than OMP by 66%, 59%, and 75%. It is worth mentioning that both PZF and OMP techniques require perfect knowledge of the CSI, and therefore require a high bandwidth feedback channel to report the full CSI in FDD scenario, which penalizes the spectral efficiency of the system.

The "Random AP selection" curves in Fig. 3.6 show the achieved SE when the BS selects the AP from the codebook randomly while obtaining the DP by substituting into (3.20) the random AP and the FDP predicted by AFP-Net. The significant performance degradation observed for the Random AP selection confirms that the AP task of the DNN actually learns the system characteristics from the dataset.

Likewise, Fig. 3.7 shows that the SE performance of the FDP obtained with the proposed AFP-Net method outperforms the ZF method, for all areas and different noise power. In

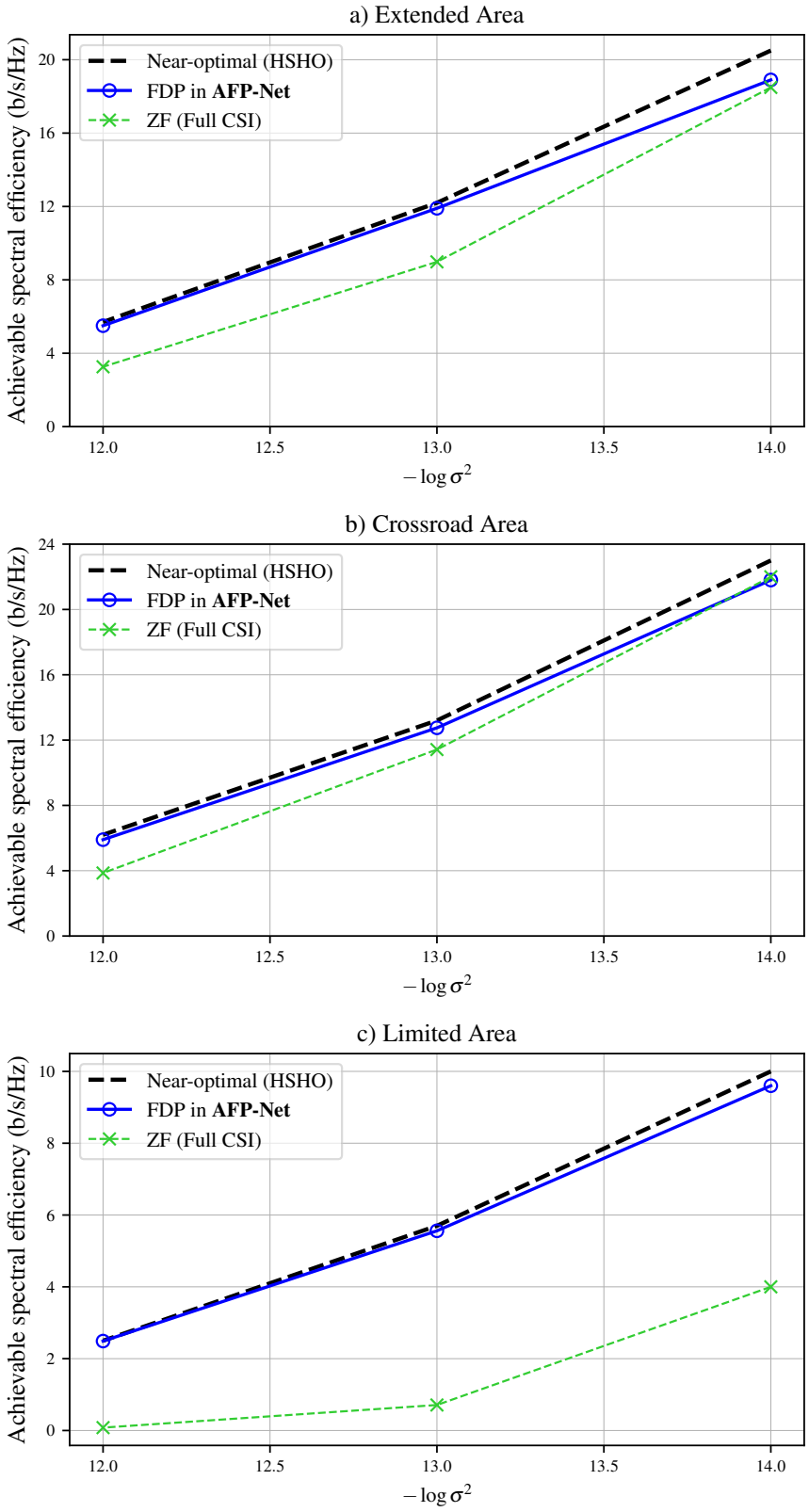

Figure 3.7: Spectral efficiency performance of FDP design in "AFP-Net" in three scenarios: a) Extended Area b) Crossroad Area c) Limited Area ($N_{\mathsf{U}} = 4, N_{\mathsf{RF}} = 8, N_{\mathsf{T}} = 64, K = 32$)

fact, the proposed unsupervised learning in AFP-Net has near-optimal FDP SE performance in all selected areas. This makes the proposed network a promising solution for FDP design in mm-wave mMIMO systems.

3.7.2 Impact of The RSSI Length and Quantization

The effect of the number K of SSBs (also the number of RSSI values) on AFP-Net is shown in Fig. 3.8, for the "Extended Area" scenario. Increasing K increases the amount of CSI available to the DNN, and we see that the achievable rate indeed improves as K increases. However, increasing K also reduces the channel efficiency because of the need to send more SSBs in Step 1. Furthermore, we see that the performance of AFP-Net with $K = 8$ is close to the performance obtained with $K = 16$ and $K = 32$.

In Fig. 3.9 we examined the proposed methods with different numbers of quantization bits N_b for the RSSIs, computed using (3.3). The "Extended Area" is considered to evaluate the performance. In fact, there is a trade-off between the SE improvement of the system and the performance of the DNN when changing the number of bits. It can be seen in Fig. 3.9 that the SE performance of the DNN for $N_b = 12$ to $N_b = 8$ is very close to the DNN performance when considering full precision for the RSSIs.

3.7.3 Impact of The Number of Users and Antennas

This section evaluates how the performance of the two proposed HBF designs scale when varying the number of users $N_{\mathsf{U}} \in \{2, 4, 6, 8\}$ and the number of antennas $N_{\mathsf{T}} \in \{16, 32, 64, 128\}$. The number of RSSIs is set to $K = 32$, the noise power is fixed to -130 dBW, and the "Extended Area" is considered. In fact, the complexity of the DNN, measured in terms of the number of parameters, can be expected to depend on the complexity of the optimization problem. Thus increasing the number of antennas in BS or the number of users should require a more complex DNN. However, the results in Figures 3.10 and 3.11 show that the proposed architecture is complex enough to have excellent performance for a wide variety of number of antennas and number of users. Fig. 3.10 shows that although our method is RSSI based, it has better performance in comparison with other CSI-based methods and the SE performance scale with the number of users. For instance, our proposed method is better than PZF by 50%, 84% and 122% for $N_{\mathsf{U}} = 4, 6, 8$, respectively. Meanwhile, the PZF and OMP methods do not scale well when the number of users increases. This can be explained by the fact that increasing the number of users and fixing the number of antennas in BS will generate more inter-user interference. Furthermore, PZF only provides near-optimal results if the ratio between the number of antennas and the number of users is large enough

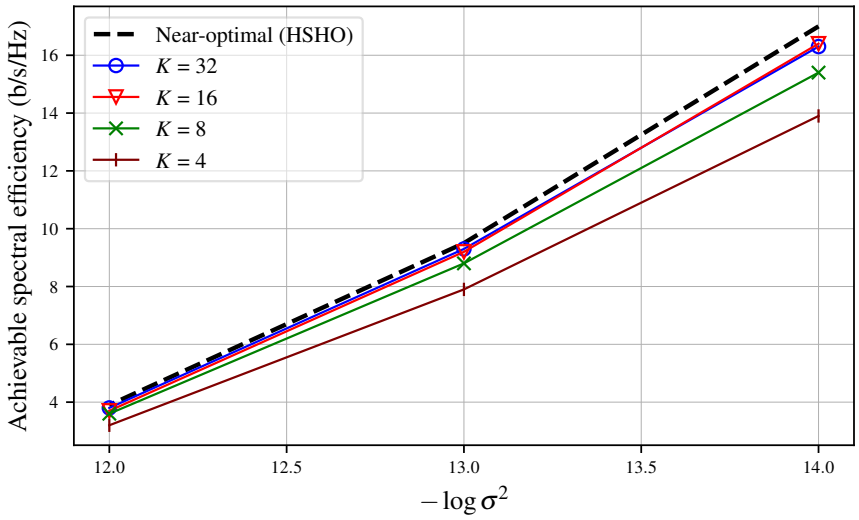

Figure 3.8: Spectral efficiency performance of HBF design in AFP-Net in different number of RSSI (K) ($N_{\mathsf{U}} = 4, N_{\mathsf{RF}} = 8, N_{\mathsf{T}} = 64$)

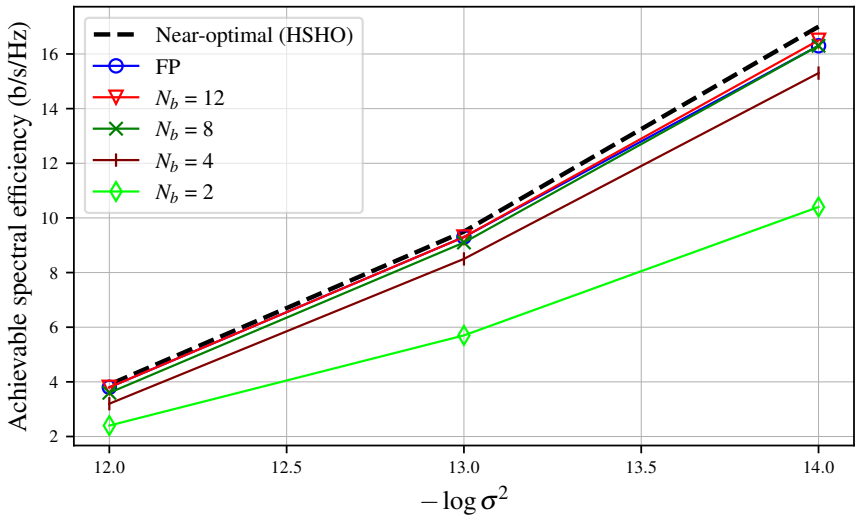

Figure 3.9: Spectral efficiency performance of HBF design in "AFP-Net" in different number of quantization bits (N_b) ($N_{\mathsf{U}} = 4, N_{\mathsf{RF}} = 8, N_{\mathsf{T}} = 64, K = 32$)

in mMIMO systems. By increasing the number of users, this ratio decreases and the SE performance of PZF collapses.

In Fig. 3.11, we evaluate our proposed method with the different number of antennas in BS (N_{T}). Again, we consider the "Extended Area" scenario where $\sigma^2 = -130$ dBW, $K = 32$ and $N_{\mathsf{T}} = 64$. As we can see, the PZF method has poor performance when the number of antennas is low whereas the SEsum-rate performance is near-optimal when the number of antennas grows up to 256. Therefore, our proposed methods outperforms PZF for the 16, 32 and 64 antennas cases by 195%, 100% and 50%, respectively. The OMP method has fair enough performance with a small number of antennas, while the SE of PZF is almost the same as our proposal for a large (128) number of antennas. However, it is worth mentioning that PZF and OMP require perfect knowledge of the CSI and by increasing the number of antennas in BS it reduces the spectral efficiency whereas our proposed methods only exploit RSSI measurements which we kept to 32 and can therefore significantly improve the data rate of the system by reducing the signaling overhead. To clarify, in $N_{\mathsf{T}} = 128$ where the proposed method and PZF have almost the same performance, our proposed method requires $K \times N_{\mathsf{U}} \times N_b = 1024$ bits to feedback the RSSIs where $N_b = 8$. On the other hand, PZF in the same configuration requires $N_{\mathsf{T}} \times N_{\mathsf{U}} \times 2 \times N_b = 4096$ bits to feedback the CSI to the BS where we find that $N_b = 4$ to keep the SE same as fully precision. As a result, in the same configuration and SE performance, PZF requires 4 times more feedback bits in comparison with our proposed method.

Fig. 3.12 shows how the number K of RSSI measurements affects the SE performance when the number of antennas is increased. It can be seen that the required number of RSSIs to achieve a near-optimal SE depends on the number of antenna. For instance, with $N_{\mathsf{T}} = 16$ using $K = 8$ or even 4, the DNN has similar performance as larger number of RSSI such as $K = 16$ or 32. However, for a larger number of antennas, the DNN needs more information to design the HBF and as a result, more RSSIs transmission is required.

3.7.4 Computational Complexity Comparison

The computational complexity of the proposed methods is analyzed in this section. First, we compare the dataset generation complexity. Second, training complexity is evaluated by comparing the number of parameters of proposed DNN architecture to other state-of-the-art DNN-based hybrid beamforming. Third, the computational complexity of the two proposed DNN methods is evaluated in the inference phase, and compared to non-DL hybrid beamforming state-of-the-art.

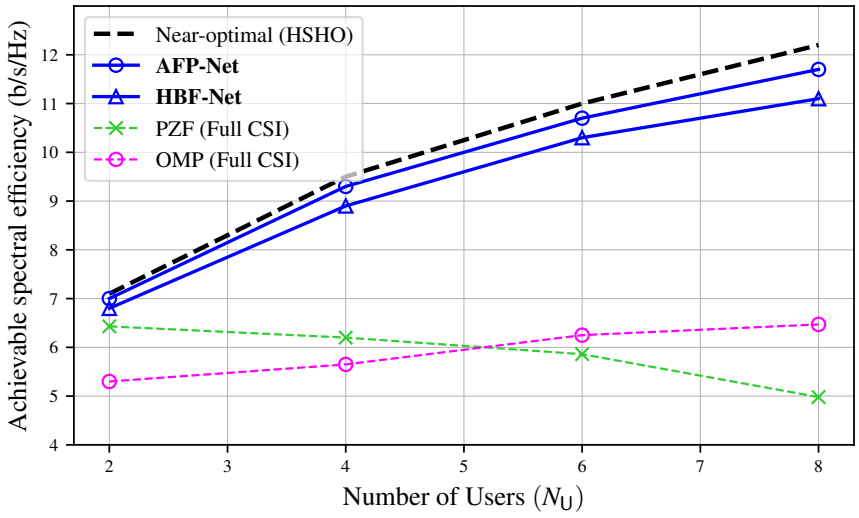

Figure 3.10: Spectral efficiency performance of HBF design in "AFP-Net" and "HBF-Net" versus different number of user (N_{U}) in "Extended area" ($\sigma^2 = -130$ dBW, $K = 32$, $N_{\mathsf{T}} = 64$, and $N_{\mathsf{RF}} = 8$)

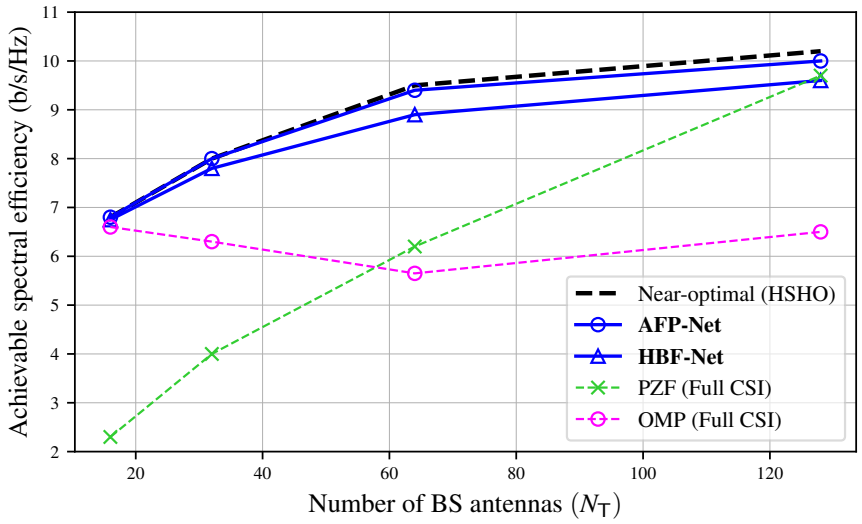

Figure 3.11: Spectral efficiency performance of HBF design in "AFP-Net" and "HBF-Net" versus different number of antenna in BS (N_{T}) in "Extended area" ($\sigma^2 = -130$ dBW, $K = 32, N_{\mathsf{U}} = 4$, and $N_{\mathsf{RF}} = 8$)

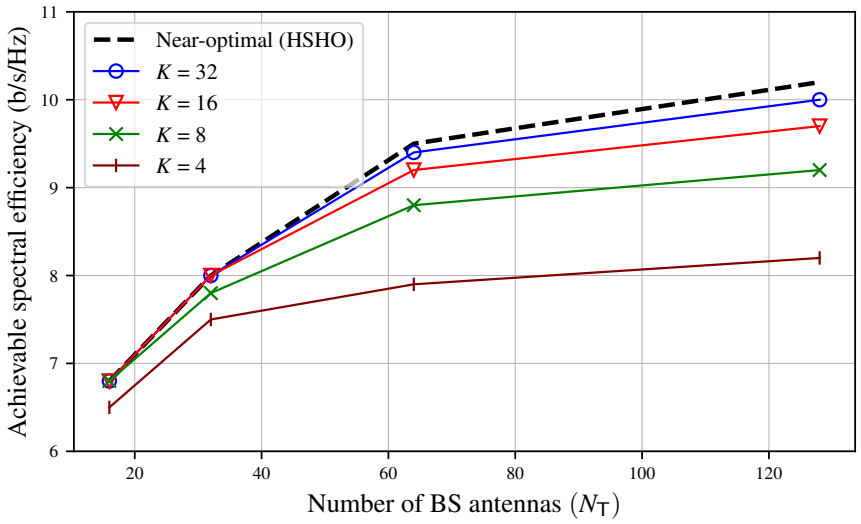

Figure 3.12: Spectral efficiency performance of HBF design in "AFP-Net" versus different number of antenna in BS (N_{T}) in "Extended area" for different number of RSSI (K) ($\sigma^2 = -130$ dBW, $N_{\mathsf{U}} = 4$, and $N_{\mathsf{RF}} = 8$)

Computational Complexity of Dataset Generation

Dataset generation plays a key role in all DNNs, and its complexity should be considered carefully so that it can be generated in a reasonable amount of time. As a point of reference, our implementation of the HSHO algorithm achieves $\mathcal{T} = 10$ seconds on one core of an Intel(R) Xeon(R) CPU E5-2620 v4 @ 2.10GHz, the processing time to generate the entire dataset for a supervised DNN would be $N_{\text{DNN}} \times \mathcal{T}$ where here we consider $N_{\text{DNN}} = 10^6$ as the size of the dataset. However, the two unsupervised DNN methods proposed in Section 3.6 do not need to have the optimal solutions as a target to design the HBF, but only a codebook, which can be generated on a smaller dataset of 10^4 samples, as explained in Section 3.5.2. As a result, the dataset generation for unsupervised learning is orders of magnitudes (100 times in this case) faster than in the case of supervised learning. As a consequence, unsupervised learning helps the system to generate the dataset as large as possible without considering the preparation time for optimal solutions.

Computational Complexity of Training Phase

Training phase of DNN is quite important in terms of time and computational complexity in the off-line mode. In Table 3.3, the number of trainable parameters of our proposed methods are compared to the ones obtained with state-of-the-art DNN-based HBF design [105, 107, 108]. This metric provides a good indication of the DNN complexity in the

Table 3.3 Number of Parameters in DNN-Based HBF

DNN-Based HBF Technique	# Parameters ($\times 10^6$)
Proposed **HBF-Net**	**2.1**
Proposed **AFP-Net**	**2.5**
CNN-Based HBF [108]	6.7
CNN-Based Beamforming [105]	10.6
CNN-MIMO [107]	72

($N_{\mathsf{U}} = 4$, $N_{\mathsf{RF}} = 8$ and $N_{\mathsf{T}} = 64$)

training phase. It is shown that our proposed methods required a much lower number of trainable parameters when compared to other DNN-based methods. As explained in Section 3.6.1, the size of the last layer for the regression task is different for the HBF-Net and AFP-Net approaches. Therefore, the number of parameters in AFP-Net is larger than HBF-Net. It is worth considering that our proposed methods, despite using the multi-tasking DNN, have less number of parameters when compared to other single task DNNs. As a result, the proposed approaches improve the training processing time by reducing the training overhead. For a fair comparison, we consider the following configuration for all considered DNNs: $N_{\mathsf{U}} = 4$, $N_{\mathsf{RF}} = 8$ and $N_{\mathsf{T}} = 64$.

Computational Complexity of Inference Phase

Since we aim to use the DL methods to reduce the complexity of hybrid beamforming design, the inference processing time should be carefully evaluated in DNN-based hybrid beamforming solution. As shown in Table 3.3, the number of parameters of the proposed methods are lower than other DNN-based hybrid beamforming design, which translates into lower processing time. Moreover, in Table 3.4, we compare the computational complexity of the inference phase of our proposed DNN methods to the complexity of conventional non-DL methods.

Analytical expressions are provided to evaluate the computational complexity in terms of the number of real multiplications (RM). We assume that one complex multiplication (CM) corresponds to 4 RMs, and 1 complex division corresponds to 8 RMs (assuming 1 real division is equal to 1 RM). Only the matrix multiplications and inversions are taken into consideration, the other operations are considered negligible. A complex multiplication between a first matrix of size $N \times P$ and a second matrix of size $P \times M$ requires NMP CMs. To invert a

Table 3.4 Complexity comparison of Proposed method and state-of-the-art

Hybrid Beamforming Technique	Analytical expression (# of real multiplications)	# Multiplications ($\times 10^6$)
Proposed **HBF-Net**	$\text{DNN}_{\mathsf{core}} + f_2(L + 2N_{\mathsf{U}}N_{\mathsf{RF}})$	2.82
Proposed **AFP-Net**	$\text{DNN}_{\mathsf{core}} + f_2(L + 2N_{\mathsf{U}}N_{\mathsf{T}}) + 4N_{\mathsf{RF}}((N_{\mathsf{RF}}-1)(2N_{\mathsf{RF}}-1)/24 + N_{\mathsf{T}}(N_{\mathsf{RF}} + 2N_{\mathsf{U}}))$	3.35
FDP design (Section 3.4.3)	$4 \times (2^{N_{\mathsf{U}}} - 1)\Big(2N_{\mathsf{U}}N_{\mathsf{T}}^2 + N_{\mathsf{U}}^2N_{\mathsf{T}} + \frac{1}{3}N_{\mathsf{T}}^3\Big)$	7.27
HSHO, AP design	$4N_gN_cN_{\mathsf{RF}}(N_{\mathsf{U}}(N_{\mathsf{T}} + N_{\mathsf{RF}}) + N_{\mathsf{RF}}^2)$	$2.2N_g$
HSHO, DP design	Similar to FDP design, replace N_{T} by N_{RF}	0.05
OMP [127]	$\approx 4L(N_{\mathsf{T}}N_{\mathsf{U}} + L) + N_{\mathsf{RF}}^2\Big(\frac{1}{3}N_{\mathsf{RF}}^2 + \frac{4}{3}N_{\mathsf{RF}}(N_{\mathsf{T}} + N_{\mathsf{U}}) + 4N_{\mathsf{T}}N_{\mathsf{U}}\Big)$	0.478
FDP + OMP	Complexity of OMP and FDP design (3.4.3)) combined	7.74
PZF [135]	$\frac{28}{3}N_{\mathsf{RF}}^3 + 8N_{\mathsf{T}}N_{\mathsf{RF}}^2$	0.036

($N_{\mathsf{U}} = 4$, $N_{\mathsf{RF}} = 8$ and $N_{\mathsf{T}} = 64$)

square matrix of size N, around $N^3/3$ CMs are required if the Gaussian elimination algorithm is employed. Finally, we consider that the eigenvalues of a square matrix (size N) are obtained using Cholesky decomposition [152], which requires approximately $4N^3$ RMs. For the HSHO AP design, N_g corresponds to the number of generations to find a solution (we noticed that typically $N_g \approx 400$). For the DNNs, the number of RMs is calculated for each layer separately, and then summed. The depth of the l^{th} fully connected layer and convolution layer are respectively denoted as f_l and c_l. Since the DNN architecture is the same for both approaches except for the output layer, we define $\text{DNN}_{\mathsf{core}} = (c_1 + c_1c_2 + c_2c_3 + c_3f_1/\kappa^2)KN_{\mathsf{U}}\kappa^2 + f_1f_2$ as the number of multiplications required to evaluate the DNN layers other than the output layers.

The same set of parameters for comparing the complexity in the training phase are considered for the inference phase. It is shown in Table 3.4 that the proposed DNNs are 1500 times less complex than the HSHO, which generates the near-optimal DP and AP solutions. When considering the OMP technique, it is important to note that it requires an FDP solution as input. Therefore, for a fair comparison, the complexity related to the design of the FDP needs to be taken into account. Assuming that the FDP is obtained using the method presented in Section 3.4.3, the proposed DNN-based methods are almost 2.5 times less complex than the OMP (with FDP) technique while achieving better SE performance. The PZF is the least complex technique, but also has very poor performance for low SNR or small number of antennas, as shown in Fig. 3.6, Fig. 3.7, and Fig. 3.11. It is worth mentioning that, for all non-DNN HBF techniques in Table 3.4, the channel is assumed to be perfectly known. In practice, channel estimation needs to be performed which further increases the complexity of the non-DNN techniques.

3.8 Conclusion

Hybrid beamforming is an essential technology for mMIMO systems that allows reducing the number of RF chains and therefore increases the energy efficiency of the system. However, the design of digital and analog precoders is challenging, and the estimation of the CSI introduces important signaling overhead, especially in FDD communication. To alleviate this issue, we instead proposed relying on RSSI feedback, improving the spectral efficiency of the communication system. The SS burst was efficiently designed so that the RSSIs provide maximum information about the CSI. We then proposed to design the hybrid beamforming by using unsupervised deep-learning methods. This unsupervised learning approach leads to decreased training time and cost since the system can be trained using only channel measurements without the costly need to obtain optimal solutions. The deep-learning methods select the AP from a codebook designed to reduce the complexity without sacrificing the SE performance. Finally, the performance of the proposed algorithm was evaluated using the realistic *deepMIMO* channel model. The results demonstrate that, despite not having access to the full CSI, the BS can be trained to robustly design the hybrid beamforming while achieving a similar SE as the HSHO near-optimal hybrid precoder that was introduced as a benchmark. Moreover, the proposed method can be implemented in real-time systems thanks to its low computational complexity.

CHAPTER 4 ARTICLE 2: DECENTRALIZED BEAMFORMING FOR CELL-FREE MASSIVE MIMO WITH UNSUPERVISED LEARNING

This chapter is a reproduction of an article published in IEEE Communications Letters on 4 March 2022.

- H. Hojatian, J. Nadal, J. -F. Frigon and F. Leduc-Primeau, "Decentralized Beamforming for Cell-Free Massive MIMO With Unsupervised Learning," in IEEE Communications Letters, vol. 26, no. 5, pp. 1042-1046, 4 March 2022.

4.1 Abstract

CF-mMIMO systems represent a promising approach to increasing the spectral efficiency of wireless communication systems. However, near-optimal beamforming solutions require a large amount of signaling exchange between access points (APs) and the network controller (NC). In this letter, we propose two unsupervised deep neural networks (DNN) architectures, fully and partially distributed, that can perform decentralized coordinated beamforming with zero or limited communication overhead between AcPs and NC, for both fully digital and hybrid precoding. The proposed DNNs achieve near-optimal spectral efficiency (SE) while also reducing complexity by $10 - 24\times$ compared to conventional near-optimal solutions.

4.2 Introduction

CF-mMIMO networks have the potential to significantly improve the efficiency of future wireless networks, as compared to cellular networks, by serving uniformly multiple users simultaneously using multi-antenna AcPs connected to a central NC [10]. Similar to standard mMIMO systems, CF-mMIMO requires designing suitable precoders for data transmission, with the added challenge that information exchange between AcPs and NC should be minimized [80]. Existing techniques tend to exhibit a trade-off in that regard. For instance, in the context of FDP, the simple and scalable CB method can be implemented locally by each AcPs and achieves acceptable performance without information exchange [82]. On the other hand, the ZF method achieves much better performance, but the precoders are computed centrally in the NC at the expense of fronthaul overhead [82].

HBF is a well-known approach to reduce energy consumption by decreasing the number

of RF chains in the transmitter without reducing the number of antennas [6]. However, designing HBF precoders that achieve near-optimal performance usually has a high computational cost. Several works have investigated the use of DL to design the HBF for single-cell communication [46, 100, 101], but extending these solutions to CF-mMIMO imposes a large signaling overhead between AcPs and NC to exchange the beamforming information. In [101], the authors proposed a supervised deep learning-based beamforming design for coordinated beamforming. However, they consider the beamforming vectors to be centrally designed in the NC, and only consider a simple analog beamforming scenario with one RF chain per base station. Moreover, all mentioned studies either assume that the CSI is known or the system operates in TDD with perfect channel reciprocity. However, in practice, the channel reciprocity may not be accurate due to calibration errors, hardware problems, or time-varying channels [153].

In this letter, we consider a FDD CF-mMIMO system with multiple AcPs, each equipped with HBF, cooperatively serving multiple users simultaneously. We propose distributed unsupervised DL-based solutions to perform decentralized HBF cooperatively and we show that appropriate training of the DNNs allows eliminating all fronthaul signaling overhead during the online phase. The proposed solutions follow a similar approach as the single-cell method proposed in [46], which used RSSI feedback to simplify the CSI acquisition. In this letter, we show how this single-cell method can be adapted to a distributed scenario. Through simulations based on the *deepMIMO* ray-tracing model [141], we show that the proposed solution can achieve near-optimal SE performance with reduced complexity compared to existing approaches. We also provide an example of the trade-off between overall computational complexity and signaling overhead by designing an alternative architecture for which complexity is further reduced at the cost of increased fronthaul signaling. In addition, we show that the proposed schemes can also be used to reduce the computational complexity and signaling overhead in a coordinated FDP system.

The rest of this letter is organized as follows. Section 4.3 gives the system model and describes the necessary optimization problems. Section 4.4 then presents the proposed DNN architectures. Numerical results are discussed in Section 4.5, and Section 4.6 concludes this letter.

4.3 System Description

We consider a CF-mMIMO network, where M APs each equipped with N_{T} antennas communicate with a NC through a fronthaul connection while serving simultaneously N_{U} single antenna users. Each AcP is assumed to have $N_{\mathsf{RF}} << N_{\mathsf{T}}$ RF chains. The signal received by

each user is

$$y_u = \sum_{\forall m} \mathbf{h}_{u,m}^{\mathrm{H}} \mathbf{A}_m \mathbf{w}_{u,m} x_u + \sum_{\forall m} \mathbf{h}_{u,m}^{\mathrm{H}} \mathbf{A}_m \sum_{j \neq u} \mathbf{w}_{j,m} x_j + \eta_u,$$

where x_u is transmit symbol for user index u, $\mathbf{h}_{u,m}$ is the channel vector between the u^{th} user and m^{th} AcP, $\mathbf{A}_m \in \{1, -1, i, -i\}^{N_{\mathsf{T}} \times N_{\mathsf{RF}}}$ is the AP selected from the m^{th} codebook ($\mathcal{A}_m$), $\mathbf{w}_{u,m} \in \mathbb{C}^{N_{\mathsf{U}} \times 1}$ is the DP for the u^{th} user, and η_u is the zero-mean Gaussian noise with variance σ^2. The SINR for the u^{th} user is given by

$$\mathrm{SINR}_u(\mathbf{A}, \mathbf{W}) = \frac{\left| \sum_{\forall m} \mathbf{h}_{u,m}^{\mathrm{H}} \mathbf{A}_m \mathbf{w}_{u,m} \right|^2}{\left| \sum_{\forall m} \mathbf{h}_{u,m}^{\mathrm{H}} \mathbf{A}_m \sum_{j \neq u} \mathbf{w}_{j,m} \right|^2 + \sigma^2}, \tag{4.1}$$

where the global AP is defined as the block diagonal matrix $\mathbf{A} = \mathrm{diag}(\mathbf{A}_1, ..., \mathbf{A}_M)$ since M separate APs are deployed, and the global DP is defined as $\mathbf{W} = [\mathbf{W}_1, \cdots, \mathbf{W}_M]^{\mathrm{T}}$. The SE of the system is therefore $R_{\mathrm{HBF}}(\mathbf{A}, \mathbf{W}) = \sum_{\forall u} \log_2(1 + \mathrm{SINR}_u(\mathbf{A}, \mathbf{W}))$. We focus on cell-free hybrid beamforming (CF-HBF) design to maximize the SE corresponding to the following optimization problem:

$$\max_{\{\mathbf{A}, \mathbf{W}\}} \quad R_{\mathrm{HBF}}(\mathbf{A}, \mathbf{W}) = \sum_{\forall u} \log_2(1 + \mathrm{SINR}_u(\mathbf{A}, \mathbf{W})) \tag{4.2a}$$

$$\text{s.t.} \quad \sum_{\forall m} \mathbf{w}_{u,m}^{\mathrm{H}} \mathbf{A}_m^{\mathrm{H}} \mathbf{A}_m \mathbf{w}_{u,m} \leq P_{\mathsf{max}}, \tag{4.2b}$$

$$\mathbf{A}_m \in \mathcal{A}_m \qquad \forall m, \tag{4.2c}$$

where P_{max} stands for the total maximum transmission power in the CF-mMIMO network. In this paper, without loss of generality, we consider $P_{\mathsf{max}} = 1$.

4.3.1 Baseline CF-mMIMO Beamforming With Perfect CSI

According to (4.1), a fully connected CF-HBF can be seen as a single mMIMO cell equipped with $M \times N_{\mathsf{T}}$ antenna and $M \times N_{\mathsf{RF}}$ RF chains. Therefore, the general approach is to first jointly design the FDP for all AcP. Then, the AP and DP are designed independently for each of the M AcPs using

$$\underset{\mathbf{A}_m}{\text{minimize}} \left\| \mathbf{U}_m - \mathbf{A}_m \mathbf{W}_m \right\|^2 \qquad \text{s.t. (4.2b), (4.2c),} \tag{4.3}$$

where $\mathbf{U} = [\mathbf{U}_1, ..., \mathbf{U}_M]$ is the global FDP matrix, $\mathbf{U}_m = [\mathbf{u}_{1,m}, ..., \mathbf{u}_{N_{\mathsf{U}},m}]^{\mathrm{T}}$ is the FDP for AcP index m and $\mathbf{u}_{u,m} \in \mathbb{C}^{N_{\mathsf{T}} \times 1}$ is the FDP vector in the m^{th} AcP for user index u. To obtain the FDP solution we define the optimization problem over all AcPs as,

$$\max_{\{\mathbf{U}\}} \quad \sum_{\forall u} R_{\mathrm{FDP}}(\mathbf{U}) \tag{4.4a}$$

$$\text{s. t.} \quad \sum_{\forall u} \mathbf{U}^{\mathrm{H}}\mathbf{U} \leq P_{\mathsf{max}}, \tag{4.4b}$$

where $R_{\mathrm{FDP}}(\mathbf{U}) = \sum_{\forall u} \log_2(1 + \mathrm{SINR}_u(\mathbf{U}))$ and

$$\mathrm{SINR}_u(\mathbf{U}) = \frac{\left| \sum_{\forall m} \mathbf{h}_{u,m}^{\mathrm{H}} \mathbf{u}_{u,m} \right|^2}{\left| \sum_{\forall m} \mathbf{h}_{u,m}^{\mathrm{H}} \sum_{j \neq u} \mathbf{u}_{j,m} \right|^2 + \sigma^2}\,. \tag{4.5}$$

We employed a method described in [52], which was demonstrated in [46]. Using the PE-AltMin solution presented in [64], the optimization problem in (4.3) can be solved. As a baseline for evaluating DNN-based systems, we consider this solution (PE-AltMin + O-FDP). However, this near-optimal method is difficult to implement in real-time systems due to its heavy computational complexity. Furthermore, it depends on having the full CSI and it is a centralized method, where the HBF vectors are computed in the NC and then sent to each AcP, thus requiring high capacity fronthaul links.

4.3.2 Beam Training

Beam training is required for IA and to obtain CSI between the AcPs and the users. CSI acquisition is a challenging task for FDD mMIMO. Therefore, we use a beam training method that relies on RSSI feedback instead of explicit CSI [140]. Our proposed beam training for CF-mMIMO follows a similar approach as in the single-cell case. However, in the CF-mMIMO, each AcP takes a turn sending its SSB, and each user measures the RSSIs from each AcP. Each burst $k \in \{1, 2, ..., K\}$ uses a different analog-only beamforming $\mathbf{a}_{\mathsf{SS,m}}^{(k)} \in \{1, -1, i, -i\}^{N_{\mathsf{T}} \times 1}$. Alternatively, the SSB of each AcP can be transmitted in parallel by all APs, during the same time slots. Our experiments indicate that this requires $K \times M$ RSSI values to achieve similar SE performance, and therefore the spectral efficiency remains identical. For simplicity, we consider the first approach where each AcP transmits its SSB sequentially. The SSBs are designed for each AcP individually using the method proposed in [46]. The SSB $\mathbf{a}_{\mathsf{SS,m}}^{(k)}$ sent by the m^{th} AcP in the downlink channel is received by all users. Therefore, the received signal at the u^{th} user for the k^{th} burst from the m^{th} AcP is $r_{u,m}^{(k)} = \mathbf{h}_{u,m}^{\mathrm{H}} \mathbf{a}_{\mathsf{SS,m}}^{(k)} + \eta_u^{(k)}$. In the next step, the RSSI values $\alpha_{u,m}^{(k)}$ are measured by the u^{th} user for the k^{th} SSB burst as $\alpha_{u,m}^{(k)} = \left| r_{u,m}^{(k)} \right|^2 + \sigma^2$. Then, each user sends a set of measured RSSIs ($\alpha_{u,m} = [\alpha_{u,m}^{(1)}, ..., \alpha_{u,m}^{(K)}]$) through a dedicated error-free feedback channel to the corresponding

AcP. Therefore each user sends back K RSSI values, and the RSSIs received by m^{th} AcP is $\alpha_m = [\alpha_{1,m}, ..., \alpha_{N_\text{u},m}]^\text{T}$. These RSSIs are then provided as input to the DNNs that design the precoding, as described in Section 4.4.

4.3.3 Codebook Design for Hybrid Beamforming

The number of possible AP phase combinations grows exponentially with the number of antennas and RF chains. However, for a given channel environment, only a subset of these combinations are useful, and we can thus seek to design an optimized *codebook* of AP phases. A 3-step codebook design is proposed in [46]. In this letter, we used the PE-AltMin algorithm proposed in [64]. Then, the codebook size is iteratively reduced by discarding the less-used AP solutions. Here, we use a similar method to design the codebook $\mathcal{A}_m$ for each AcP individually. Thus, the codebook size for each AcP may differ due to its location and channel environment. Note that the codebooks are designed only once in the offline phase.

4.4 Distributed DNNs for Cell-Free Beamforming

We propose two possible architectures for DNN-based cell-free beamforming in Fig.4.1, each achieving a different trade-off between computational complexity and signaling overhead. In the first architecture, fully decentralized beamforming, the trained DNN is fully distributed and the NC does not participate in beamforming design. In the second architecture, partially decentralized beamforming, only the last two layers of the DNN are distributed at each AcP, and the NC remains involved in the online phase for beamforming design.

4.4.1 Fully Decentralized Beamforming

The proposed fully distributed architecture, called "FullDeC-HBF" for HBF or "FullDeC-FDP" for FDP, is shown in Fig 4.1-(a). The main idea is to completely transfer the signaling exchange of the beamforming from the online phase to the offline phase. To do so, the architecture is composed of M parallel local-DNNs, each taking as input only the RSSIs α_m associated with the m^{th} AP, which have been obtained using the beam training described in Section 4.3.2. These networks are trained jointly, but during the online mode, each AcP uses only its trained local-DNN, and designs its beamforming vector locally, which eliminates the fronthaul signaling overhead.

In *FullDeC-HBF*, a multi-tasking DNN is considered, which jointly performs the regression and classification task to respectively design the DP and the AP. Each local-DNN consists of 2 CLs with 32 channels and 3×3 kernels, followed by 2 FLs with 512 neurons connected

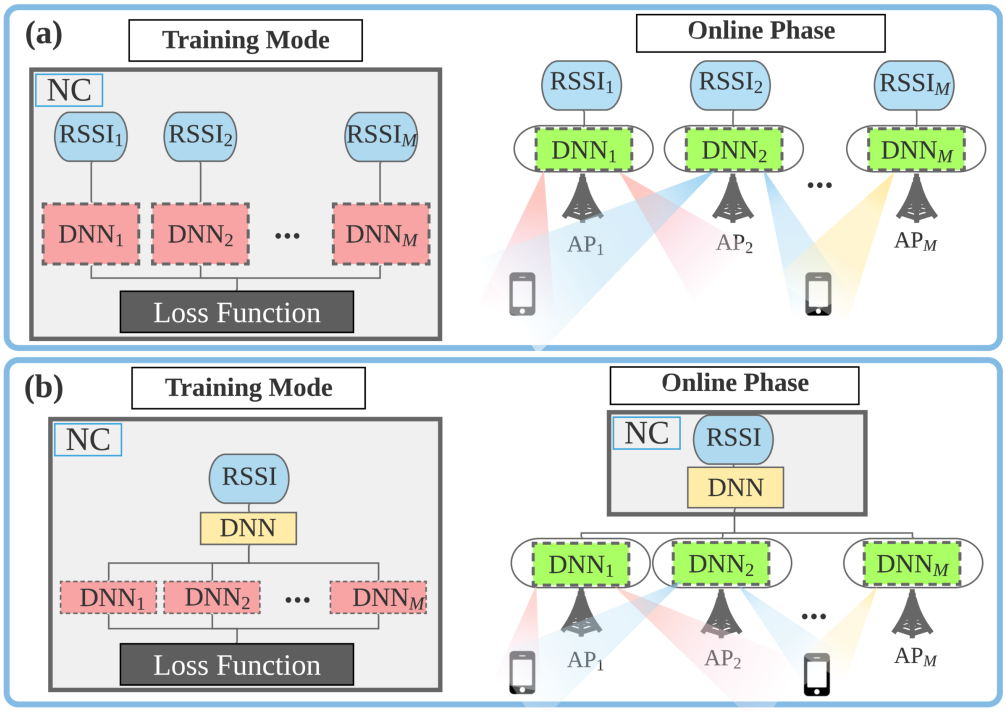

Figure 4.1: a) Fully distributed DNN "FullDeC-HBF" or "FullDeC-FDP", b) Partially distributed DNN "PartDeC-HBF" or "PartDeC-FDP"

to the output layer. Since we use real-valued DNNs, the output layer for the regression task has size $2 \times N_{\mathsf{RF}} \times N_{\mathsf{U}}$ for each local-DNN. All non-output layers use the "LeakyReLU" activation function and for the output layer of the classifier, the "Softmax" is used to assign a probability to each codeword in the codebook. Hence, we define $\mathbf{p}_m = [p_{1,m}, ..., p_{l,m}, ..., p_{L_m,m}]$ as the output of each classifier, where $p_{l,m}$ corresponds to the probability of the l^{th} codeword in the codebook of the m^{th} AcP and $L_m = |\mathcal{A}_m|$ is the size of m^{th} codebook. The size of the classifier in each local-DNN corresponds to the length of the local codebook. For the FDP case, the architecture of *FullDeC-FDP* is the same as *FullDeC-HBF*, except for the output layer which only consists of a regression task since there is no AB.

Since we design M parallel local-DNNs, the complexity scales linearly in terms of the number of AcPs. To address this concern, we propose another architecture in the following based on the auto-encoder concept, enabling lower computational complexity than fully decentralized beamforming.

4.4.2 Partially Decentralized Beamforming

The second architecture, called "PartDeC-HBF" for HBF or "PartDeC-FDP" for FDP, is shown in Fig 4.1-(b). Here, we designed the DNN partially distributed with a combination

of shared and unshared layers in the offline phase. The first idea behind this architecture is to use some shared layers to reduce the total computational complexity both in the offline phase and the online phase. To do so, we used 2 shared CLs with 32 channels, one FL with 1024 neurons followed by M parallel groups of unshared layers. Each group consists of 2 FLs with 200 and 1024 neurons. The second idea is to use the last shared layer and a first unshared layer to form an auto-encoder to reduce the signaling overhead. The activation functions are the same as in the fully decentralized case. For the FDP case, *PartDeC-FDP* is derived from *PartDeC-HBF* by keeping only the regression task in the output layer.

4.4.3 Training Mode (Offline Phase)

As shown in Fig4.1-(a), all local-DNNs in *FullDeC-HBF* or *FullDeC-FDP* are trained jointly, for instance inside the NC, and all of them are fed with quantized RSSIs obtained from users, as described in Section 4.3. Since we aim to train the DNN with unsupervised learning, we propose the following loss function to train the DNNs for HBF:

$$\mathcal{L}_{\mathrm{HBF}} = -\sum_{l_1=1}^{L_1} ... \sum_{l_M=1}^{L_M} \left(R_{\mathrm{HBF}}(\bar{\mathbf{A}}_{l_1,...,l_M}, \bar{\mathbf{W}}) \prod_{m=1}^{M} p_{l_m,m} \right), \tag{4.6}$$

where $\bar{\mathbf{W}}$ is the DP output of the DNN, $\bar{\mathbf{A}}_{l_1,...,l_M} = \mathrm{diag}(\bar{\mathbf{A}}_{l_1}, ..., \bar{\mathbf{A}}_{l_M})$, and $\bar{\mathbf{A}}_{l_m}$ is the AB corresponding to the l_m^{th} codeword. Thus, the loss function is defined by the expected SE of the system for the given codeword combinations for all local DNNs. Likewise, we define $\mathcal{L}_{\mathrm{FDP}} = -R_{\mathrm{FDP}}(\bar{\mathbf{U}})$ for the FDP where $\bar{\mathbf{U}}$ is the output of the DNN in *FullDeC-FDP*. The CSI is assumed to be known only during DNN training. In practice, CSI could be acquired once during an initial measurement campaign by the APs.

Moreover, batch normalization and dropout are used during training. Finally, to satisfy $\sum_{\forall m} ||\bar{\mathbf{A}}_{l_m} \bar{\mathbf{w}}_m||^2 = 1$, we further normalize $\bar{\mathbf{w}}_m$ using the approach proposed in [82] for power allocation. The offline phase for *PartDeC-HBF* or *PartDeC-FDP* shown in Fig 4.1-(b) follows the same procedures.

4.4.4 Testing Mode (Online Phase)

In the evaluation phase, each AcP is assumed to have a local copy of a portion of the DNN (green boxes in Fig. 4.1). In the case of the fully distributed systems (*FullDeC-HBF* or *FullDeC-FDP*), the local DNNs are fully independent, and each AcP is able to directly design the precoding as soon as it receives its quantized RSSI feedback. In the case of the partially distributed systems (*PartDeC-HBF* or *PartDeC-FDP*), the local DNNs receive inputs from

Table 4.1 Comparison of Beamforming Type, Signaling Exchange, and Complexity ($N_{\mathsf{T}} = 64$, $N_{\mathsf{RF}} = 8$, $N_{\mathsf{U}} = 4$, $K = 16$, $M = 4$)

Technique	Beamforming Type	# RF chains (per AP)	Signaling Exchange AcPs → NC	Signaling Exchange NC → AcPs	# multiplications ($\times 10^6$)	SE (bit/s/Hz)	Architecture Type
O-FDP [52]	FDP (Perfect CSI)	N_{T}	$2MN_{\mathsf{T}}N_{\mathsf{U}}$	$2MN_{\mathsf{T}}N_{\mathsf{U}}$	358.2	24.6 (100%)	Centralized
ZF [82]	FDP (Perfect CSI)	N_{T}	$2MN_{\mathsf{T}}N_{\mathsf{U}}$	$2MN_{\mathsf{T}}N_{\mathsf{U}}$	24.4	24.4 (99%)	Centralized
FullDeC-FDP	FDP (**RSSI-based**)	N_{T}	0	0	2.9	**23.3** (95%)	Decentralized
PartDeC-FDP	FDP (**RSSI-based**)	N_{T}	KMN_{U}	$200M$	1.3	**23.2** (94%)	Centralized
CB [82]	FDP (Perfect CSI)	N_{T}	0	0	0	13.1 (52%)	Decentralized
PE-AltMin [64] + O-FDP	HBF (Perfect CSI)	N_{RF}	$2MN_{\mathsf{T}}N_{\mathsf{U}}$	$2MN_{\mathsf{RF}}(N_{\mathsf{T}} + N_{\mathsf{U}})$	369.2	20.2 (100%)	Centralized
PE-AltMin [64] + ZF [82]	HBF (Perfect CSI)	N_{RF}	$2MN_{\mathsf{T}}N_{\mathsf{U}}$	$2MN_{\mathsf{RF}}(N_{\mathsf{T}} + N_{\mathsf{U}})$	26.2	19.7 (97%)	Centralized
FullDeC-HBF	HBF (**RSSI-based**)	N_{RF}	0	0	2.7	**19.5** (96%)	Decentralized
PartDeC-HBF	HBF (**RSSI-based**)	N_{RF}	KMN_{U}	$200M$	1.1	**19.4** (96%)	Centralized

(Hyper-parameters: Mini-batch size = 1000, Initial lr = 0.001, Weight decay = 10^{-6}, Dropout = .05, Zero padding = 1, BatchNorm $\epsilon = 10^{-5}$)

the shared DNN layers (yellow box) in the NC. Consequently, the quantized RSSI input is first processed by the NC, and then the real-valued outputs of the shared DNN are sent from the NC to the APs, which then evaluate the last layers to output the precoding. Note that, although the NC is engaged in the online mode, the signaling overhead is nonetheless reduced compared to a conventional method since the last layer in the NC and the first layer in each AcP is sized to form an auto-encoder.

4.5 Simulation Results

In this section, the performance of the four proposed architectures (two for HBF and two for FDP), implemented using the PyTorch DL framework, are evaluated numerically. The deepMIMO channel model [141] is employed to generate the dataset, with parameters `active_BS` $= \{3 : 10\}$, `active_user_first` $= 1100$ and `active_user_last` $= 2200$. The training dataset consists of only RSSIs and CSI, which could be obtained in practice through an initial measurement campaign. There are M AcPs ($M \in \{2, 4, 8\}$), each equipped with $N_{\mathsf{T}} = 64$ antennas and $N_{\mathsf{RF}} = 8$ RF chains with 2-bit phase shifters serving $N_{\mathsf{U}} = 4$ users located randomly. The number of SSBs is $K = 16$, and the RSSI feedback values are quantized on 8 bits. The size of the DNN dataset is set to 10^6 samples, with 85% of the samples used for the training set and the remaining ones used to evaluate the performance as the test set. The mini-batch size, learning rate, and weight decay are set to 1000, 0.001, and 10^{-6}, respectively. Due to the lack of space, the DNN training and testing curves are not shown. However, no overfitting or underfitting was observed, and the training procedure converged after approximately 120 epochs.

Table 4.1 compares the amount of signaling exchange, the computational complexity, and the SE performance of the proposed methods with existing approaches for $\sigma^2 = -130$ dBW. The top and bottom rows of Table 4.1 respectively present results for FDP and HBF techniques.

Counting the number of transferred real matrix coefficients between the AcPs and NC reveals the amount of signal exchange. For the computational complexity, we consider the number of real multiplications (RM) for each matrix multiplication and inversion involved in the algorithms. We assume that one complex multiplication (CM) corresponds to 4 RMs. General expressions for the number of RMs required by O-FDP and by each DNN layer can be found in [46]. In order to fairly compare the complexity of the alternative solutions, the DNNs are sized such that the "Full" and "Part" DNNs achieve approximately the same SE.

As a near-optimal baseline for HBF, we adapted *PE-AltMin* [64] for the case of 2-bit phase shifters. For FDP, we compare with ZF and CB. Since the *PE-AltMin* method is based on knowing the FDP matrix, Table 4.1 considers both a high complexity near-optimal approach (O-FDP) and a low complexity approach (ZF). The average number of iterations for *PE-AltMin* to converge is $\ell = 18$. Therefore, considering that the singular-value decomposition of an $m \times n$ matrix requires $4m^2n + 22n^3$ RMs [154], the number of RMs for *PE-AltMin* can be expressed as $\ell M(8N_{\mathsf{RF}}N_{\mathsf{U}}(N_{\mathsf{T}} + N_{\mathsf{U}}) + 22N_{\mathsf{RF}}^3)$.

When compared to the *PE-AltMin* + ZF technique, *PartDeC-HBF* has a slight SE loss of 1%, but requires 80% less signaling exchange (uplink + downlink), and is 24× less complex. Moreover, perfect CSI is used for all reference approaches, whereas the proposed DNNs only rely on RSSI measurements as described in Section 4.3. On the other hand, *FullDeC-HBF* also has a SE loss of 1%, but requires no signaling exchange while being almost 10× less complex. In comparison to the *PE-AltMin* + O-FDP, *FullDeC-HBF* and *PartDeC-HBF* are respectively 136× and 335× less complex at the cost of a 4% SE reduction compared to *PE-AltMin* + O-FDP. Therefore, proposed DNNs provide near-optimal HBF solutions with significantly less complexity and signaling exchange than traditional methods. As expected, for FDP, O-FDP and ZF provide the best SE in a high SNR regime. The complexity of ZF is given by $4M^2N_{\mathsf{T}}^2(2N_{\mathsf{U}} + MN_{\mathsf{T}}/3)$. However, *FullDeC-FDP* and *PartDeC-FDP* have almost 8× and 18× lower computational complexity than ZF, respectively, at the cost of 4% SE loss. For *PartDeC-FDP*, the signaling exchange between AcPs and the NC is reduced by 60% when compared to the ZF solution, while there is no signaling exchange for *FullDeC-FDP*. CB is the less complex of all techniques and requires no signaling overhead. However, both proposed DNN-based FDP solutions outperform CB by 77%. It is worth noting that FDP requires one RF chain per antenna and is thus less energy efficient compared to HBF techniques. We can note also that the amount K of feedback can be reduced at a moderate cost in SE. For instance, compared to $K = 16$, $K = 8$ and $K = 4$ achieve 86% and 64% of the SE, respectively, for all the proposed methods and under the same conditions as in Table 4.1.

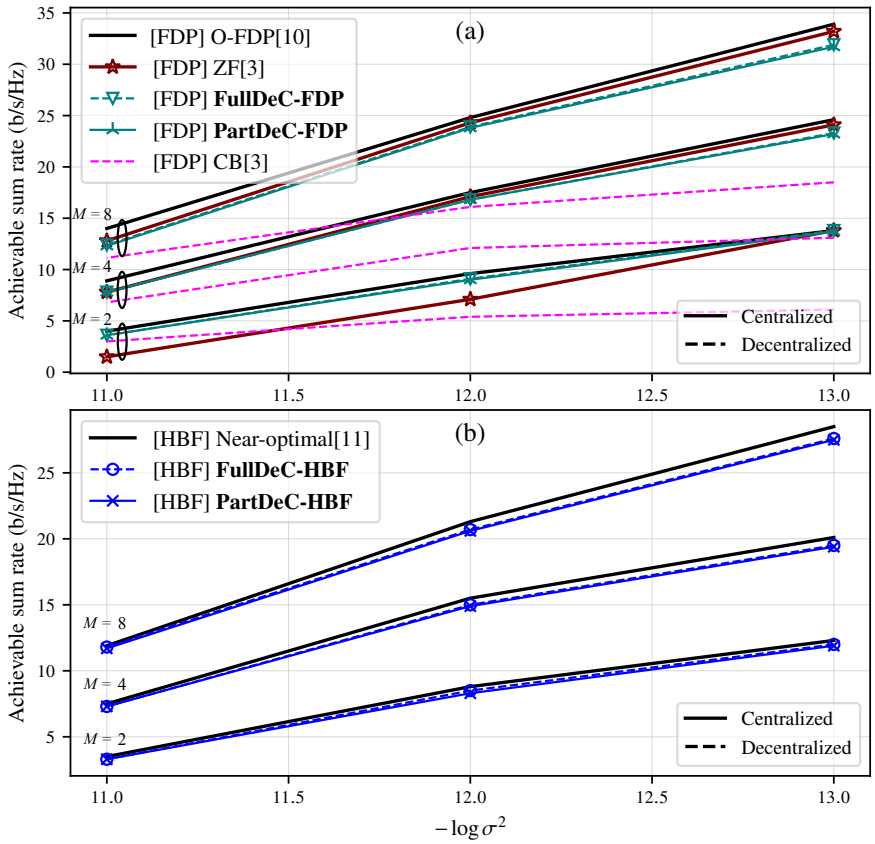

Figure 4.2: Achievable spectral efficiency (b/s/Hz) performance (a) FDP, (b) HBF

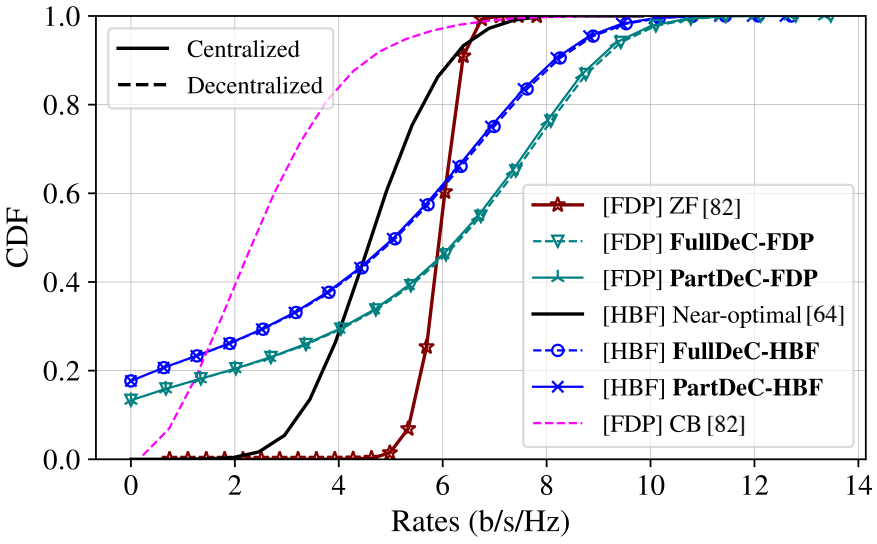

Figure 4.3: CDFs of the per-user spectral efficiency ($\sigma^2 = -130$ dBW, $M = 4$, $N_{\mathsf{T}} = 64$)

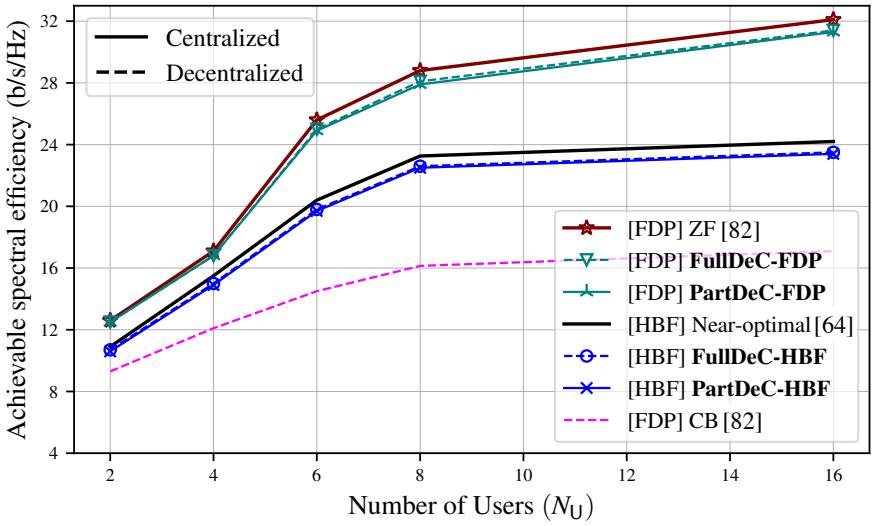

Figure 4.4: Spectral efficiency versus N_{U} ($\sigma^2 = -120$ dBW, $M = 4$, $N_{\mathsf{T}} = 64$)

In Fig. 4.2, we evaluated the SE of the proposed solutions for FDP and HBF, where in Fig. 4.2 (a) we compared the FDP solution with O-FDP [52], ZF and CB [82], and in Fig. 4.2 (b), the proposed HBF solution is compared with the near-optimal PE-AltMin solution [64]. We consider different noise power values σ^2 ranging from -110 dBW to -130 dBW. When considering the channel attenuation, the average SNRs are between 3.1 dB and 23.1 dB. It shows that the proposed HBF and FDP solutions provide near-optimal SE performance with a decentralized architecture over this noise power range. Among FDP solutions, CB has poor performance in the high SNR regime because user interference is more dominant. On the other hand, ZF has poor performance when the number of AcPs is low. Fig. 4.3 shows the cumulative distribution function (CDF) of the per-user rates. It is shown that the proposed DNNs focus on maximizing the average SE and neglect users with worse channels. This is expected since no notion of fairness has been included in the loss function used to train the DNNs. Finally, we evaluate in Fig. 4.4 the proposed solutions for different numbers of users. It can be seen that the performance remains comparable to the near-optimal schemes. Since the number of RF chains ($N_{\mathsf{RF}} = 8$) is fixed, the performance gap between HBF and FDP increases with the number of users.

4.6 Conclusion

CF-mMIMO is a promising technique to increase the throughput and improve the coverage, but conventional approaches for designing the precoder are complex and require a significant communication overhead, both in the case of FDP and HBF architectures. In this paper, we

proposed two RSSI-based DNNs with distributed architectures to design a coordinated FDP or HBF precoder. The experiments on a ray-tracing channel model show that the proposed DNNs can achieve near-optimal performance for both FDP and HBF systems, while significantly reducing the computational complexity and the signaling overhead. Furthermore, the signaling overhead can be completely eliminated at the cost of increased complexity.

CHAPTER 5 ARTICLE 3: LEARNING ENERGY-EFFICIENT TRANSMITTER CONFIGURATIONS FOR MASSIVE MIMO BEAMFORMING

This chapter is a reproduction of an article submitted to IEEE Transactions on Machine Learning in Communications and Networking on 11 August 2023.

- H. Hojatian, Z.Mlika, J. Nadal, J. -F. Frigon and F. Leduc-Primeau, "Learning Energy-Efficient Transmitter Configurations for Massive MIMO Beamforming," in IEEE Transactions on Machine Learning in Communications and Networking, submitted, Aug. 2023.

5.1 Abstract

Hybrid beamforming (HBF) and antenna selection are promising techniques for improving the energy efficiency (EE) of massive multiple-input multiple-output (mMIMO) systems. However, the transmitter architecture may contain several parameters that need to be optimized, such as the power allocated to the antennas and the connections between the antennas and the radio frequency chains. Therefore, finding the optimal transmitter architecture requires solving a non-convex mixed integer problem in a large search space. In this paper, we consider the problem of maximizing the EE of fully digital precoder (FDP) and hybrid beamforming (HBF) transmitters. First, we propose an energy model for different beamforming structures. Then, based on the proposed energy model, we develop an unsupervised deep learning method to maximize the EE by designing the transmitter configuration for FDP and HBF. The proposed deep neural networks can provide different trade-offs between spectral efficiency and energy consumption while adapting to different numbers of active users. Finally, to ensure that the proposed method can be implemented in practice, we investigate the ability of the model to be trained exclusively using imperfect channel state information (CSI), both for the input to the deep learning model and for the calculation of the loss function. Simulation results show that the proposed solutions can outperform conventional methods in terms of EE while being trained with imperfect CSI. Furthermore, we show that the proposed solutions are less complex and more robust to noise than conventional methods.

5.2 Introduction

Wireless communication has been revolutionized by mMIMO technologies, which are already one of the key enabling technologies in the fifth-generation (5G) of wireless networks thanks to their potential to increase the transmission capacity through the deployment of large-scale antenna arrays at the transmitter or receiver side [4]. As a result, mmWave communications can be used at longer ranges, thus greatly increasing the bandwidth available to wireless networks [17].

The conventional implementation of MIMO systems utilizes a dedicated RF chain for each antenna element. Even though this approach is appropriate for common small-scale MIMO systems, it is inadvisable for mMIMO systems equipped with a large number of antenna elements due to the high production costs and power consumption associated with the RF circuitry. Therefore, even though mMIMO is an important technology for future generations of wireless networks, it still faces many technical challenges to improve its EE and, to date, it remains a subject of ongoing research [155]. In light of this, HBF and antenna selection are proposed as an effective way to facilitate the implementation and to improve the EE of mMIMO systems [6]. Indeed HBF reduces the number of RF chains and DACs, helping to improve EE. Accordingly, for better EE, HBF techniques are being examined for 5G cellular networks in the mmWave frequency bands, and will likely also be found in sixth-generation (6G) networks [8].

Different HBF structures have been proposed to achieve different trade-offs between cost, energy consumption, and SE, which can be grouped into three general categories, FC-HBF [133], FSA-HBF [156], and DSA-HBF [65]. Each category has its advantages and limitations. FC-HBF offers flexibility but has higher implementation complexity. FSA-HBF balances SE and complexity. Finally, DSA-HBF provides adaptability but with additional design complexities. To configure a HBF structure, one of the most prominent techniques consists in minimizing the Euclidean distance between the desired FDP and its hybrid counterpart [64]. However, this technique requires designing the FDP, which is computationally complex and not necessarily energy-efficient. Furthermore, the number of possible HBF structures is extremely large, making it complicated to find an optimal HBF structure. Therefore, the question that arises is how to efficiently design the best HBF structure in terms of energy consumption and SE. Towards answering this question, our first step consists of proposing an accurate energy model that finds the power consumption of each component in different beamforming structures. Our second step involves applying machine learning-based approaches to design the beamforming structure instead of using complex optimization-based ones.

Thanks to the enormous success of DL, in a wide variety of engineering fields, DNNs have received significant attention in recent years and have been widely applied to wireless communication systems [36,86]. Despite the fact that training DNNs to solve wireless communication problems can be computationally intensive, it can take place offline and only the trained DNN model will be used to make online decisions, thus reducing the overall complexity. Different studies used DNNs to address complex problems within the physical layer [9]. In supervised learning approaches, the time spent during the data labeling procedure is not negligible. In addition, this procedure must be performed each time a new dataset is used for training. In reinforcement learning (RL) approaches, an agent collects online data as it interacts with its environment in a trial-and-error manner. In mMIMO systems, since the HBF action space is large, the convergence of the RL model requires a large number of experiments. As a consequence, unsupervised learning demonstrates superiority over supervised learning and reinforcement learning in terms of its ability to autonomously extract meaningful patterns and insights from large datasets without relying on explicit labels or large training overhead.

To summarize, in this study, we aim to optimize the EE of mmWave mMIMO systems by designing HBF structures and FDP using DL-based techniques. The problem consists of jointly designing the transmitter configuration and beamforming weights that maximize the EE. To accomplish this, we first propose an accurate energy model that takes into account the power consumption of the different components of the mMIMO system. Second, we propose an unsupervised deep learning approach that incorporates two key components to design an energy-efficient beamforming structure: (i) a novel loss function that considers different trade-offs between SE, energy consumption, and active users, and (ii) imperfect CSI during both the training and inference phases.

5.2.1 Related Works

In [157], the authors compared the EE of six different PS-based and switch-based HBF structures. However, given the hardware available today, the energy model in [157] overstates the power consumption of PSs, which makes the conclusion unfair to PS-based approaches. Many studies are proposed in the context of DL-aided HBF design and antenna selection algorithms [46, 47, 99, 103, 104, 108–110, 112, 118, 140, 158, 159]. In particular, a RSSI-based FC-HBF design implemented with supervised learning is proposed in [140]. The authors of [104] suggested a supervised learning approach for FC-HBF design under perfect CSI. Another form of supervised learning is also proposed for the FSA-HBF design with perfect CSI in [109]. The authors of [118] proposed a reinforcement learning (RL) approach to design the HBF. However, they assumed that the CSI is known perfectly, and due to the continuous

action space, their method relies on deep deterministic policy gradient (DDPG), which is computationally complex [123]. In the context of unsupervised learning for the FC-HBF design, the authors in [46, 47] presented a novel HBF design employing imperfect CSI for single BS and cell-free mMIMO (CF-mMIMO), respectively. However, their approaches are only for FC-HBF. In [110], the authors proposed an unsupervised learning approach for HBF and antenna selection using a differentiable activation function for 1-bit PSs. However, the main objective is to maximize the SE of the mMIMO system, and the authors neither optimized the EE nor considered an accurate energy model. In [99, 103, 108], the authors proposed a joint antenna selection and precoding design with an iterative algorithm and a DL solution to maximize the SE of multi-user multiple-antenna downlink systems. The proposed ML approach assumes perfect CSI for the training data, does not optimize the EE, and requires a complex iterative algorithm to generate the training samples. In [158, 159], the authors proposed a supervised learning approach to solve the antenna selection problem. However, the proposed method only applies to FDP.

5.2.2 Contributions

In this paper, we consider both FDP and HBF transmitters and develop new unsupervised deep learning solutions that jointly design beamforming and antenna selection while taking into account the power consumption and insertion loss (IL) of all components. For FDP, the proposed solution designs the FDP vectors along with the antenna selection solution, while for HBF, thanks to a multi-tasking DNN, the proposed solution directly provides the AP and DP with the power allocation among the antennas. A preliminary version of this work was published in [160], where we only considered maximizing the SE by designing the HBF for fixed and dynamic HBF structures.

In summary, the contributions of this work are as follows:

- We propose an accurate energy model for the FDP and HBF structures while considering the latest state-of-the-art hardware solutions.
- We propose an unsupervised deep learning solution robust against imperfect CSI to find the optimal energy-efficient antenna selection for FDP and transmit power allocation for HBF considering the proposed accurate energy model. Due to the binary constraints of beamforming connections, our unsupervised deep learning approach makes use of the Gumbel-Sigmoid technique inspired by Gumbel-Softmax. The Gumbel-Sigmoid technique is designed such that it considers the constraints of all components involved in the beamforming connections.

- We design an unsupervised loss function that takes into account the SE, the energy consumption (EC) as well as the number of active users. Thanks to this loss function, the proposed solution is flexible and can intelligently adjust the power consumption according to the number of active users and can provide an optimal trade-off between SE and EC.
- We train the proposed unsupervised deep learning solution using imperfect CSI for both the DNN input and the loss function computation. We also investigate the noise tolerance of our approach by showing that imperfect inputs can be beneficial and improve the EE of the mMIMO system.
- The proposed solutions are evaluated in a realistic ray-tracing channel model generated using a three-dimensional model of an urban environment to capture the geometry-based characteristics of the channel. The simulation results show that the proposed solution outperforms conventional solutions in terms of EE with lower computational complexity, and can be adapted to achieve different trade-offs between SE and EC.

5.2.3 Paper Organization and Notation

The rest of the paper is organized as follows: In Section 5.3, we present the system setup followed by the baseline solutions and the channel model. The proposed energy model for the different beamforming structures is provided in Section 5.4. Section 5.5 presents the proposed energy-efficient unsupervised learning solutions for HBF and FDP, including a discussion of the DNN structure, the training phase, and the online phase. In Section 5.6, we evaluate the performance of the proposed algorithms by comparing them with state-of-the-art solutions using a realistic ray-tracing channel model. Finally, Section 5.7 concludes the paper.

Matrices, vectors, and scalars are denoted by boldface uppercase, boldface lowercase, and normal letters, respectively. The notations $(\cdot)^{\mathrm{H}}$, $(\cdot)^{\mathrm{T}}$, $(\cdot)^{\dagger}$, $|\cdot|$, $\|\cdot\|_F$, $\|\cdot\|_2$, $\Re[\cdot]$, $\Im[\cdot]$, $\mathbb{I}_n$, $\otimes$ denote Hermitian transpose, transpose, Moore-Penrose pseudoinverse, absolute value, Frobenius norm, ℓ^2-norm, real part, imaginary part, the $n \times n$ identity matrix, and element-wise product, respectively.

5.3 System Model and Baselines

Let us assume a TDD multi-user mMIMO system where channel reciprocity is available such that the uplink channel estimate can be used for the downlink transmission. The mMIMO system consists of a single BS in a single-cell equipped with N_{T} antennas and N_{RF} RF chains

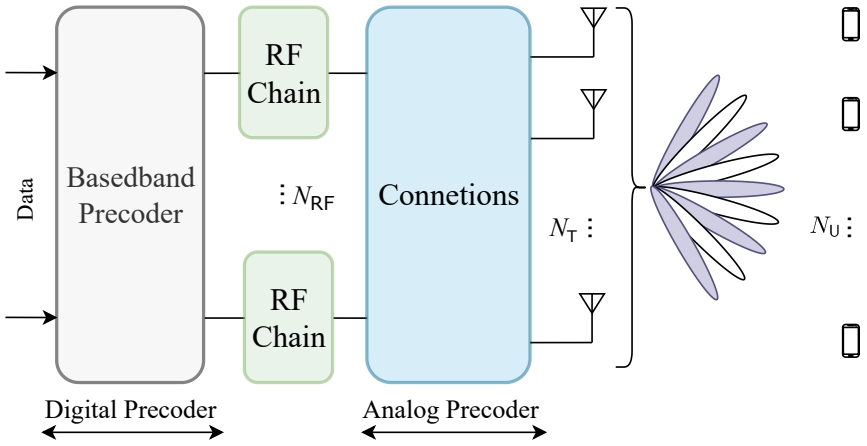

Figure 5.1: Massive MIMO system model structure with one transmitter BS employing HBF to serve a set of users

serving N_{U} single antenna users simultaneously as shown in Figure 5.1. The DP is performed in the baseband and then the output signal goes through the RF chains. Each RF chain is composed of a DAC, a low pass filter (LPF), a local oscillator (LO) and a mixer, and is connected to the N_{T} antennas. The resolution for all DACs and PSs are fixed respectively to b_D and q. The RF chains are connected to the antennas through PSs. The network of these connections and PSs, known as AP, can be tuned based on different HBF structures.

5.3.1 Conventional Beamforming Structures

We first review the three conventional beamforming structures followed by their non-DL design methods, which are used as baselines for our proposed solutions. Connections between the RF chains and the antennas are represented by a binary matrix $\mathbf{\Omega}$. For HBF, $\mathbf{\Omega} = \mathbf{\Omega}_{\mathsf{HB}} \in \{0,1\}^{N_{\mathsf{T}} \times N_{\mathsf{RF}}}$, and $[\mathbf{\Omega}_{\mathsf{HB}}]_{n,m} = 1$ if antenna n is connected to RF chain m. For FDP, $\mathbf{\Omega} = \mathbf{\Omega}_{\mathsf{FD}}$ is an $N_{\mathsf{T}} \times N_{\mathsf{T}}$ diagonal binary matrix, with $\mathbf{\Omega}_{\mathsf{FD}} = \mathrm{diag}(\boldsymbol{\omega})$, where $\boldsymbol{\omega} = [\omega_1, \ldots, \omega_{N_{\mathsf{T}}}]$ and $\omega_n = 1$ if antenna n is activated.

Fully Digital Precoder (FDP)

In FDP, each antenna is connected to an RF chain through the circuit of DAC, LPF, LO, and a mixer. The signal received by each user can be written as

$$\mathbf{y}_u = \mathbf{h}_u^{\mathrm{H}} \sum_{u=1}^{N_{\mathsf{U}}} \mathbf{u}_u x_u + \boldsymbol{\eta}, \tag{5.1}$$

where $\mathbf{h}_u \in \mathbb{C}^{N_\mathsf{T}\times 1}$ stands for the channel vector from the N_T antennas of the BS to the user index u, $\mathbf{x} = [x_1, \ldots, x_u, \ldots, x_{N_\mathsf{U}}]$ is the matrix of transmitted symbols for all users, normalized to $\mathbb{E}[\mathbf{x}\mathbf{x}^\mathrm{H}] = \frac{1}{N_\mathsf{U}}\mathbb{I}_{N_\mathsf{U}}$, $\boldsymbol{\eta}$ is the AWGN with mean 0 and variance σ^2, and $\mathbf{u}_u$ denotes the precoder vector for the u^{th} user. The SE of the O-FDP, $\mathbf{U}_{\mathsf{opt}} = [\mathbf{u}_1, \ldots, \mathbf{u}_u, \ldots, \mathbf{u}_{N_\mathsf{U}}]$ for single-antenna users is obtained by solving the following problem:

$$\max_{\{\mathbf{U}_{\mathsf{opt}}\}} \quad R_{\mathsf{FDP}}(\mathbf{U}_{\mathsf{opt}}) \tag{5.2a}$$

$$\text{s. t.} \quad \sum_{u=1}^{N_\mathsf{U}} \mathbf{u}_u^\mathrm{H}\mathbf{u}_u \leq P_{\mathsf{TX}}\,, \tag{5.2b}$$

where $R_{\mathsf{FDP}}(\mathbf{U}_{\mathsf{opt}}) = \sum_{u=1}^{N_\mathsf{U}} \log_2(1 + \mathrm{SINR}(\mathbf{u}_u))$, the SINR of the u^{th} user is given by

$$\mathrm{SINR}(\mathbf{u}_u) = \frac{\left|\mathbf{h}_u^\mathrm{H}\mathbf{u}_u\right|^2}{\sum\limits_{\substack{j=1\\ j\neq u}}^{N_\mathsf{U}} \left|\mathbf{h}_u^\mathrm{H}\mathbf{u}_j\right|^2 + \sigma^2}\,, \tag{5.3}$$

and P_{TX} is the normalized total transmit power constraint. The baseline results presented in this paper are obtained by solving (5.2) based on [161]. We refer to this approach as optimal FDP (O-FDP). For a given connection matrix $\boldsymbol{\Omega}_{\mathsf{FD}}$, the FDP is given by $\mathbf{U} = \boldsymbol{\Omega}_{\mathsf{FD}} \times \mathbf{U}_{\mathsf{opt}}$.

Fully Connected Hybrid Beamforming (FC-HBF)

In all HBF structures, we assume $N_{\mathsf{RF}} << N_\mathsf{T}$. Regardless of the chosen HBF structure, the signal received by each user can be written as

$$\mathbf{y}_u = \mathbf{h}_u^\mathrm{H}\mathbf{A}\sum_{u=1}^{N_\mathsf{U}} \mathbf{w}_u x_u + \boldsymbol{\eta}\,. \tag{5.4}$$

The HBF vectors consist of a DP, $\mathbf{W} = [\mathbf{w}_1, \ldots, \mathbf{w}_u, \ldots, \mathbf{w}_{N_\mathsf{U}}] \in \mathbb{C}^{N_{\mathsf{RF}}\times N_\mathsf{U}}$, and an AP, $\mathbf{A} \in \mathbb{C}^{N_\mathsf{T}\times N_{\mathsf{RF}}}$. Since the AP is a combination of the PSs and combiners and it depends on HBF structure and connection between the antennas and RF chains, we define it as follows:

$$\mathbf{A} = \mathbf{P}_q \otimes \boldsymbol{\Omega}_{\mathsf{HB}}, \tag{5.5}$$

where $\mathbf{P}_q \in \mathbb{C}^{N_\mathsf{T}\times N_{\mathsf{RF}}}$ is the coefficient of the q bits PS connecting the n^{th} antenna and m^{th} RF chain, where $[\mathbf{P}_q]_{n,m} \in \{e^{j2\pi k/2^q} : k \in \{1, \ldots, 2^q\}\}$. Therefore, the SE for a given HBF

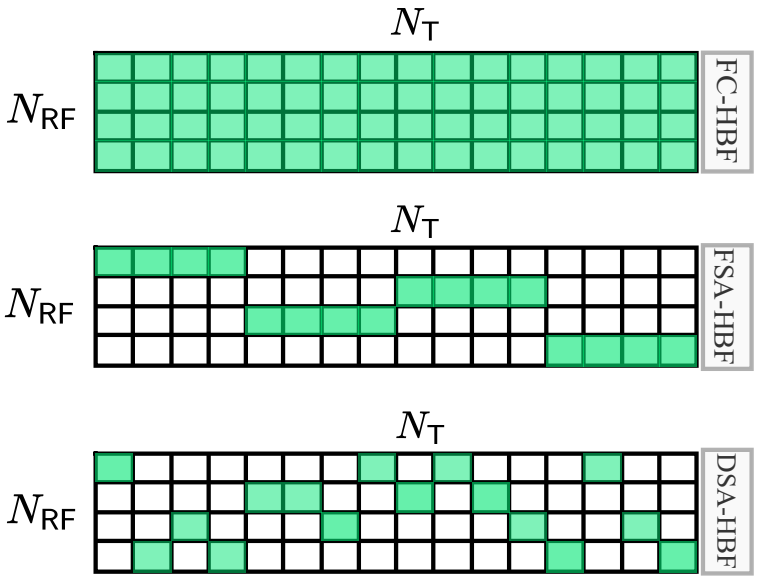

Figure 5.2: Example of connection matrices ($\mathbf{\Omega}_{\mathsf{HB}}$) of some conventional HBF structures. Each green square indicates a connection. Top: FC-HBF. Middle: FSA-HBF. Bottom: DSA-HBF

$(\mathbf{A}, \mathbf{W})$ is given by

$$R_{\mathsf{HBF}}(\mathbf{A}, \mathbf{W}) = \sum_{u=1}^{N_{\mathsf{U}}} \log_2\Big(1 + \mathrm{SINR}(\mathbf{A}, \mathbf{w}_u)\Big)\,, \tag{5.6}$$

and the SINR of the u^{th} user can be expressed as

$$\mathrm{SINR}(\mathbf{A}, \mathbf{w}_u) = \frac{\left|\mathbf{h}_u^{\mathrm{H}} \mathbf{A} \mathbf{w}_u\right|^2}{\sum\limits_{\substack{j=1 \\ j \neq u}}^{N_{\mathsf{U}}} \left|\mathbf{h}_u^{\mathrm{H}} \mathbf{A} \mathbf{w}_j\right|^2 + \sigma^2}\,. \tag{5.7}$$

In FC-HBF, we set $\mathbf{\Omega}_{\mathsf{HB}} = \mathbf{\Omega}_{\mathsf{FC}}$, and all RF chains are connected to all antennas through PSs, combiners, and power amplifier (PA) as shown in Figure 5.2 (top), where the green boxes show the connections. This structure thereby enables maximum design flexibility and therefore requires a large number of PSs and combiners, which increase the implementation cost and energy consumption. The AP of the FC-HBF can be expressed according to (5.5) with

$$[\mathbf{\Omega}_{\mathsf{HB}}]_{n,m} = 1 \quad \forall n, m\,, \tag{5.8}$$

$$[\mathbf{P}_q]_{n,m} \in \{e^{j2\pi k/2^q} : k \in \{1, \ldots, 2^q\}\} \quad \forall n, m\,. \tag{5.9}$$

Since all the antennas are connected to all the RF chains through a PS with q-bit quantization, the feasible analog precoder for n^{th} antenna and m^{th} RF chain is $[\mathbf{A}]_{n,m} \in \{e^{j2\pi k/2^q} : k \in \{1,\ldots,2^q\}\}$. Conventional HBF solutions either rely on codebook-based solutions to limit the number of feasible solutions [127] or, more rarely, use real-valued PSs [64]. The conventional approach consists of first designing the O-FDP matrix in (5.2). Then, the AP and DP are designed in such a way that the resulting precoders approximate $\mathbf{U}_{\mathsf{opt}}$ as follows:

$$\underset{\mathbf{A},\mathbf{W}}{\text{minimize}} \quad \left\|\mathbf{U}_{\mathsf{opt}} - \mathbf{A}\mathbf{W}\right\|_F^2 \tag{5.10a}$$

$$\text{s. t.} \quad (5.5), (5.8), (5.9), \|\mathbf{A}\mathbf{W}\|_F^2 = N_{\mathsf{U}}. \tag{5.10b}$$

We obtain the FC-HBF solution of (5.10) using "PE-AltMin" and "MO-AltMin" proposed in [64].

Subarray Hybrid Beamforming

Each antenna in a subarray structure is connected to only one RF chain through a PS. Consequently, the total number of PSs is reduced to N_{T}, instead of $N_{\mathsf{T}} \times N_{\mathsf{RF}}$ in the FC-HBF. In the subarray HBF structure, we consider two types of connection: (i) a structure equipped with fixed connections, known as fixed subarray HBF (FSA-HBF), or (ii) a structure equipped with dynamic connections, known as dynamic subarray HBF (DSA-HBF). Examples of possible connection matrices for each case are shown in Figure 5.2. The DSA-HBF structure enables the antennas and the RF chains to be dynamically switched at each time interval in response to changing conditions. It was shown that such a dynamic structure significantly enhances the SE of the system by providing more degrees of freedom in the HBF design compared to a FSA-HBF structure, and reduces the power consumption compared to the FC-HBF structure [65]. Therefore, based on the general definition of the AP ($\mathbf{A} = \mathbf{P}_q \otimes \mathbf{\Omega}_{\mathsf{HB}}$), the constraint on matrix $\mathbf{\Omega}_{\mathsf{HB}}$ for subarray HBF is given by

$$\sum_{m=1}^{N_{\mathsf{RF}}} [\mathbf{\Omega}_{\mathsf{HB}}]_{n,m} = 1 \quad \forall\, n\,. \tag{5.11}$$

To find the precoder matrices for FSA-HBF, the general approach described in (5.10) for FC-HBF can be used. For the DSA-HBF, the connection pattern ($\mathbf{\Omega}_{\mathsf{HB}}$) between the RF chains and the antennas is dynamic and needs to be optimized, resulting in a large design space.

5.3.2 Problem Definition

The main objective of this paper is to maximize the EE of the mMIMO system by selecting the antennas and designing the BF structure. For the FDP case, the problem consists of finding the precoder matrix $\mathbf{U}$ and antenna selection $\mathbf{\Omega}_{\mathsf{FD}} = \mathrm{diag}(\boldsymbol{\omega})$ that maximize the EE, while achieving a desired minimum average SE denoted as R_{d}. More formally, we seek to solve the following optimization problem:

$$\begin{aligned}
\underset{\mathbf{U},\mathbf{\Omega}_{\mathsf{FD}}}{\text{maximize}} \quad & R_{\mathsf{FDP}}(\mathbf{U} \times \mathbf{\Omega}_{\mathsf{FD}})/P_{\mathrm{FDP}} && \text{(5.12a)}\\
\text{s. t.} \quad & \sum_{u=1}^{N_{\mathsf{U}}} \mathbf{u}_u^{\mathrm{H}}\mathbf{u}_u \leq P_{\mathsf{TX}}\,, && \text{(5.12b)}\\
& [\mathbf{\Omega}_{\mathsf{FD}}]_{n,n} \in \{0,1\},\ \forall n, && \text{(5.12c)}\\
& R_{\mathsf{FDP}}(\mathbf{U} \times \mathbf{\Omega}_{\mathsf{FD}}) \geq N_{\mathsf{U}} R_{\mathsf{d}}, && \text{(5.12d)}
\end{aligned}$$

where P_{FDP} is the total power consumed by the BF components.

Similarly, the HBF design consists in finding the precoder matrices $\mathbf{W}$ and $\mathbf{A}$ and the power allocation that maximizes the EE. Therefore, we have the following optimization problem:

$$\begin{aligned}
\underset{\mathbf{A},\mathbf{W}}{\text{maximize}} \quad & R_{\mathsf{HBF}}(\mathbf{A},\mathbf{W})/P_{\mathrm{HBF}}, && \text{(5.13a)}\\
\text{s.t.} \quad & \sum_{u=1}^{N_{\mathsf{U}}} \mathbf{w}_u^{\mathrm{H}}\mathbf{A}^{\mathrm{H}}\mathbf{A}\mathbf{w}_u \leq P_{\mathsf{TX}}\,, && \text{(5.13b)}\\
& \mathbf{A} = \mathbf{P}_q \otimes \mathbf{\Omega}_{\mathsf{HB}}, && \text{(5.13c)}\\
& [\mathbf{\Omega}_{\mathsf{HB}}]_{n,m} \in \{0,1\},\ \forall n,m, && \text{(5.13d)}\\
& R_{\mathsf{HBF}}(\mathbf{A},\mathbf{W}) \geq N_{\mathsf{U}} R_{\mathsf{d}}, && \text{(5.13e)}
\end{aligned}$$

where P_{HBF} is the total power consumed by the HBF transmitter, and again R_{d} is the minimum average required SE. The power consumption P_{FDP} and P_{HBF} will be described in detail in Section 5.4. In this paper, for simplicity, we consider a total power constraint for the transmitter, where the power transmitted by each antenna is not necessarily equal or limited to $P_{\mathsf{TX}}/N_{\mathsf{T}}$. It should be noted that in HBF turning off an antenna is not necessarily corresponding to deactivating an RF chain. On the contrary, since in FDP, each antenna is connected to one RF chain, and the power consumed by RF chains is noticeable, turning off the RF chains leads to the deactivation of the corresponding antennas.

5.3.3 Channel Model

The experiments presented in this paper are based on the generic deep learning dataset for mmWave mMIMO systems (known as deepMIMO) [141], which provides a channel vector $\mathbf{h}$ of length N_{T} for each user position on a quantized grid. An $N_{\mathsf{T}} \times N_{\mathsf{U}}$ channel matrix entries in the dataset are obtained by concatenating the N_{U} channel vectors randomly selected from the available user positions of the considered area.

Since we consider TDD communication with channel reciprocity, the estimated CSI in the uplink can be employed for downlink. However, due to channel estimation errors, the downlink channel cannot be perfectly estimated. Thus, to model the channel estimation error, the BS uses the minimum mean square error such that the estimated channel matrix is given by [44]:

$$\hat{\mathbf{H}} = \sqrt{1-\beta^2}\mathbf{H} + \beta\boldsymbol{\epsilon}, \tag{5.14}$$

where $\mathbf{H} = [\mathbf{h}_1, ..., \mathbf{h}_{N_{\mathsf{U}}}]^{\mathrm{T}}$ is the actual channel matrix, the scaling coefficient $\beta \in [0, 1]$ represents the reliability of the estimate, and $\boldsymbol{\epsilon} \sim \mathcal{N}(0, \sigma_e^2)$ is an error matrix modeled as a zero-mean Gaussian noise with variance σ_e^2. Unlike previous DL-based studies, where perfect CSI is available during the training of the DNN, in this work, we propose to use the imperfect CSI ($\hat{\mathbf{H}}$) not only as the input to the DNN but also to compute the loss function during the training phase. In Section 5.6, we further evaluate the impact of the imperfect CSI by varying the value of β and show that a moderate level of imperfection in CSI can act as a regularizer for the DNN and slightly improve the SE.

5.4 Energy Model

In this section, we present an energy model for the different FDP and HBF hardware configurations, considering both the direct energy consumption as well as the energy consumption resulting from IL of each component.

5.4.1 General Beamforming Structure

We consider a regularity assumption where components of the same type have the same input/output interface, i.e. their inputs and outputs are connected to the same type and number of components. This assumption is generally true because it eases the conception of generic circuits.

To better represent each HBF structure, we suggest a general template form as shown in Figure 5.3 (a), where a given antenna is connected to a combiner having $c \in \{1, \ldots, N_{\mathsf{RF}}\}$

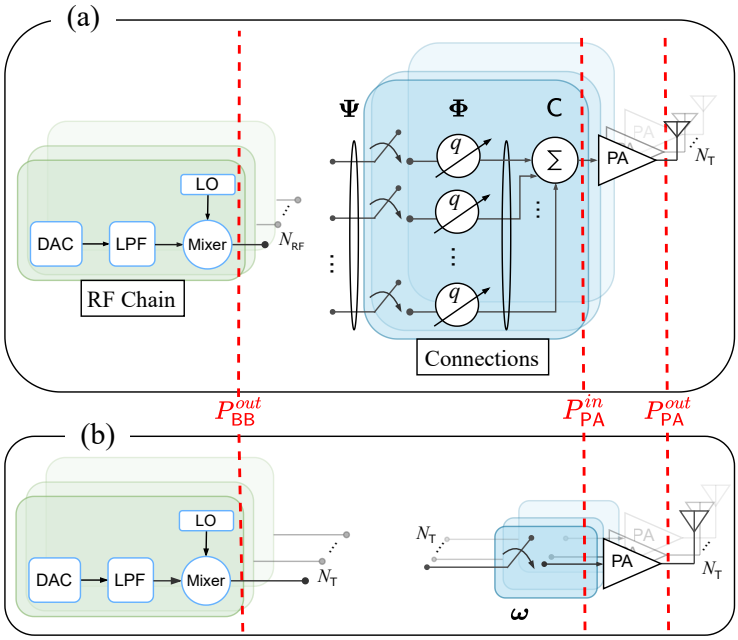

Figure 5.3: General beamforming structure. (a) Hybrid beamforming structure. (b) Fully digital precoder structure

inputs. Each input of a combiner is connected to the output of a phase shifter. Then, each phase shifter is connected to an RF chain through a switch. The number of switches is $\psi \in \{1, \ldots, N_{\mathsf{RF}}\}$. As a result, the analog precoder can be fully characterized by specifying the tuple (ψ, c). For instance, for the three conventional HBF structures that we discussed previously, we have:

- $(N_{\mathsf{RF}}, N_{\mathsf{RF}})$ for the FC-HBF structure. In the FC-HBF structure, all the switches are connected (i.e., $\psi = N_{\mathsf{RF}}$), while the outputs of all the PSs are combined before each antenna i.e., $c = N_{\mathsf{RF}}$.
- $(N_{\mathsf{RF}}, 1)$ for the DSA-HBF structure. In DSA-HBF, only one switch can be connected at each time interval, therefore $c = 1$, while there are possible connections for all the switches, thus $\psi = N_{\mathsf{RF}}$. It should be noted that such configuration for switches works like a multiplexer. Thus, in a practical system, the switches are replaced by a $\psi \times 1$ multiplexer.
- $(1, 1)$ for the FSA-HBF structure. In FSA-HBF, each antenna is only connected to a fixed RF chain (i.e., $c = 1$), while the connection is fixed i.e., $\psi = 1$.

The hardware complexity of different beamforming techniques is compared in Table 5.2.

Table 5.1 Energy Model Notations and Parameters

Component	Notation $\langle c \rangle$	Parameter x
Digital analog convert	D	# bits b_D
Low pass filter	L	-
Mixer	M	-
Local oscillator	LO	-
Switches (multiplexers)	$\mathbf{\Psi}$	# inputs ψ
Phase shifters	$\mathbf{\Phi}$	-
Combiners	C	-
Power amplifier	PA	-

Table 5.2 Hardware Complexity Comparison

Beamforming technique	Hardware components				
	RF chains	Antennas	PS	Combiners	Switches
FDP	N_{T}	N_{T}	-	-	-
FC-HBF	N_{RF}	N_{T}	$N_{\mathsf{RF}}N_{\mathsf{T}}$	N_{T}	-
FSA-HBF	N_{RF}	N_{T}	N_{T}	-	-
DSA-HBF	N_{RF}	N_{T}	N_{T}	-	N_{T}

5.4.2 Energy Consumption Analysis

We now describe the energy consumption of each component, and we list the most recent state-of-the-art hardware solutions. We consider components that are suitable for operating in the frequency range of 20-40 GHz.

A component of the set $\{\mathsf{D}, \mathsf{L}, \mathsf{M}, \mathsf{LO}, \mathbf{\Psi}, \mathbf{\Phi}, \mathsf{C}, \mathsf{PA}\}$ is denoted by o and the correspondence between a component and its notation is defined in Table 5.1. We denote IL_o as the insertion loss of passive component o and when o depends on some parameter x, we use $\mathrm{IL}_o(x)$. The average power dissipated by the active component o is denoted as P_o, or $P_o(x)$ if o depends on the parameter x. See Table 5.1 for the list of components and their parameters. Note that the power dissipated by the wires is neglected and when $c = 1$ there is no need for a combiner (i.e., $\mathrm{IL}_{\mathsf{C}}(1) = 0\,\mathrm{dB}$). Likewise, the switches can be replaced with wires when $\psi = 1$ or $\psi = c$, that is $\mathrm{IL}_{\mathbf{\Psi}}(1) = \mathrm{IL}_{\mathbf{\Psi}}(c) = 0\,\mathrm{dB}$, since all possible connections are always established.

In our energy model, we consider the possibility of turning off the RF chains or antennas to save power. The n^{th} antenna or the m^{th} RF chain is turned off when the n^{th} row or the m^{th} column of the matrix $\mathbf{\Omega}$ is zero, respectively. Therefore, we can define $N_{\mathsf{T}}(\mathbf{\Omega}) = \{n : \sum_{m=1}^{N_{\mathsf{RF}}} [\mathbf{\Omega}]_{n,m} > 0\}$ and $N_{\mathsf{RF}}(\mathbf{\Omega}) = \{m : \sum_{n=1}^{N_{\mathsf{T}}} [\mathbf{\Omega}]_{n,m} > 0\}$, as the set of activated antennas and

RF chains, respectively.

RF Front-End

The RF front-end corresponds to the circuitry between the antenna and the DAC. As shown in Figure 5.3 (b), for the FDP, this consists of low pass filters (LPFs), mixers, local oscillators (LOs), switches, and power amplifiers (PAs). On the other hand, in Figure 5.3 (a), the HBF requires a network of PSs, splitters, and combiners in addition to the components described for the FDP. Mixers, combiners, switches, and PSs are assumed to be passive devices that introduce IL.

For the mixer, based on the recent solution in [162], we consider $\mathrm{IL}_{\mathsf{M}} = 6.4$ dB. The IL of the PS and the combiner plays a key role in designing energy-efficient HBF, especially for the FC-HBF, where all the RF chains are connected to all the antennas through PSs and combiners. In Table 5.3, we list the ILs of PSs from some recent state-of-the-art references. Based on this table, we choose $\mathrm{IL}_{\mathbf{\Phi}} = 3.7$ dB with $q = 9.4$ bits resolution, and we assume $\mathrm{IL}_{\mathsf{C}} = 1.8$ dB [163]. For DSA-HBF, the switches dynamically change the connections between the RF chains and the antennas to improve the flexibility of the structure. Since these ILs are in low power and they do not have a big impact on the final power consumption, we assume $\mathrm{IL}_{\mathbf{\Psi}}(\psi) = 1.1$ dB for the other values of ψ, by considering single pole single throw (SPST) switch [164].

Now, denoting by P_{BB}^{out} the output power of each RF chain, the input power of the PA before the n^{th} antenna for all structures of the HBF (in mW) can be written as

$$P_{\mathsf{PA,HBF}}^{in,n} = \frac{P_{\mathsf{BB}}^{out}}{\mathrm{IL}_{\mathsf{C}}\mathrm{IL}_{\mathbf{\Psi}}(\psi)\mathrm{IL}_{\mathbf{\Phi}}\mathrm{IL}_{\mathsf{M}}} \sum_{m \in N_{\mathsf{RF}}(\mathbf{\Omega})} \frac{[\mathbf{\Omega}_{\mathsf{HB}}]_{n,m}}{\sum_{n=1}^{N_{\mathsf{T}}} [\mathbf{\Omega}_{\mathsf{HB}}]_{n,m}}, \tag{5.15}$$

where $\mathrm{IL}_{\mathbf{\Phi}}$ denotes the IL of PSs and IL values are expressed in a linear scale. In the FC-HBF, where all the RF chains are connected to the antennas ($\mathbf{\Omega}_{\mathsf{HB}}$ given in (5.8)), we have $(\psi, c) = (N_{\mathsf{RF}}, N_{\mathsf{RF}})$ and $\mathrm{IL}_{\mathbf{\Psi}}(\psi = c) = 1$. For DSA-HBF with the structure of (ψ, c) $= (N_{\mathsf{RF}}, 1)$ and the connection matrix $\mathbf{\Omega}_{\mathsf{HB}}$ in (5.11), due to IL of switches, we have $\mathrm{IL}_{\mathbf{\Psi}}(\psi) = 1.1$. In FSA-HBF that has a structure $(\psi, c) = (1, 1)$, there are neither combiners nor switches. As a result, $\mathrm{IL}_{\mathbf{\Psi}}(1) = 1$, and $\mathrm{IL}_{\mathsf{C}} = 1$. Similarly for the FDP, as shown in Figure 5.3 (b), the input power of the PA on the n^{th} antenna can be obtained as

$$P_{\mathsf{PA,FDP}}^{in,n} = \frac{P_{\mathsf{BB}}^{out}}{\mathrm{IL}_{\mathsf{M}}}. \tag{5.16}$$

Table 5.3 Passive Phase Shifter IL Comparison

Reference	Year	Frequency (GHz)	bits q	$\mathrm{IL}_{\mathbf{\Phi}}$ (dB)
[165]	2019	24-28	-	5
[166]	2018	28	-	4
[167]	2018	22-36	3	5.6
[168]	2018	28	9.4	3.7

Finally, the direct current (DC) power drawn by the n^{th} active PA P_{PA}, can be written as

$$P_{\mathsf{PA,BF}}^{\mathrm{DC},n} = \frac{P_{\mathsf{TX}}^{n} - P_{\mathsf{PA,BF}}^{in,n}}{\alpha}, \tag{5.17}$$

where α is the power-added efficiency (PAE) of the linear power amplifier (LPA), P_{TX}^{n} is the transmit power of the n^{th} antenna, and BF should be replaced with HBF or FDP according to the chosen transmitter type. Based on the recent solution for PA listed in [169–171], we consider an average PAE of $\alpha = 36$.

Digital to Analog Converter

DACs are among the components having the largest power consumption in wireless applications. The power consumed by a DAC (P_{D}) is a linear function of the sampling frequency (f_s) and the figure of merit ($\mathrm{FoM}_{\mathsf{D}}$) of the converter, and grows exponentially with the number of bits of resolution (b_D) as $P_{\mathsf{D}} = \mathrm{FoM}_{\mathsf{D}} \times f_s \times 2^{b_D}$ [172]. The sampling frequencies for ultra wide-band applications are in the range of 0.5-1 GHz. It is shown in [172] that in terms of required signal-to-quantization noise ratio (SQNR), FDP required 2 bits less than HBF. Therefore, we assume $b_D = 4$ for FDP and $b_D = 6$ for HBF, respectively. Moreover, based on [173], we consider $\mathrm{FoM}_{\mathsf{D}} = 54.5$ fJ/conv.

Low Pass Filter in TX

The output of the DACs will require analog LPF to reject spectral images and maintain out-of-band emission limits. For an m'-th order active LPF with cutoff frequency f_c, the $\mathrm{FoM}_{\mathsf{L}}$ is the power consumed per pole per Hertz [174]. The power drawn by LPF is given by $P_{\mathsf{L}} = \mathrm{FoM}_{\mathsf{L}} \times f_c \times m'$. Based on [174], we assume a first order LPF with $f_c = 500$MHz, and $\mathrm{FoM}_{\mathsf{L}} = 1.4$ mW/GHz. Furthermore, we define P_{LO} as the power consumed by the mixer from the LO and we consider $P_{\mathsf{LO}} = 10$ dBm [175].

Total Energy Consumption

Now, putting it all together, the total power consumed by a given beamforming structure can be written as follows:

$$P_{\mathsf{BF}} = \left|N_{\mathsf{RF}}(\mathbf{\Omega})\right|(P_{\mathsf{L}} + P_{\mathsf{LO}} + P_{\mathsf{D}}(b_D)) + \sum_{n \in N_{\mathsf{T}}(\mathbf{\Omega})} P_{\mathsf{PA,BF}}^{\mathrm{DC},n}, \tag{5.18}$$

where $P_{\mathsf{PA,BF}}$ should be replaced with either $P_{\mathsf{PA,HBF}}$ or $P_{\mathsf{PA,FDP}}$ according to the transmitter type and $\mathbf{\Omega} \in \{\mathbf{\Omega}_{\mathsf{FD}}, \mathbf{\Omega}_{\mathsf{HB}}\}$. In this paper, we focus on passive PS, but we note that active PS can be easily considered in the model by setting $\mathrm{IL}_{\mathbf{\Phi}}$ to 1 and adding the power consumption of all active PSs to (5.18). The energy consumption E_{BF} can then be obtained with $E_{\mathsf{BF}} = T_s \times P_{\mathsf{BF}}$, where T_s is the duration of a symbol. When considering a fixed symbol duration, minimizing the power consumption is equivalent to minimizing the energy. Therefore, we evaluate the EE as b/s/Hz/W. It is interesting to see that based on (5.15), considering passive PSs and combiners, the power consumed by different HBF structures is similar since the IL of the passive components is applied on the low power signals, before the PAs. However, in terms of hardware complexity and cost, shown in Table 5.2, the subarray HBF is more efficient than FC-HBF.

In equations (5.6) and (5.18), we observe that both the SE and the EE are influenced by the matrix $\mathbf{\Omega}$. This matrix defines the connection between the RF chains and the antennas. Having more connections results in higher SE as it increases beamforming flexibility. However, each connection corresponds to the use of an RF chain in FDP, and in the case of HBF, it involves a PS and a combiner, leading to increased costs and energy consumption. This dependency makes the optimization problem in (5.13) difficult to solve. Consequently, to address this issue, we propose a novel unsupervised learning solution in the following sections. This approach aims to jointly optimize both SE and EE.

5.5 Energy-Efficient Beamforming Driven By Deep Unsupervised Learning

In this section, we describe the unsupervised learning solution to design the antenna selection and efficient HBF as well as FDP. We start by describing the architecture of the proposed DNN in Section 5.5.1. Then, the proposed method is divided into two phases: the training phase is described in Section 5.5.2, and the online phase is described in Section 5.5.3.

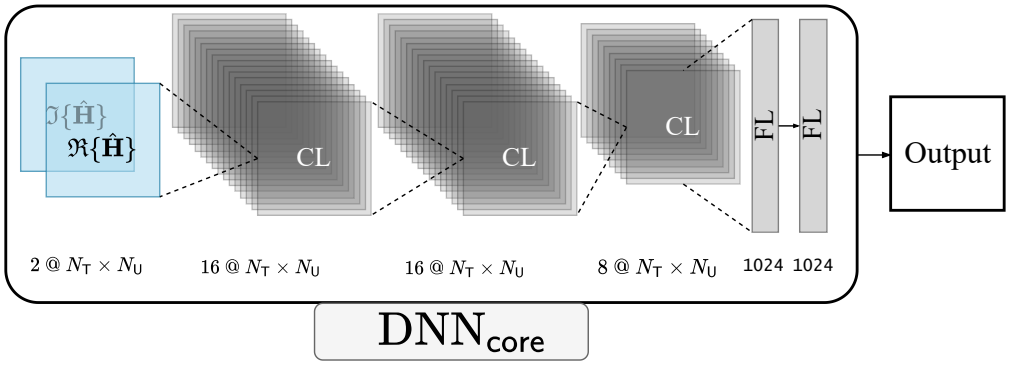

Figure 5.4: $\mathrm{DNN}_{\mathsf{core}}$ architecture which is identical for both HBF and FDP

5.5.1 Deep Neural Network Architecture

The input and the hidden layers of the proposed DNN architecture are common for both the FDP and the HBF structures. However, the output layers are different for each BF structure. We start by describing the architecture of the input and the hidden layers denoted as $\mathrm{DNN}_{\mathsf{core}}$ as shown in Figure 5.4. Then in the following subsections, we describe the architectures of the output layers of the HBF and the FDP.

The input of the DNN is given by the imperfect channel matrix $\hat{\mathbf{H}}$ given in (5.14). To improve the representation learning, we normalize the input to $\bar{\mathbf{H}} = \hat{\mathbf{H}}/\|\hat{\mathbf{H}}\|_F^2$ such that $\|\bar{\mathbf{H}}\|_F^2 = 1$. Then, we separate the real part $\Re\{\bar{\mathbf{H}}\}$ and the imaginary part $\Im\{\bar{\mathbf{H}}\}$ of $\bar{\mathbf{H}}$ into two channels that are fed to the first CL. $\mathrm{DNN}_{\mathsf{core}}$ consists of 2 CLs $16@N_\mathsf{T} \times N_\mathsf{U}$ where 16 is the number of channels and $N_\mathsf{T} \times N_\mathsf{U}$ is the dimension of each channel followed by 1 CL $8@N_\mathsf{T} \times N_\mathsf{U}$. The kernel size is 3×3 for all CLs. The CLs are followed by 2 FLs, each with 1024 neurons. The "Leaky ReLU" activation function and batch normalization are used after all layers except for the output layers. This $\mathrm{DNN}_{\mathsf{core}}$ is then combined with different output layers to form the HBF model, called efficient HBF network (E-HBF-Net), and the FDP model, called efficient FDP network (E-FDP-Net). The models are relatively small. For example, for $N_\mathsf{T} = 64$, $N_\mathsf{U} = 8$, the total number of parameters including the output layers in E-HBF-Net is 5.8M (with $N_{\mathsf{RF}} = 8$), and 4.9M in E-FDP-Net. A detailed complexity analysis is presented in Section 5.6.4.

Output Layers for HBF

As shown in Figure 5.5 (a), we divide the output of the last FL into 4 parallel layers. The first and second parallel layers, both of size $N_{\mathsf{RF}} \times N_\mathsf{U}$, generate the real and imaginary part of the DP. The output of the third parallel layer generates the AP, thus its dimension is

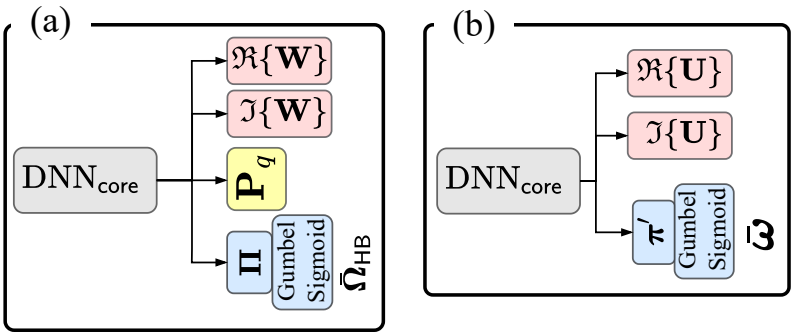

Figure 5.5: Proposed DNN architecture for (a) Hybrid beamforming, (b) Fully digital precoder

$N_{\mathsf{RF}} \times N_{\mathsf{T}}$. The output of AP can also be adapted to different PS resolutions. It is shown in [160] that using the straight-through estimator (STE) technique, we are able to have different numbers of quantization bits for the PSs. In this paper we again consider the same approach for the output of the DNN dedicated for PS quantization in AP. The fourth layer of size $N_{\mathsf{RF}} \times N_{\mathsf{T}}$ designs the matrix $\mathbf{\Omega}_{\mathsf{HB}}$.

As we described before, $\mathbf{\Omega}_{\mathsf{HB}}$ must be a binary matrix. Typically, this binary constraint requires using the "Sigmoid" function during training and then, during the online phase, applying a rounding technique to transform the real values into binary values. However, we found that this approach does not lead to good results for unsupervised learning, because the SE measured during training can be very different from the actual SE measured during testing. To solve this problem, we propose to use a differentiable approximation, called "Gumbel-Sigmoid" during training inspired by the "Gumbel-Softmax" estimator [176]. The Gumbel-Softmax approximation is a technique that allows sampling from a categorical distribution during the forward pass of a neural network, by combining a re-parameterization trick and a smooth relaxation. The connection between the RF chains and the antennas can be represented using a categorical binary distribution. Hence, defining $\pi_{n,m}$ as the probability that antenna n is connected to the RF chain m, then we can form an $N_{\mathsf{T}} \times N_{\mathsf{RF}}$ matrix $\mathbf{\Pi}$ that corresponds to the probability states between antenna n and the RF chain m. The Gumbel-Softmax function, $G(\mathbf{\Pi})$, applied to each element of the matrix $\mathbf{\Pi}$ can then be defined as

$$\bar{\mathbf{\Omega}}_{\mathsf{HB}} = G(\mathbf{\Pi}) = \frac{\exp((\log(\mathbf{\Pi}) + \mathbf{g})/\tau)}{\exp((\log(\mathbf{\Pi}) + \mathbf{g})/\tau) + \exp(\mathbf{g}'/\tau)}, \tag{5.19}$$

where $\bar{\mathbf{\Omega}}_{\mathsf{HB}}$ is the output of the DNN, and $\mathbf{g}$ and $\mathbf{g}'$ are independent samples with zero mean and unit variance, drawn from the Gumbel distribution. Note that the $\exp(\cdot)$ and $\log(\cdot)$ functions are applied element-wise when taking a matrix as input. The parameter τ is called

the "Gumbel temperature". When $\tau \to 0$, $G(\mathbf{\Pi})$ tends to the categorical distribution, but when $\tau \to \infty$, it converges to the uniform distribution [176]. Therefore, there is a trade-off between small temperatures, where sample vectors are close to one-hot but the variance of the gradient is large, and large temperatures, where samples are more uniform but the variance of the gradient is small. We thus consider τ as a hyper-parameter to be optimized in our implementation.

Output Layers for FDP

The proposed architecture for FDP is shown in Figure 5.5 (b). We divide the output layer into 3 parallel layers. The first two layers are dedicated to the real and imaginary part of the FDP with dimension $N_{\mathsf{T}} \times N_{\mathsf{U}}$. The third layer, similar to the one for HBF, designs the antenna selection vector ($\boldsymbol{\omega}$) described in Section 5.3.1. Here again, we use the Gumbel-Sigmoid described in (5.19) to obtain the binary variables from $\boldsymbol{\omega}$. Let π'_n denotes the probability of activating the n-th antenna and $\boldsymbol{\pi}' = [\pi'_1, \ldots, \pi'_{N_{\mathsf{T}}}]$. Then, we have $\bar{\mathbf{\Omega}}_{\mathsf{FD}} = \text{diag}(\bar{\boldsymbol{\omega}})$, where $\bar{\boldsymbol{\omega}} = G(\boldsymbol{\pi}')$.

5.5.2 Training Phase: Unsupervised Learning

In the training phase, thanks to unsupervised learning, the data samples consist of only imperfect channel matrices without the need for labels. The imperfect channel ($\hat{\mathbf{H}}$) is modeled as in (5.14) and it includes a coefficient β that determines the magnitude of the estimation error and thus helps us study the impact of the estimation error of the channel on the DNN training.

Although the approach to train the DNN is similar for E-HBF-Net and E-FDP-Net, there are differences in their hardware configurations. Therefore, we first present the common aspects

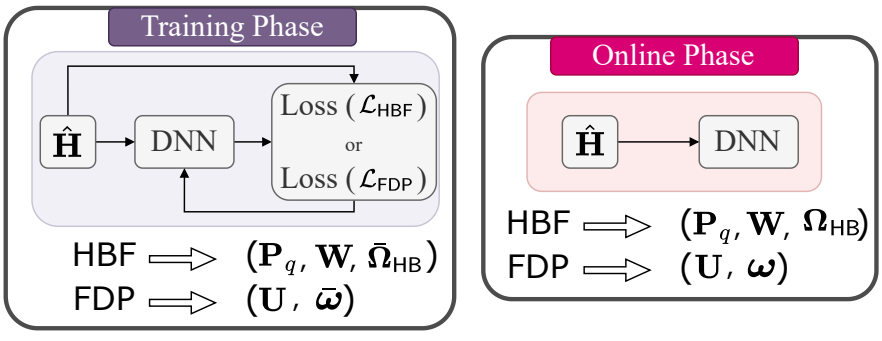

Figure 5.6: Training (left) and online (right) phases for efficient beamforming. The outputs of the DNN depend on the BF structure (HBF, FDP)

shared by both DNN models and then proceed to explain the parts specific to each model.

The objective of the proposed solutions is to design the beamforming configuration to not only maximize the SE but also to minimize the EC while being adaptive to the number of active users, i.e., when the number of active users is small, it intelligently turns off part of the antennas since they will no longer be needed. Consequently, it will reduce the EC. To achieve this objective, we design the following unsupervised loss function to train the DNN:

$$\mathcal{L}_{\mathsf{BF}} = \gamma \mathcal{L}_{\mathsf{EC}} + \mathcal{L}_{\mathsf{AAS}}, \tag{5.20}$$

where the first term is related to EC and the second term is related to both the SE and the active number of users and is called the adaptive antenna selection (AAS) term. The hyper-parameter γ is required to achieve proper training convergence and should be tuned in the training phase. Each term of the loss function is described in detail in the sequel.

EC term ($\mathcal{L}_{\mathsf{EC}}$): This term is introduced to add a penalty to the total loss function to reduce EC. It is given as:

$$\mathcal{L}_{\mathsf{EC}} = \bar{P}_{\mathsf{BF}}, \tag{5.21}$$

where $\bar{P}_{\mathsf{BF}}$ is the total power consumption for either HBF ($\bar{P}_{\mathsf{HBF}}$) or FDP ($\bar{P}_{\mathsf{FDP}}$) given in (5.18) as discussed in Section 5.4, which depends on $\bar{\mathbf{\Omega}} \in \{\bar{\mathbf{\Omega}}_{\mathsf{FD}}, \bar{\mathbf{\Omega}}_{\mathsf{HB}}\}$. Thus, $\bar{\mathbf{\Omega}}_{\mathsf{BF}}$ affects both the SE as well as the EC.

AAS term ($\mathcal{L}_{\mathsf{AAS}}$): This term of the loss function $\mathcal{L}_{\mathsf{AAS}}$ is given by:

$$\mathcal{L}_{\mathsf{AAS}} = \left(\frac{\bar{R}}{N_{\mathsf{U}}} - R_{\mathsf{d}} \right)^2, \tag{5.22}$$

where as discussed in Section 5.3.2, parameter R_{d} denotes the desired average SE value for each user, and $\bar{R}$ is either $\bar{R}_{\mathsf{HBF}}(\bar{\mathbf{A}}, \mathbf{W})$ for HBF or $\bar{R}_{\mathsf{FDP}}(\mathbf{U} \times \bar{\mathbf{\Omega}}_{\mathsf{FD}})$ for FDP. Thanks to the AAS term, the SE is forced to approach R_{d} while parts of the antennas can be turned off to reduce the EC (according to the EC term $\mathcal{L}_{\mathsf{EC}}$). As a result, the AAS term aims to consume minimum power to satisfy an average desired SE (R_{d}), possibly pushing down the power consumption.

Efficient Hybrid Beamforming Network (E-HBF-Net)

To design an efficient HBF structure, a programmable switch is employed for each connection ($N_{\mathsf{T}} \times N_{\mathsf{RF}}$) to find the best matrix ($\mathbf{\Omega}_{\mathsf{HB}}$) that maximizes the EE. As shown in the "Training Phase" of Figure 5.6, the proposed DNN for HBF, E-HBF-Net, is designing jointly the

DP ($\mathbf{W} = \Re[\mathbf{W}] + i\Im[\mathbf{W}]$), the PSs ($\bar{\mathbf{P}}_q$), and the connections matrix ($\bar{\mathbf{\Omega}}_{\mathsf{HB}}$) by employing the proposed "Gumbel Sigmoid" function as in (5.19).

Obtaining $\bar{P}_{\mathsf{HBF}}$ requires computing (5.18) and thus we first need to know the power consumed by the PAs. Thus, based on (5.17), we would need the input and output power of the PAs. The output power of the PAs $1, \ldots, N_T$ is given by

$$\bar{\mathbf{p}}_{\mathsf{TX}} = \sum_{u=1}^{N_{\mathsf{U}}} |\bar{\mathbf{A}}\mathbf{w}_u|^2, \tag{5.23}$$

where $\bar{\mathbf{p}}_{\mathsf{TX}} = [\bar{P}^1_{\mathsf{TX}}, \ldots, \bar{P}^{N_{\mathsf{T}}}_{\mathsf{TX}}]^{\mathsf{T}}$ and $\bar{\mathbf{A}}$ and $\mathbf{W} = [\mathbf{w}_1, \ldots, \mathbf{w}_{N_{\mathsf{U}}}]$ are the AP and DP outputs designed by the proposed DNN. Due to the total power constraint assumed at the BS in (5.13c), we should normalize the power such $\|\bar{\mathbf{A}}\mathbf{W}\|_F^2 = \sum_{n=1}^{N_{\mathsf{T}}} \sum_{u=1}^{N_{\mathsf{U}}} |\bar{\mathbf{A}}\mathbf{w}_u|^2 \leq P_{\mathsf{TX}}$. To respect the inequality of the power constraint, we introduce a new power threshold $\bar{P}_{\mathsf{TX}}$ that is a function of the connection matrix as follows:

$$\bar{P}_{\mathsf{TX}} = \sum_{\forall m,n} [\bar{\mathbf{\Omega}}_{\mathsf{HB}}]_{n,m} P_{\mathsf{TX}}/(N_{\mathsf{RF}} N_{\mathsf{T}}). \tag{5.24}$$

Therefore, the maximum transmitted power is limited to P_{TX} when all connections are established ($[\bar{\mathbf{\Omega}}_{\mathsf{HB}}]_{n,m} = 1 \; \forall n, m$), while reducing the number of connections reduces the transmit power. After power normalization, we can obtain the input power of the PAs according to (5.15). However, for the DNN loss function, we cannot have a sum over a dynamic set as defined in (5.15). Therefore, we reformulate (5.15) as

$$\bar{\mathbf{p}}^{in}_{\mathsf{PA,HBF}} = \frac{P^{out}_{\mathsf{BB}}}{\mathrm{IL}_{\mathsf{C}} \mathrm{IL}_{\mathbf{\Psi}}(\psi) \mathrm{IL}_{\mathbf{\Phi}} \mathrm{IL}_{\mathsf{M}}} \bar{\mathbf{\Omega}}_{\mathsf{HB}} \mathrm{diag}(\bar{\mathbf{\Omega}}^{\mathrm{T}}_{\mathsf{HB}} \mathbf{1}_{N_{\mathsf{T}}})^{\dagger} \mathbf{1}_{N_{\mathsf{RF}}}, \tag{5.25}$$

where $\bar{\mathbf{p}}^{in}_{\mathsf{PA,HBF}} = [\bar{P}^{in,1}_{\mathsf{PA,HBF}}, \ldots, \bar{P}^{in,N_{\mathsf{T}}}_{\mathsf{PA,HBF}}]$ is the vector of input power of the APs, $\bar{\mathbf{\Omega}}_{\mathsf{HB}}$ is the output of Gumbel-Sigmoid function for HBF, and $\mathbf{1}_N$ denotes the all-one column vector of size N. According to (5.17) and (5.23)-(5.25), we can obtain $\bar{P}^{\mathrm{DC},n}_{\mathsf{PA,HBF}}$.

To compute the power consumption of all activated RF chains as in (5.18), we need to determine the number of activated RF chains (i.e., $N_{\mathsf{RF}}(\bar{\mathbf{\Omega}}_{\mathsf{HB}})$). However, finding $N_{\mathsf{RF}}(\bar{\mathbf{\Omega}}_{\mathsf{HB}})$ again requires a summation over a dynamic set and it is not appropriate for the loss function. As a consequence, we use an alternative linear algebra formulation. First, we compute the expectation over all antennas of each RF chain as $\bar{\mathbf{\Omega}}^{\mathrm{T}}_{\mathsf{HB}} \mathbf{1}_{N_{\mathsf{T}}}/N_{\mathsf{T}}$. Then, we find the expected number of activated RF chains as follows:

$$\bar{N}_{\mathsf{RF}}(\bar{\mathbf{\Omega}}_{\mathsf{HB}}) = \mathbf{1}^{\mathrm{T}}_{N_{\mathsf{RF}}} \bar{\mathbf{\Omega}}^{\mathrm{T}}_{\mathsf{HB}} \mathbf{1}_{N_{\mathsf{T}}}/N_{\mathsf{T}}. \tag{5.26}$$

Finally, the total power consumption is given by

$$\bar{P}_{\mathsf{HBF}} = \bar{N}_{\mathsf{RF}}(\bar{\mathbf{\Omega}}_{\mathsf{HB}})(P_{\mathsf{L}} + P_{\mathsf{LO}} + P_{\mathsf{D}}(b_D)) + \sum_{n=1}^{N_{\mathsf{T}}} \bar{P}^{\mathrm{DC},n}_{\mathsf{PA,HBF}}, \tag{5.27}$$

where $\bar{P}_{\mathsf{HBF}}$ is the power consumption terms that has been employed in (5.21).

Algorithm 3: Efficient HBF (E-HBF-Net)

Training Phase:

Input: $\hat{\mathbf{H}}$
Output: $\Re[\mathbf{W}]$, $\Im[\mathbf{W}]$, $\mathbf{P}_q$, and $\bar{\mathbf{\Omega}}_{\mathsf{HB}}$
for i ***in range(****epochs)* **do**
  FeedForward E-HBF-Net.train()
  $\mathbf{W} = \Re[\mathbf{W}] + i\Im[\mathbf{W}]$
  $\mathbf{A} = \mathbf{P}_q \otimes \bar{\mathbf{\Omega}}_{\mathsf{HB}}$,
  $\bar{P}^{n}_{\mathsf{TX}}$, $\bar{P}^{in,n}_{\mathsf{PA,HBF}}$, and $\bar{N}_{\mathsf{RF}}(\bar{\mathbf{\Omega}}_{\mathsf{HB}})$ in (5.23) in (5.25), and (5.26)
  compute P_{HBF} based on (5.27)
  compute $R_{\mathsf{HBF}}(\bar{\mathbf{A}}, \mathbf{W})$ based on (5.6)
  Loss: $\mathcal{L}_{\mathsf{BF}} = \gamma\mathcal{L}_{\mathsf{EC}} + \mathcal{L}_{\mathsf{AAS}}$
  compute gradient over layers
  update weights and biases with **AdamW** optimizer

Online Phase:

Input: $\hat{\mathbf{H}}$
Output: $\mathbf{W}$, $\mathbf{P}_q$, and $\mathbf{\Omega}_{\mathsf{HB}}$
FeedForward E-HBF-Net.eval()
$\mathbf{\Omega}_{\mathsf{HB}} = \lfloor \bar{\mathbf{\Omega}}_{\mathsf{HB}} \rceil$
$\mathbf{W} = \Re[\mathbf{W}] + i\Im[\mathbf{W}]$
$\mathbf{A} = \mathbf{P}_q \otimes \mathbf{\Omega}_{\mathsf{HB}}$,

Fully Digital Precoder (E-FDP-Net)

E-FDP-Net provides the precoder $\mathbf{U} = \Re[\mathbf{U}] + i\Im[\mathbf{U}]$ and the vector $\bar{\boldsymbol{\omega}}$ for antenna selection, where $\bar{\mathbf{\Omega}}_{\mathsf{FD}} = \mathrm{diag}(\bar{\boldsymbol{\omega}})$. To evaluate the first term of the loss function detailed in (5.20), the total power consumption of FDP ($\bar{P}_{\mathsf{FDP}}$) is required. Computing $\bar{P}_{\mathsf{FDP}}$ for E-FDP-Net is simpler than HBF because in FDP each antenna is connected to one RF chain. Consequently, the input power of each PA is simply P^{out}_{BB}. Similar to HBF, to respect the power constraint for FDP, $\|\bar{\mathbf{U}}\|^2_F \leq P_{\mathsf{TX}}$, the output power should be a function of $\bar{\boldsymbol{\omega}} = [\bar{\omega}_1, ..., \bar{\omega}_{N_{\mathsf{T}}}]$. As a

Algorithm 4: Efficient FDP (E-FDP-Net)

Training Phase:
Input: $\hat{\mathbf{H}}$
Output: $\Re[\mathbf{U}]$, $\Im[\mathbf{U}]$, and $\bar{\mathbf{\Omega}}_{\mathsf{FD}}$
for i ***in range(****epochs)* **do**
  FeedForward E-FDP-Net.train()
  $\bar{\mathbf{\Omega}}_{\mathsf{FD}} = \mathrm{diag}(\bar{\boldsymbol{\omega}})$
  compute $\bar{P}^n_{\mathsf{TX}}$ as (5.28)
  $\bar{\mathbf{U}} = \Re[\mathbf{U}] + i\Im[\mathbf{U}]$
  compute P_{FDP} based on (5.27)
  compute $R_{\mathsf{FDP}}(\bar{\mathbf{\Omega}}_{\mathsf{FD}} \times \mathbf{U})$ based on (5.3)
  Loss: $\mathcal{L}_{\mathsf{BF}} = \gamma\mathcal{L}_{\mathsf{EC}} + \mathcal{L}_{\mathsf{AAS}}$
  compute gradient over layers
  update weights and biases with **AdamW** optimizer

Online Phase:
Input: $\hat{\mathbf{H}}$
Output: $\mathbf{U}$, and $\mathbf{\Omega}_{\mathsf{FD}}$
FeedForward E-FDP-Net.eval()
$\mathbf{\Omega}_{\mathsf{FD}} = \mathrm{diag}(\lfloor\bar{\boldsymbol{\omega}}\rceil)$
$\mathbf{U} = \Re[\mathbf{U}] + i\Im[\mathbf{U}]$

consequence, we denote the output power of the n^{th} antenna as

$$\bar{P}^n_{\mathsf{TX}} = \sum_{u=1}^{N_{\mathsf{U}}} |[\mathbf{U}]_{n,u}|^2 \bar{\omega}_n \,. \tag{5.28}$$

Therefore, the power consumed by the PAs is given by (5.17). Finally, the power consumed by the active RF chains is also easy to compute because the number of active RF chains is given by $\bar{N}_{\mathsf{RF}}(\bar{\mathbf{\Omega}}_{\mathsf{FD}}) = \sum_{n=1}^{N_{\mathsf{T}}} \bar{\boldsymbol{\omega}}$.

5.5.3 Online Phase: Transmitting Data

Once the DNN has been trained, the online phase can start as shown in Figure 5.6 (right). In the online phase, the DNN input is only given by the imperfect channel matrices $\hat{\mathbf{H}}$. In the online phase, like the training phase, the outputs of the DNN: the AP ($\mathbf{P}_q$) and the DP ($\mathbf{W}$) in HBF and ($\mathbf{U}$) in FDP can be employed as is without any further processing, which is not the case for the connection matrix $\bar{\mathbf{\Omega}}$. Since the connection matrix ($\bar{\mathbf{\Omega}}_{\mathsf{HB}}$ in HBF or $\bar{\boldsymbol{\omega}}$ in FDP) should be binary, once it is output by the DNN in the online phase, it requires binary quantization. To do so, we can use the element-wise round function ($\lfloor\cdot\rceil$) on each element of the connection matrix as follows: $\mathbf{\Omega}_{\mathsf{HB}} = \lfloor\bar{\mathbf{\Omega}}_{\mathsf{HB}}\rceil$ for HBF and $\boldsymbol{\omega} = \lfloor\bar{\boldsymbol{\omega}}\rceil$,

and $\mathbf{\Omega}_{\mathsf{FD}} = \text{diag}(\boldsymbol{\omega})$ for FDP. The output power of the n^{th} antenna for E-HBF-Net is given by the n^{th} element of the power vector defined in (5.23) while for E-FDP-Net it is given by (5.28). The two proposed DNN solutions, E-HBF-Net and E-FDP-Net, are described in Algorithm 3, Algorithm 4, respectively.

5.6 Performance Evaluation

In this section, the performance of the proposed DNN, implemented using the PyTorch deep learning library, is numerically evaluated. The scenario "O1-28 GHz" of the deepMIMO channel model [141] is employed to generate the unlabeled dataset (the channel coefficients $\mathbf{h}_u$ for user u) for the training and testing. In the deepMIMO dataset [141], realistic channel information is generated by applying ray-tracing methods to a three-dimensional model of an urban environment to capture the geometry-based characteristics, such as the correlation between the channels at different locations, and the dependence on the materials of the various environmental elements, among others. The parameters to generate the deepMIMO dataset are shown in Table 5.4, where the channel model parameters `active_user_first` and `active_user_last` are set to 1100 and 2200 respectively. The BS is equipped with $N_{\mathsf{T}} = 64$ antennas and $N_{\mathsf{RF}} = 8$ RF chains with PSs serving $N_{\mathsf{U}} = 4$ users randomly located in a dedicated area (**S1** in Figure 5.7). Scenario "O1" consists of several users' locations being randomly placed in two streets surrounded by buildings. These two streets are orthogonal and intersect in the middle of the considered area. The size of the DNN dataset is set to 2×10^6 samples, with 85% of the samples used for the training set and the remaining used to evaluate the performance. We used "AdamW" as the DNN training optimizer. The hyper-parameters used in our DNN model are listed in Table 5.5. In addition, hyper-parameter τ known as the Gumbel-Sigmoid temperature is set to 0.1 and 0.5 for E-HBF-Net and E-FDP-Net, respectively, while the best value for hyper-parameter γ, described in (5.20), depends on R_{d}, and ranges from $\gamma = 0.1$ for $R_{\mathsf{d}} = 1$, to $\gamma = 0.005$ for $R_{\mathsf{d}} = 8$. The training procedure required 200 epochs.

5.6.1 Spectral Efficiency and Power Consumption Analysis

We first verify the maximum SE that can be achieved by the proposed DNNs, when they are trained without considering their power consumption, and compare them with the baseline solutions presented in Section 5.3.1. This maximal SE is shown in Figure 5.8 when varying the noise power. Taking into account channel attenuation, the average SNR ranges from -7.8 dB to 22.2 dB. To obtain the maximum SE, we set $\gamma = 0$ so that the loss function for E-HBF-Net and E-FDP-Net in (5.21) depends only on $\mathcal{L}_{\mathsf{AS}}$ and we set $R_{\mathsf{d}} = 15$ to have no constraint

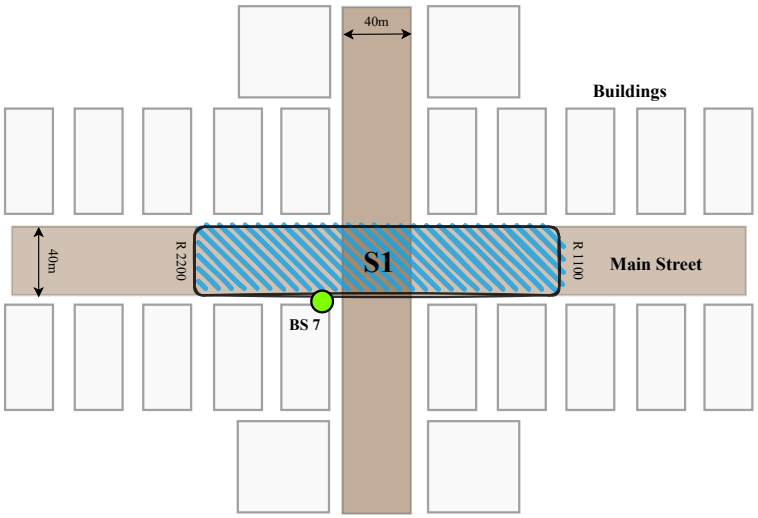

Figure 5.7: Illustration of the selected covered area from deepMIMO channel model [141]

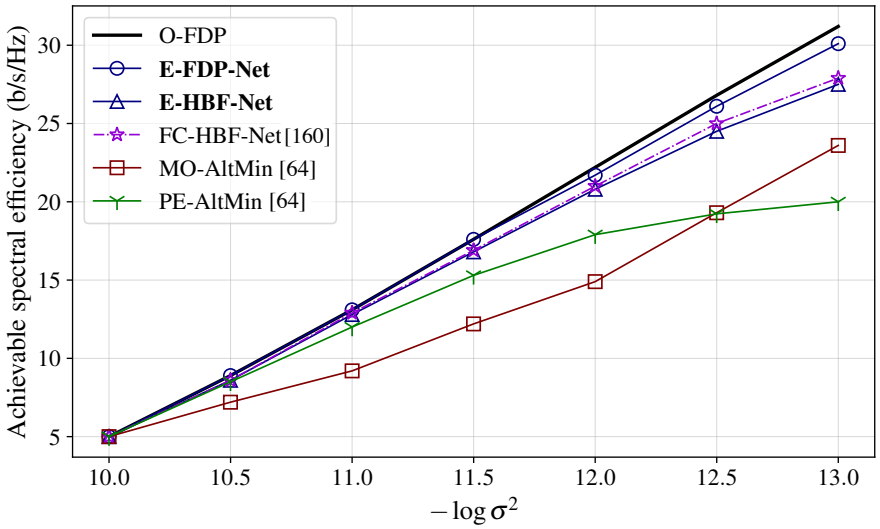

Figure 5.8: Maximum spectral efficiency of E-FDP-Net and E-HBF-Net, compared to other conventional approaches. System parameters are set to: $N_{\mathsf{U}} = 4$, $N_{\mathsf{RF}} = 8$, $N_{\mathsf{T}} = 64$

Table 5.4 Parameter selection for the deepMIMO channel model

System		Antennas	
Parameter	Value	Parameter	Value
`scenario`	"O1-28 GHz"	`num_ant_x`	1
`bandwidth`	0.5 GHz	`num_ant_y`	8
`num_OFDM`	512	`num_ant_z`	8
`num_paths`	2	`ant_spacing`	0.5

Table 5.5 Proposed DNN hyper-parameters

Parameter	Set Value
Mini-batch size	1000
Initial learning rate	0.005
ReduceLROnPlateau (factor)	0.4
ReduceLROnPlateau (patience)	10
Weight decay	10^{-5}
Dropout keep probability	.95
Kernel size	3
Zero padding	1
"ϵ" in BatchNorm (1D & 2D)	10^{-5}

on SE. On the one hand, the proposed E-FDP-Net gives a close-to-optimal performance. On the other hand, E-HBF-Net, outperforms other conventional solutions and is very close to E-FDP-Net performance. In the low-noise regime, the SE of all solutions continues to increase. However, both E-HBF-Net and E-FDP-Net outperform other conventional non-DL solutions in high SNR regimes.

In Figure 5.9, we compare the power consumption of different BF hardware configurations at a given SE. It is shown that by adjusting R_{d} for E-FDP-Net and E-HBF-Net, different SE and power consumption trade-offs can be obtained, where for each proposed technique we set R_{d} in $\{1, 3, 5, 6, 8\}$. To cover a range of SE values, we also adjust the transmitted power for the conventional methods by setting P_{TX} in $\{0.1, 1, 10\}$W. We see that the optimal FDP and the proposed E-FDP-Net with $R_{\mathsf{d}} = 8$ achieve the best SE. However, they also consume the most power because they require to activate all N_{T} RF chains. In this figure, we see that when the desired SE parameter R_d is reduced, both E-FDP-Net and E-HBF-Net are able to reduce their power consumption. For example, when R_{d} is decreased from 8 to 5 bits/s/Hz/user, the consumed power for both E-FDP-Net and E-HBF-Net is reduced

Table 5.6 Simulation parameters for the energy model

Parameter	Value	Parameter	Value
FoM_{L}	1.4 mW/GHz	IL_{C}	1.8 dB
FoM_{D}	54.5 fJ/conv	IL_{M}	5.5 dB
f_s	0.5 GHz	$\text{IL}_{\mathbf{\Phi}}$	3.7 dB
f_c	500 MHz	$\text{IL}_{\mathbf{\Psi}}$	1 dB
P_{TX}	40 dBm	P_{LO}	10 mW
α	36%	P_{L}	0.7 mW
P_{BB}^{out}	-5.6 dBm	b_D	6 bits

significantly (64% less for E-FDP-Net and 68% less for E-HDF-Net). By decreasing R_{d} further, both the power consumption and the SE continue to decrease. Furthermore, we see that E-FDP-Net and E-HBF-Net achieve must better energy efficiency than the baseline approaches. For example, when $R_{\mathsf{d}} = 6$, it can be seen that E-HBF-Net achieves similar SE compared to FC-HBF solved with MO-AltMin, but with almost 1.7 times less consumed power. Further, the baseline solutions exhibit a power floor, shown by red lines in the figure, that corresponds to the power consumed by RF chains. When the transmit power of O-FDP and FC-HBF is decreased to $P_{\mathsf{TX}} = 1$W and $P_{\mathsf{TX}} = 0.1$W, the SE is degraded due to the lower transmit power. However, there is constant power consumption for each beamforming technique due to the operation of RF chains. On the contrary, E-FDP-Net and E-HBF-Net have the ability to reduce their power consumption below these floors by adaptively turning off their RF chains.

To illustrate how many antennas are activated by E-FDP-Net, we plot in Figure 5.10 the connection matrix $\bar{\mathbf{\Omega}}_{\mathsf{FD}}$ for one sample of the test set, for different values of R_{d}, where a blue square represents the value 1 and a white square represents the value 0. It can be seen that large values of R_{d} lead to more active antennas (and thus more active RF chains), and thus to a higher power consumption. In Figure 5.11, we show the average value of $\bar{\mathbf{\Omega}}_{\mathsf{HB}}$ over the inputs, for different values of R_{d}. When decreasing R_{d}, the number of active antennas (non-zero columns) remains constant, while the number of active RF chains (non-zero rows) is reduced. This is because the power consumption of an antenna depends on its transmit power, which can be adjusted, whereas RF chains consume a fixed amount of power and must be turned off to save power. It is interesting to see that with a lower value of R_{d}, the E-HBF-Net designs the connection matrix such that a small number of RF chains are activated that are connected to several antennas, which helps to increase the spatial multiplexing gain

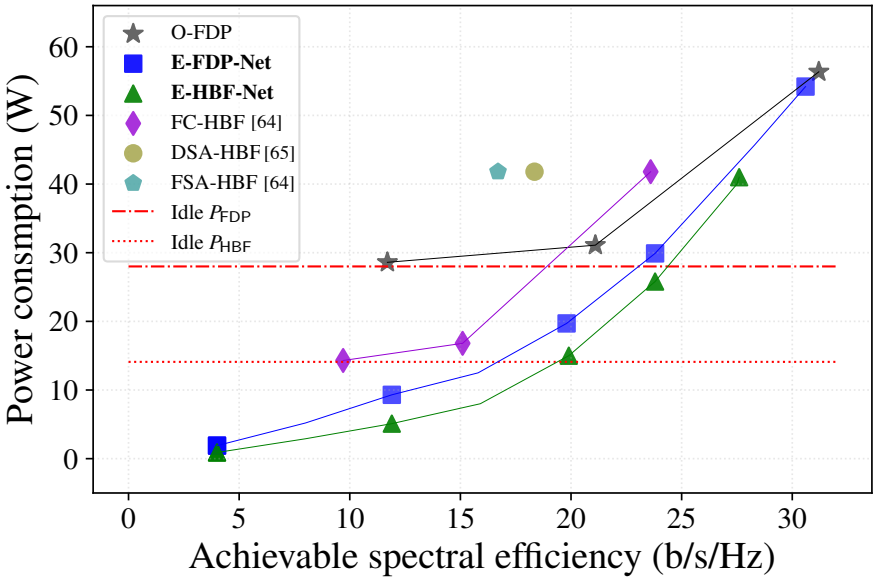

Figure 5.9: Power required to achieve a given SE for the various transmitter configurations. Idle P_{BF} is the power consumed by the BF structure when $P_{\mathsf{TX}} = 0$. The parameters are set to: $N_{\mathsf{U}} = 4$, $N_{\mathsf{T}} = 64$, $N_{\mathsf{RF}} = 8$, and $\sigma^2 = -130$ dBm

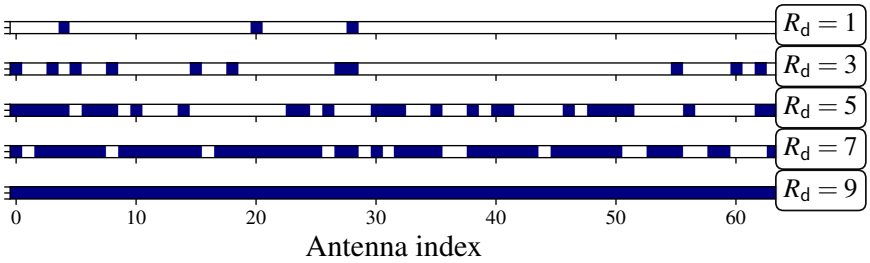

Figure 5.10: The connection matrix $\bar{\mathbf{\Omega}}_{\mathsf{FD}} = \mathrm{diag}(\bar{\boldsymbol{\omega}})$ of E-FDP-Net for one input sample, and for different values of hyper-parameter R_{d}, where a blue square represents the value 1 and a white one represents the value 0. System parameters are set to: $N_{\mathsf{U}} = 4$, $N_{\mathsf{T}} = 64$, and $\sigma^2 = -130$ dBm

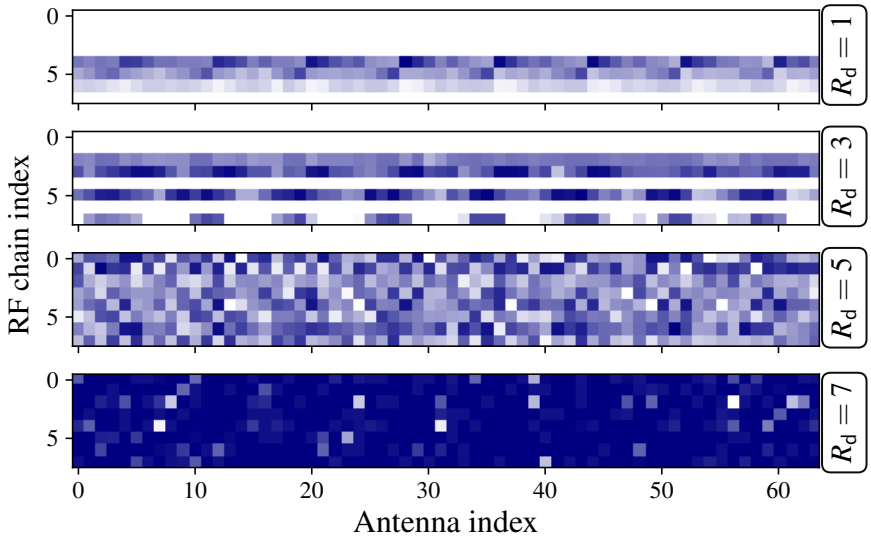

Figure 5.11: The average value of the connection matrix $\bar{\mathbf{\Omega}}_{\mathsf{HB}}$ of E-HBF-Net given for different values of hyper-parameter R_{d}, where the shade of each square represents the range of values from 0 (light) to 1 (dark). System parameters are set to: $N_{\mathsf{U}} = 4$, $N_{\mathsf{T}} = 64$, $N_{\mathsf{RF}} = 8$, and $\sigma^2 = -130$ dBm

and degrees of freedom. Finally, we see that as R_{d} increases, more antennas and more RF chains are activated, and thus more power is used.

Figure 5.12 presents the EE versus SE comparison for the proposed E-FDP-Net and E-HBF-Net, with varying adjustments to R_{d}. Notably, as SE decreases, E-HBF-Net demonstrates superior EE performance compared to E-FDP-Net. This outcome is attributed to the behavior of E-HBF-Net at lower SE values, where it intelligently deactivates RF chains while keeping multiple antennas active. Conversely, in E-FDP-Net, turning off an RF chain also turns off the associated antenna. Consequently, E-HBF-Net excels in conserving energy while simultaneously offering enhanced SE due to its higher flexibility. Furthermore, as SE increases, E-HBF-Net maintains its efficiency advantage over E-FDP-Net, although the performance gap between the two approaches diminishes.

5.6.2 Varying the Number of Users

To show the impact of antenna and RF chain selection when varying the number of active users, we present Figure 5.13 for $R_{\mathsf{d}} = 3$ and $R_{\mathsf{d}} = 5$, where the left-side sub-plots present E-FDP-Net and the right-side ones shows E-HBF-Net. To improve the presentation we use the normalized number of active RF chains ($\frac{N_{\mathsf{RF}}(\mathbf{\Omega})}{N_{\mathsf{RF}}}$), which in the case of FDP is equal to the number of active antennas. In the proposed solutions, we see that by increasing the

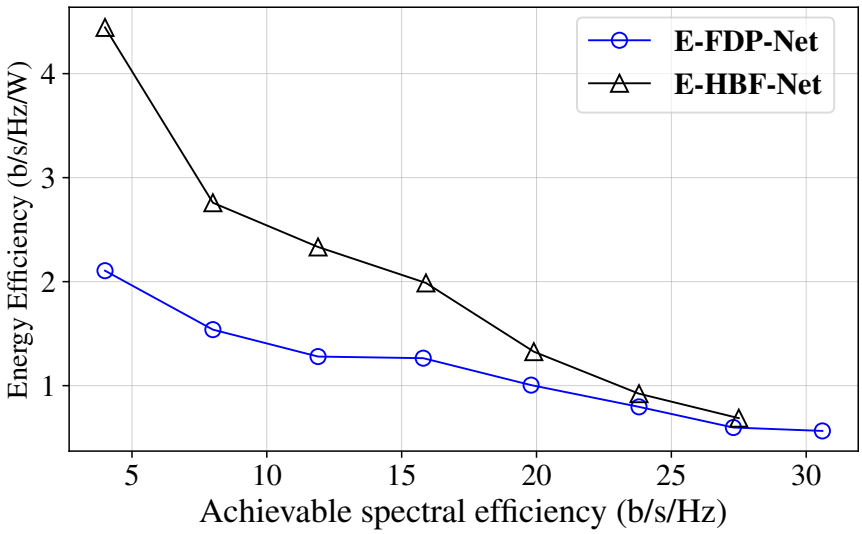

Figure 5.12: EE versus SE for the proposed E-HBF-Net and E-FDF-Net. The parameters are set to: $N_{\mathsf{U}} = 4$, $N_{\mathsf{T}} = 64$, $N_{\mathsf{RF}} = 8$, and $\sigma^2 = -130$ dBm

number of active users, the DNN not only activates more RF chains but also increases the transmitted power to meet R_{d}. Moreover, when R_{d} is small, the DNN requires a smaller number of active RF chains while minimizing the transmitted power, thus lowering power consumption and consequently increasing EE. Figure 5.13 shows that the proposed DNN approaches are adaptive to the number of active users in the network. That is, depending on the scenario, the DNN designs the beamforming structures to adapt to the varying number of users in each scenario. For instance, in a high-traffic scenario, when the number of active users is large, the DNN will activate more antennas and RF chains to meet the average SE. On the other hand, in a low-traffic scenario, when the number of users is low, the DNN has no need to activate a large number of antennas and RF chains, and thus can significantly increase its EE. Finally, we notice that by controlling the value of R_{d}, which depends on the application and the objective of the service provider, the power consumption can be adjusted.

5.6.3 Training with Imperfect CSI

Unlike other studies that assume perfect CSI for DNN training, in this work, we employed imperfect CSI not only for the input of the DNN but also for the computation of the loss function. The robustness of the proposed methods against imperfect CSI is evaluated and compared to other non-DL methods in Figure 5.14. Here we train the DNN with different β in $\{0, 0.1, 0.2, 0.3, 0.4, 0.5\}$. It is clear that the SE performance decreases as the value of β increases. In particular, when β increases from 0 to 0.5, the SE performance for O-FDP

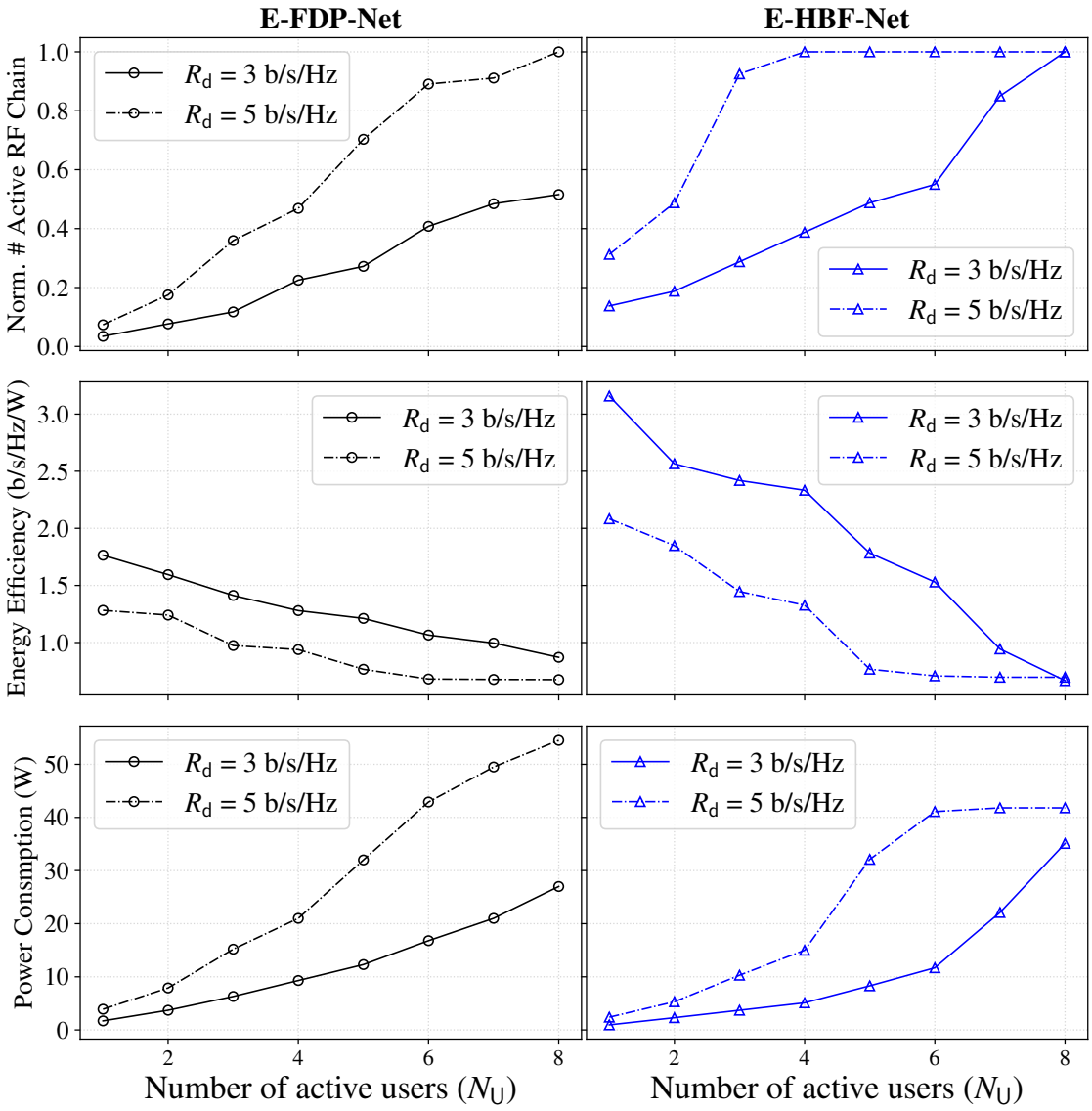

Figure 5.13: The normalized number of active RF chains, EE, and power consumption of the proposed E-FDP-Net (left sub-plots), E-HBF-Net (right sub-plots) versus different numbers of users. System parameters are set to: $N_{\mathsf{RF}} = 8$, $N_{\mathsf{T}} = 64$, and $\sigma^2 = -130$ dBm

degraded by 38%. For PE-AltMin, the degradation is around 25%, whereas it is around 27%, for MO-AltMin. The lowest degradation in terms of SE performance is achieved for E-HBF-Net and E-FDP-Net, (e.g., the degradation is around 9% and 11%, respectively). Therefore, the proposed methods are more robust against estimation errors. Moreover, the red lines in Figure 5.14 shows the ideal case of perfect CSI when $\beta = 0$. It is interesting to see that for a small β (i.e. 0.1) the SE performance did not degrade, but in contrast, it slightly improved in the online phase. This is due to the fact that training with imperfect CSI can act as a regularization technique known as noise injection in the machine learning literature and thus can improve the generalization of the DNN in the online phase [177].

In Figure 5.15, we present the convergence of the training of the proposed E-FDP-Net in terms of SE, power consumption, and EE, when $R_{\mathsf{d}} = 3$ and $N_{\mathsf{U}} = 4$. We see in the top subplot that the DNN learns quickly to design the connection matrix and the FDP to obtain an SE of $N_{\mathsf{U}} R_{\mathsf{d}} = 12$, i.e., after few epochs, the achieved SE for each user is around R_{d}. Then, while the SE target is respected, the DNN learns to gradually reduce power consumption by turning off some RF chains until it achieves the minimum power consumption as shown in the middle subplot.

5.6.4 Computational Complexity Analysis

To evaluate the computational complexity of the proposed DNNs, we derive the analytical expression of the number of real multiplications (RM) and compare it with other approaches. We assume that one complex multiplication (CM) corresponds to 4 RMs and that the 1 complex division corresponds to 8 RMs (assuming that the real division of 1 is equal to 1 RM). Only the matrix multiplications and inversions are taken into consideration, the other operations are considered negligible. A CM between a matrix of size $N \times P$ and a matrix of size $P \times M$ requires NMP CMs. To invert a square matrix of size N, around $N^3/3$ CMs are required if the Gaussian elimination algorithm is employed. Finally, we consider that the eigenvalues of a square matrix of size N are obtained using the Cholesky decomposition [152], which requires approximately $4N^3$ RMs.

O-FDP requires $4(2^{N_{\mathsf{U}}} - 1)(2N_{\mathsf{U}}N_{\mathsf{T}}^2 + N_{\mathsf{U}}^2 N_{\mathsf{T}} + \frac{1}{3}N_{\mathsf{T}}^3)$ RMs as described in [46]. In the specified scenario, we replicate the implementation of SoTA algorithms. Our observations reveal that the PE-AltMin algorithm typically achieves convergence within an average of $\ell_{\mathsf{PE}} = 15$ iterations. Given that the computation of the singular-value decomposition of a $p \times q$ matrix necessitates approximately $4p^2q + 22q^3$ resource modules (RMs), we can formulate the total number of RMs required for PE-AltMin as $\ell_{\mathsf{PE}}(8N_{\mathsf{RF}}N_{\mathsf{U}}(N_{\mathsf{T}} + N_{\mathsf{U}}) + 22N_{\mathsf{RF}}^3)$. MO-AltMin has a much higher complexity than PE-AltMin [64]. MO-AltMin is composed of a main loop

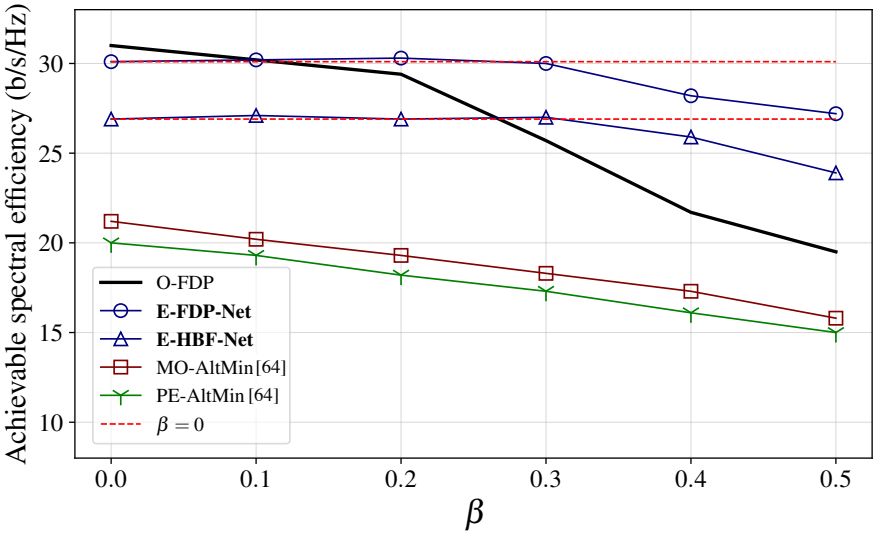

Figure 5.14: The SE comparison of the different BF solutions with different values of β. System parameters are set to: $N_{\mathsf{U}} = 4$, $N_{\mathsf{RF}} = 8$, $N_{\mathsf{T}} = 64$, $\gamma = 0$, $\sigma^2 = -130$ dBm

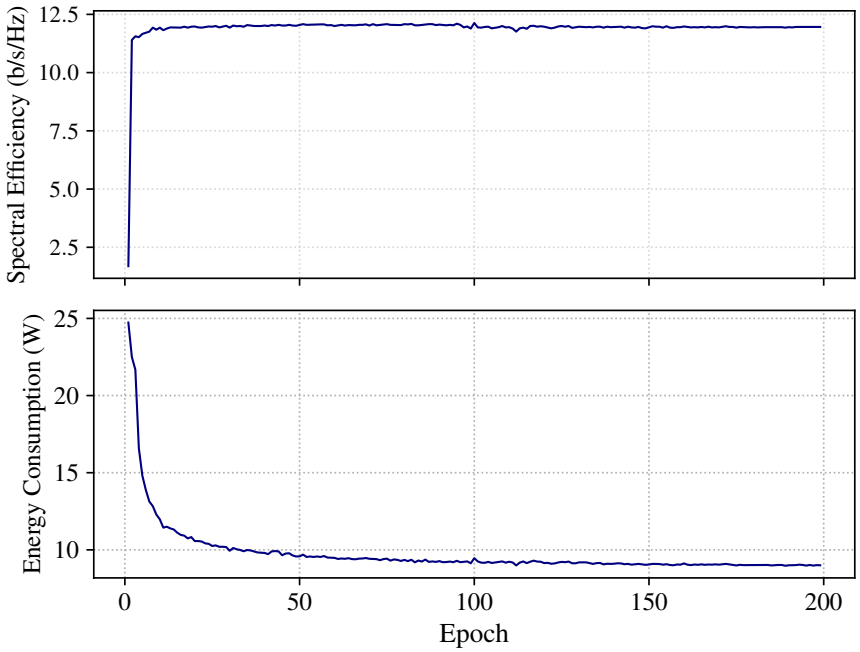

Figure 5.15: Training steps of E-FDP-Net. The parameters are set to: $N_{\mathsf{U}} = 4$, $N_{\mathsf{RF}} = 8$, $N_{\mathsf{T}} = 64$, and $R_{\mathsf{d}} = 3$

that computes the DP, and of an inner loop applying the "Conjugate Gradient" algorithm to find the HBF. In the main loop, computing the DP requires $4N_{\mathsf{T}}N_{\mathsf{U}}N_{\mathsf{RF}}$ RMs, while in the inner loop, the Kronecker product of a $N_{\mathsf{RF}} \times N_{\mathsf{T}}$ matrix with a $N_{\mathsf{U}} \times N_{\mathsf{T}}$ matrix is computed, which requires $4N_{\mathsf{T}}^2N_{\mathsf{U}}N_{\mathsf{RF}}$ RMs. Based on the defined scenario the outer loop is repeated $\ell_{\mathsf{MO}} = 2$ times while the inner loop is repeated $\ell' = 30$ times, the total number of RMs used by MO-AltMin is $4\ell_{\mathsf{MO}}N_{\mathsf{T}}N_{\mathsf{U}}N_{\mathsf{RF}}\Big(1+\ell' N_{\mathsf{T}}\Big)$. To design the HBF, both PE-AltMin and MO-AltMin require designing the FDP as discussed in (5.10), thus the complexity of obtaining the FDP should be added to the complexity of PE-AltMin and MO-AltMin.

On the other hand, to compute the computational complexity of the DNN approaches, we need to compute the number of parameters of the DNN architectures. Both DNN architectures, E-HBF-Net and E-FDP-Net, have the same $\text{DNN}_{\mathsf{core}}$ but their output layers are different due to different output dimensions. The number of RMs in the $\text{DNN}_{\mathsf{core}}$ is calculated for each layer separately, then summed up. The width of the l^{th} FC and CL are respectively denoted as f_l and c_l. The number of multiplications required for $\text{DNN}_{\mathsf{core}}$ is $\mathcal{M}(\text{DNN}_{\mathsf{core}}) = (2c_1 + c_1c_2 + c_2c_3 + c_3f_1/\kappa^2)N_{\mathsf{T}}N_{\mathsf{U}}\kappa^2 + f_1f_2$, where κ is the kernel size i.e. $\kappa = 3$ [46]. Considering that for E-HBF-Net there are 4 output layers, one layer for the AP, two layers for the DP, and one layer for the connection matrix, then the total number of multiplications is $\mathcal{M}(\text{DNN}_{\mathsf{core}}) + f_2(N_{\mathsf{T}}N_{\mathsf{RF}} + 2N_{\mathsf{U}}N_{\mathsf{RF}} + N_{\mathsf{T}}N_{\mathsf{RF}})$. Likewise, for E-FDP-Net, the total number of multiplications is $\mathcal{M}(\text{DNN}_{\mathsf{core}}) + f_2(2N_{\mathsf{U}}N_{\mathsf{T}} + N_{\mathsf{T}})$. Examples of the numerical values of these analytical expressions are shown in Table 5.7. It can be seen that for HBF transmitters, E-HBF-Net reduces the complexity by 38% compared to the least complex conventional approach (PE-AltMin), while for FDP transmitters, O-FDP is 1.5 times more complex than E-FDP-Net.

Table 5.7 Computational Complexity Comparison

Transmitter type	Method	# RMs ($\times 10^6$)
FDP	O-FDP	7.27
HBF	PE-AltMin [64]	8.48
HBF	MO-AltMin [64]	38.7
FDP	**E-FDP-Net**	**4.69**
HBF	**E-HBF-Net**	**5.21**

($N_{\mathsf{U}} = 4$, $N_{\mathsf{RF}} = 8$ and $N_{\mathsf{T}} = 64$)

5.7 Conclusion

In this paper, we studied the problem of antenna selection and beamforming design in a massive multiple-input multiple-output (mMIMO) system with the objective of maximizing energy efficiency (EE). First, we derived an accurate energy model for the mMIMO system. Our proposed energy model takes into account the transmit power as well as the power consumed by the hardware by considering the insertion loss and the direct power consumption of different components such as the combiners and the power amplifiers. Next, based on our energy model, we designed unsupervised deep learning approaches to intelligently and adaptively select the BF structures and the transmitting antennas. Specifically, we proposed two deep neural networks models, called E-HBF-Net and E-FDP-Net, for hybrid BF and for fully digital precoding, respectively. Both DNNs optimize the EE of the mMIMO system by intelligently selecting the transmitting antennas and choosing the precoding matrices for HBF and FDP, which allows them to achieve significantly better EE than conventional solutions. Simulation results confirm that the proposed DNNs can adapt to the number of active users and that they provide different trade-offs between SE and EC that can be controlled by tuning a hyper-parameter. Furthermore, we show that the DNN models can be trained exclusively using imperfect channel information (CSI), i.e., the imperfect CSI was used as input to our DNN models as well as to compute the loss function during training.

CHAPTER 6 GENERAL DISCUSSION

Applied DL techniques have shown promise in addressing the challenges and improving the performance of beamforming in mMIMO systems. Deep learning algorithms, particularly DNNs, offer the ability to automatically learn complex mappings between input data and optimal SE beamforming parameters, enabling efficient and adaptive beamforming designs. One of the primary advantages of DL in beamforming is its ability to handle the high-dimensional and nonlinear nature of mMIMO systems. Deep learning models can effectively capture the intricate relationships and dependencies among a large number of antennas, users, CSI, and propagation environments. By processing extensive training data, DNNs can learn complex patterns and extract relevant features to improve beamforming performance.

The general discussion in this thesis centers on the contributions made in the realm of beamforming techniques and transmitter configurations for mMIMO communication systems, harnessing the potential of deep learning. These contributions have been articulated through a series of research papers, all driven by the shared objective of enhancing spectral efficiency, reducing computational complexity, and fortifying solutions against the challenges posed by imperfect CSI. In this chapter, we delve into the evolutionary journey of the thesis, outlining the key advancements and insights gained throughout the research process.

In the literature review presented in CHAPTER 2, it becomes evident that conventional beamforming methods frequently encounter obstacles concerning computational complexity, dependence on precise CSI, and limited adaptability. These challenges have motivated the exploration of novel approaches to address the limitations of traditional techniques. As a consequence, we present an approach to address the challenges of implementing hybrid beamforming in practical MIMO systems in CHAPTER 3. By relying solely on RSSI feedback from each user, this chapter introduces an unsupervised DL-based method to optimize the hybrid precoder. While the hybrid beamforming design in MIMO system with supervised learning is studied in [140], in CHAPTER 3, we take a step further by proposing a novel unsupervised deep learning approach for mMIMO system. By eliminating the reliance on explicit labels or feedback, the unsupervised learning framework opens new avenues for more flexible and adaptive beamforming solutions. The multi-tasking deep neural network in the second paper learns to optimize the hybrid precoding matrix based solely on the RSSI from each user, enabling a more streamlined and computationally efficient implementation.

This innovative solution significantly reduces the need for CSI feedback in FDD communication, resulting in a substantial reduction in signaling overhead. The proposed method

achieves near-optimal sum-rates comparable to complex full-CSI solutions while operating with reasonable complexity. Furthermore, the research showcases how the proposed technique greatly improves the spectral efficiency of the system compared to existing methods, making it efficient and practical for real-world applications.

In addition to the unsupervised learning aspect, CHAPTER 3 also delves into optimizing SS in IA and designing the codebook for the analog precoder. These additional contributions add valuable insights into enhancing the overall efficiency and performance of massive mMIMO systems. Evaluating the proposed method through a realistic channel model in various scenarios, the study demonstrates its ability to significantly increase spectral efficiency, particularly in FDD communication, by utilizing partial CSI feedback. Moreover, the proposed unsupervised deep learning approach showcases its capability to achieve near-optimal sum-rates, outperforming state-of-the-art full-CSI solutions while reducing the computational complexity. By building upon the foundation laid by the first paper, the second paper sets new benchmarks in hybrid beamforming for massive mMIMO systems and opens avenues for more intelligent, self-adaptive, and efficient beamforming techniques.

We then in CHAPTER 4 represent a notable extension of our previous work on "Unsupervised Deep Learning for Massive MIMO Hybrid Beamforming" by addressing the challenges associated with CF-mMIMO systems. Cell-free mMIMO systems offer a promising approach to enhance spectral efficiency by utilizing a large number of distributed AcP instead of traditional base stations. The CF-mMIMO beamforming is generally divided into two approaches, centralized and decentralized. Centralized methods are considered optimal SE as they achieve near-optimal SE beamforming solutions; however, they come with high complexity and cost. These methods rely on extensive signaling exchange between the AcPs and the NC, which can become impractical and resource-intensive in large-scale deployments, hindering their widespread adoption. On the other hand, decentralized methods are more straightforward and cost-effective, but they often suffer from performance limitations compared to their centralized counterparts.

The challenges posed by both approaches led us to explore an innovative solution using unsupervised deep learning techniques. Our proposed approach introduces two distinct unsupervised DNNs architectures: fully distributed and partially distributed. The fully distributed architecture empowers each AcP to independently optimize its beamforming strategy using only local information without the need for extensive communication with the centralized NC. This results in a cost-effective and simplified solution that reduces the signaling overhead between the AcPs and the NC. On the other hand, the partially distributed architecture allows limited communication between AcPs and the NC, striking a balance between per-

formance and complexity. This architecture outperforms fully distributed methods without incurring the high signaling overhead of centralized schemes. By leveraging unsupervised learning, both architectures achieve near-optimal sum-rates, effectively addressing the limitations of conventional centralized and decentralized approaches in CF-mMIMO systems. These innovative propositions and successful results showcase the potential of unsupervised deep learning in overcoming challenges and advancing beamforming techniques for cell-free massive mMIMO systems, paving the way for more efficient and scalable communication systems.

In CHAPTER 2, we explored various types of subarray beamforming techniques for mMIMO systems. Subarray beamforming architectures, FSA-HBF and DSA-HBF, are promising approaches that can further enhance the energy efficiency of mMIMO systems by reducing the number of phase shifters required. However, the design of hybrid beamforming vectors for subarrays presents significant challenges due to the discrete nature of subarray connections and phase-shifter quantization. Finding the optimal connections between RF chains and antennas in a large search space becomes a non-convex problem, and conventional solutions often assume the availability of perfect CSI, which is not practical in real-world scenarios.

To address these challenges, we proposed an innovative unsupervised learning approach in [48] where we aimed to improve the energy efficiency of FDP and HBF transmitters. The transmitter architecture often contains multiple parameters that need to be optimized, such as power allocation to antennas and connections between antennas and RF chains. To tackle this optimization problem, we developed an energy model for different beamforming structures and applied unsupervised deep learning to maximize energy efficiency by designing the transmitter configuration for FDP and HBF. Additionally, we introduced a loss function that offers trade-offs between spectral efficiency and energy consumption, enabling system customization based on specific requirements while being adaptive to the number of active users. In this research, we made the assumption of using passive components between the RF chains and antennas. Consequently, the primary takeaway here is that relocating the PAs to the antennas, as opposed to embedding them within the RF chains, leads to reduced dissipated power attributed to the IL caused by passive elements.

Furthermore, we investigated the ability of the proposed model to be trained exclusively using imperfect CSI, both for input to the deep learning model and for the calculation of the loss function. Our simulation results showed that the proposed solutions outperformed conventional methods in terms of energy efficiency while also exhibiting enhanced robustness to noise. By optimizing power allocation and antenna selection through unsupervised learning, our approach achieved higher energy efficiency and improved overall system performance in

massive MIMO communication. These advancements contribute to the development of cost-effective and energy-efficient wireless communication systems for future networks, and they push the system toward intelligent beamforming.

In conclusion, the general discussion of this thesis showcases the contributions achieved in the field of beamforming techniques and transmitter configurations for mMIMO communication systems through the power of deep learning. These contributions have collectively aimed to enhance spectral efficiency, reduce computational complexity, and improve the robustness of beamforming solutions against the challenges presented by imperfect CSI. By leveraging the capabilities of deep learning algorithms, particularly DNNs, we have successfully addressed various obstacles and limitations faced by conventional methods. The insights gained from this thesis lay the groundwork for further exploration and innovation in the field of beamforming for mMIMO systems, driving the industry towards more sophisticated, intelligent, and sustainable wireless networks.

CHAPTER 7 CONCLUSION AND RECOMMENDATIONS

In this chapter, we provide a summary of the major contributions, achievements, and publications originating from this thesis. Additionally, complementary considerations and methods are suggested for future work to make the proposed methods more adaptive and efficient.

7.1 Summary of Works and Contributions

This thesis has presented a series of research papers that collectively contribute to advancements in the field of beamforming techniques and transmitter configurations for mMIMO communication systems using the power of deep learning. The works presented in this thesis aimed to enhance spectral efficiency, reduce computational complexity, and improve the robustness of beamforming solutions against the challenges posed by imperfect CSI. The contributions made in this research lay the groundwork for more efficient and intelligent wireless communication systems, pushing the boundaries of traditional beamforming methods.

The journey began with "RSSI-Based Hybrid Beamforming Design with Deep Learning" [140], where we proposed a supervised deep learning-based approach for hybrid beamforming design in practical MIMO systems. By relying solely on RSSI feedback, the method significantly reduced the need for CSI feedback and minimized signaling overhead. The results demonstrated near-optimal sum-rates comparable to complex full-CSI solutions, showcasing its efficiency and practicality for real-world applications.

Building on the success of the first paper, "Unsupervised Deep Learning for Massive MIMO Hybrid Beamforming" [46], explored unsupervised deep learning methods for hybrid beamforming in massive mMIMO systems. By eliminating the reliance on explicit labels or feedback, the proposed framework provided more flexible and adaptive beamforming solutions. The study demonstrated its capability to achieve sum-rates close to the optimal levels, surpassing the performance of state-of-the-art solutions based on full-CSI, and concurrently achieving a notable reduction in computational complexity. This extension opened new avenues for more streamlined and efficient beamforming designs.

Expanding our focus to "Decentralized Beamforming for Cell-Free Massive MIMO With Unsupervised Learning" [47], we tackled the challenges of CF-mMIMO systems. Two innovative unsupervised DNNs architectures, fully distributed and partially distributed, were proposed, offering cost-effective and simplified solutions with reduced signaling overhead. Both architectures achieved near-optimal sum-rates, bridging the performance gap between centralized

and decentralized approaches in CF-mMIMO systems, making it a promising approach for future wireless networks.

We then delved into subarray beamforming techniques in "Flexible Unsupervised Learning for Massive MIMO Subarray Hybrid Beamforming" [160], introducing an unsupervised learning approach that optimized hybrid beamforming for various subarray structures. The research effectively addressed the challenges posed by discrete subarray connections and phase-shifter quantization, achieving higher sum-rates compared to existing methods.

Taking one step further, "Learning Energy-Efficient Transmitter Configurations for Massive MIMO Beamforming" [48] aimed to enhance energy efficiency in mMIMO systems. By applying unsupervised deep learning techniques, the approach optimized power allocation and antenna selection, achieving higher energy efficiency and improved system performance, even with imperfect CSI.

Overall, the works presented in this thesis significantly contributed to the advancement of beamforming techniques in mMIMO communication systems. Leveraging the potential of deep learning algorithms, we overcame various challenges and limitations faced by conventional methods. The insights gained from this research laid the foundation for more efficient, scalable, and intelligent wireless communication systems, paving the way for future advancements in beamforming technology and its applications in 5G and beyond. This thesis contributed to the growing body of knowledge in the field, ultimately driving the industry towards more sustainable, high-performing, and cost-effective wireless networks.

7.2 Future Research

As the field of beamforming techniques and transmitter configurations for mMIMO communication systems continues to evolve, there are several exciting avenues for future research that can further enhance the performance and adaptability of these systems. One key direction is to make beamforming solutions more adaptive to different scenarios and network conditions. Current deep learning-based approaches have shown promising results, but further research is needed to develop more adaptive models, potentially utilizing Meta-learning, that can dynamically adjust beamforming parameters based on changing network conditions, user requirements, and channel characteristics. This adaptability can significantly improve the efficiency and reliability of mMIMO communication systems in real-world deployments.

Another crucial area for future research is improving the training of DNNs for beamforming. Current methods often require large datasets and complex training processes, which can be computationally expensive and time-consuming. Researchers should explore novel techniques

to improve the efficiency and effectiveness of DNN training, such as transfer learning, where models trained on one dataset can be fine-tuned on a different dataset with limited labeled data. Transfer learning allows models trained on one task or domain to be adapted for a related task or domain. Applying transfer learning to beamforming can be highly beneficial, as it enables the knowledge learned from one set of scenarios to be transferred and fine-tuned for new scenarios, leading to more efficient and accurate beamforming solutions in different environments. This can help reduce the data requirements for training and enhance the scalability of deep learning-based beamforming solutions.

Generating representative and diverse datasets for training DNNs is another critical aspect that requires further investigation. High-quality datasets are essential for training accurate and robust models. Researchers can explore new techniques for generating synthetic datasets that capture a wide range of channel conditions and user scenarios. Additionally, efforts can be made to collect real-world data from different environments and deployment scenarios to create more comprehensive and reliable datasets.

Furthermore, future research can explore the integration of beamforming with other emerging technologies such as edge computing and artificial intelligence. Combining beamforming with edge computing can enhance the efficiency of data processing and reduce latency, especially in latency-sensitive applications. Moreover, artificial intelligence techniques, such as reinforcement learning, can be explored to develop adaptive and self-learning beamforming algorithms that continuously improve their performance based on real-time feedback from the network.

Moreover, the deployment and testing of deep learning-based beamforming techniques in real-world scenarios are essential for practical adoption. Future research should focus on conducting large-scale field trials to validate the effectiveness and reliability of these techniques in real-world mMIMO deployments. This can provide valuable insights into the real-world performance of deep learning-based beamforming and highlight areas for improvement and optimization.

Finally, DL-based solutions should be extended to more realistic scenarios such as high mobility users and channel aging, both of which pose unique challenges in the context of mMIMO communication systems. With the proliferation of mobile and IoT devices, the presence of high-speed user mobility is increasingly prevalent in wireless communication environments. Future research efforts should thus prioritize the development of beamforming strategies capable of seamlessly adapting to and tracking fast-moving users. This adaptability ensures uninterrupted connectivity and optimized performance, even in dynamic scenarios characterized by rapid user mobility.

In conclusion, the future of research in beamforming techniques for mMIMO communication systems is promising, with several exciting directions to explore. Advancements in adaptability, training efficiency, dataset generation, transfer learning, and integration with other technologies can significantly enhance the performance, reliability, and energy efficiency of mMIMO systems. The successful implementation of these future research directions will pave the way for more intelligent, scalable, and sustainable wireless communication networks, revolutionizing the way we communicate and connect in the 5G era and beyond.

7.3 Publications

1. **H. Hojatian**, V. N. Ha, J. Nadal, J.-F. Frigon, and F. Leduc-Primeau, "RSSI-Based Hybrid Beamforming Design with Deep Learning," ICC 2020 - IEEE International Conference on Communications (ICC), Dublin, Ireland, 2020, pp. 1-6.

2. **H. Hojatian**, J. Nadal, J.-F. Frigon, and F. Leduc-Primeau, "Unsupervised Deep Learning for Massive MIMO Hybrid Beamforming," in IEEE Transactions on Wireless Communications, vol. 20, no. 11, pp. 7086-7099, Nov. 2021.

3. **H. Hojatian**, J. Nadal, J.-F. Frigon, and F. Leduc-Primeau, "Decentralized Beamforming for Cell-Free Massive MIMO With Unsupervised Learning," in IEEE Communications Letters, vol. 26, no. 5, pp. 1042-1046, May 2022.

4. **H. Hojatian**, J. Nadal, J.-F. Frigon, and F. Leduc–Primeau, "Flexible Unsupervised Learning for Massive MIMO Subarray Hybrid Beamforming," GLOBECOM 2022 - IEEE Global Communications Conference, Rio de Janeiro, Brazil, 2022, pp. 3833-3838.

5. **H. Hojatian**, F. Leduc-Primeau, J. Nadal, J.-F. Frigon, and Z. Mlika, "Learning Energy-Efficient Massive MIMO Beamforming," U.S patent, filed by Ericsson, PCT/IB2023/053214, Feb. 2023.

6. **H. Hojatian**, Z. Mlika, J. Nadal, J.-F. Frigon, and F. Leduc-Primeau, "Learning Energy-Efficient Transmitter Configurations for Massive MIMO Beamforming," in IEEE Transactions on Machine Learning in Communications and Networking, submitted, Aug. 2023.

REFERENCES

[1] M. Z. Chowdhury, M. Shahjalal, S. Ahmed, and Y. M. Jang, "6G wireless communication systems: Applications, requirements, technologies, challenges, and research directions," *IEEE Open Journal of the Communications Society*, vol. 1, pp. 957–975, 2020.

[2] P. Yang, Y. Xiao, M. Xiao, and S. Li, "6G wireless communications: vision and potential techniques," *IEEE Network*, vol. 33, no. 4, pp. 70–75, 2019.

[3] T. L. Marzetta, "Noncooperative cellular wireless with unlimited numbers of Base station antennas," *IEEE Transactions on Wireless Communications*, vol. 9, no. 11, pp. 3590–3600, Nov. 2010.

[4] ——, "Massive MIMO: An introduction," *Bell Labs Technical Journal*, vol. 20, pp. 11–12, 2015.

[5] L. Lu, G. Y. Li, A. L. Swindlehurst, A. Ashikhmin, and R. Zhang, "An overview of massive MIMO: Benefits and challenges," *IEEE Journal of Selected Topics in Signal Processing*, vol. 8, no. 5, pp. 742–758, 2014.

[6] A. F. Molisch, V. V. Ratnam, S. Han, Z. Li, S. L. H. Nguyen, L. Li, and K. Haneda, "Hybrid beamforming for massive MIMO: A survey," *IEEE Communications Magazine*, vol. 55, no. 9, pp. 134–141, 2017.

[7] I. Goodfellow, Y. Bengio, and A. Courville, *Deep Learning*. MIT Press, 2016, http://www.deeplearningbook.org.

[8] K. B. Letaief, W. Chen, Y. Shi, J. Zhang, and Y.-J. A. Zhang, "The roadmap to 6G: AI empowered wireless networks," *IEEE Communications Magazine*, vol. 57, no. 8, pp. 84–90, 2019.

[9] Z. Qin, H. Ye, G. Y. Li, and B.-H. F. Juang, "Deep learning in physical layer communications," *IEEE Wireless Communications*, vol. 26, no. 2, pp. 93–99, 2019.

[10] H. Q. Ngo, A. Ashikhmin, H. Yang, E. G. Larsson, and T. L. Marzetta, "Cell-free massive MIMO versus small cells," *IEEE Transactions on Wireless Communications*, vol. 16, no. 3, pp. 1834–1850, 2017.

[11] B. Gopinath, "On the control of linear multiple input-output systems," *The Bell System Technical Journal*, vol. 50, no. 3, pp. 1063–1081, 1971.

[12] P. Rudnick, "Digital beamforming in the frequency domain," *Journal of the Acoustical Society of America (USA)*, vol. 46, no. 5, pp. 1089–90, 1969/11/. [Online]. Available: http://dx.doi.org/10.1121/1.1911828

[13] T. L. Marzetta and H. Yang, *Fundamentals of massive MIMO*. Cambridge University Press, 2016.

[14] E. G. Larsson, O. Edfors, F. Tufvesson, and T. L. Marzetta, "Massive MIMO for next generation wireless systems," *IEEE Communications Magazine*, vol. 52, no. 2, pp. 186–195, 2014.

[15] E. Björnson, J. Hoydis, and L. Sanguinetti, *Massive MIMO Networks: Spectral, Energy, and Hardware Efficiency*, 2017.

[16] J. G. Andrews, S. Buzzi, W. Choi, S. V. Hanly, A. Lozano, A. C. Soong, and J. C. Zhang, "What will 5G be?" *IEEE Journal on Selected Areas in Communications*, vol. 32, no. 6, pp. 1065–1082, Jun. 2014.

[17] A. Swindlehurst, E. Ayanoglu, P. Heydari, and F. Capolino, "Millimeter-wave massive MIMO: The next wireless revolution?" *IEEE Communications Magazine*, vol. 52, no. 9, pp. 56–62, 2014.

[18] J. Zhang, X. Ge, Q. Li, M. Guizani, and Y. Zhang, "5G millimeter-wave antenna array: Design and challenges," *IEEE Wireless Communications*, vol. 24, no. 2, pp. 106–112, 2017.

[19] I. F. Akyildiz, A. Kak, and S. Nie, "6G and beyond: The future of wireless communications systems," *IEEE Access*, vol. 8, pp. 133 995–134 030, 2020.

[20] G. Caire and S. Shamai, "On the achievable throughput of a multiantenna Gaussian broadcast channel," *IEEE Transactions on Information Theory*, vol. 49, no. 7, pp. 1691–1706, 2003.

[21] J. Hoydis, S. ten Brink, and M. Debbah, "Massive MIMO in the UL/DL of cellular networks: How many antennas do we need?" *IEEE Journal on Selected Areas in Communications*, vol. 31, no. 2, pp. 160–171, 2013.

[22] A. Adhikary, J. Nam, J.-Y. Ahn, and G. Caire, "Joint spatial division and multiplexing—The large-scale array regime," *IEEE Transactions on Information Theory*, vol. 59, no. 10, pp. 6441–6463, 2013.

[23] H. Huh, G. Caire, H. C. Papadopoulos, and S. A. Ramprashad, "Achieving "Massive MIMO"' spectral efficiency with a Not-so-Large number of antennas," *IEEE Transactions on Wireless Communications*, vol. 11, no. 9, pp. 3226–3239, 2012.

[24] T. S. Rappaport, S. Sun, R. Mayzus, H. Zhao, Y. Azar, K. Wang, G. N. Wong, J. K. Schulz, M. Samimi, and F. Gutierrez, "Millimeter wave mobile communications for 5G cellular: It will work!" *IEEE Access*, vol. 1, pp. 335–349, 2013.

[25] P. Viswanath, D. Tse, and R. Laroia, "Opportunistic beamforming using dumb antennas," *IEEE Transactions on Information Theory*, vol. 48, no. 6, pp. 1277–1294, 2002.

[26] S. Kutty and D. Sen, "Beamforming for millimeter wave communications: An inclusive survey," *IEEE Communications Surveys & Tutorials*, vol. 18, no. 2, pp. 949–973, 2016.

[27] T. M. Mitchell, *Machine learning.* New York, 1997.

[28] Y. Lecun, Y. Bengio, and G. Hinton, "Deep learning," *Nature*, vol. 521, no. 7553, pp. 436–444, 2015.

[29] A. Esteva, B. Kuprel, R. A. Novoa, J. Ko, S. M. Swetter, H. M. Blau, and S. Thrun, "Dermatologist-level classification of skin cancer with deep neural networks," *Nature*, vol. 542, no. 7639, pp. 115–118, 2017. [Online]. Available: https://doi.org/10.1038/nature21056

[30] A. Geiger, P. Lenz, C. Stiller, and R. Urtasun, "Vision meets robotics: The KITTI dataset," *The International Journal of Robotics Research*, vol. 32, no. 11, pp. 1231–1237, 2013. [Online]. Available: https://doi.org/10.1177/0278364913491297

[31] N. J. Zakaria, M. I. Shapiai, R. A. Ghani, M. N. M. Yassin, M. Z. Ibrahim, and N. Wahid, "Lane detection in autonomous vehicles: A systematic review," *IEEE Access*, vol. 11, pp. 3729–3765, 2023.

[32] C. M. Bishop and N. M. Nasrabadi, *Pattern recognition and machine learning.* Springer, 2006.

[33] R. S. Sutton and A. G. Barto, *Reinforcement learning: An introduction.* MIT press, 2018.

[34] N. C. Luong, D. T. Hoang, S. Gong, D. Niyato, P. Wang, Y.-C. Liang, and D. I. Kim, "Applications of deep reinforcement learning in communications and networking: A survey," *IEEE Communications Surveys & Tutorials*, vol. 21, no. 4, pp. 3133–3174, 2019.

[35] R. Li, Z. Zhao, X. Zhou, G. Ding, Y. Chen, Z. Wang, and H. Zhang, "Intelligent 5G: When cellular networks meet artificial intelligence," *IEEE Wireless Communications*, vol. 24, no. 5, pp. 175–183, 2017.

[36] Q. Mao, F. Hu, and Q. Hao, "Deep learning for intelligent wireless networks: A comprehensive survey," *IEEE Communications Surveys & Tutorials*, vol. 20, no. 4, pp. 2595–2621, 2018.

[37] C. K. Wen, W. T. Shih, and S. Jin, "Deep learning for massive MIMO CSI feedback," *IEEE Wireless Communications Letters*, vol. 7, no. 5, pp. 748–751, 2018.

[38] H. Ye, G. Y. Li, and B. H. Juang, "Power of deep learning for channel estimation and signal detection in OFDM systems," *IEEE Wireless Communications Letters*, vol. 7, no. 1, pp. 114–117, 2018.

[39] H. He, C. K. Wen, S. Jin, and G. Y. Li, "Deep learning-based channel estimation for beamspace mmwave massive MIMO systems," *IEEE Wireless Communications Letters*, vol. 7, no. 5, pp. 852–855, 2018.

[40] P. Dong, H. Zhang, G. Y. Li, I. S. Gaspar, and N. Naderializadeh, "Deep CNN-based channel estimation for mmwave massive MIMO systems," *IEEE Journal on Selected Topics in Signal Processing*, vol. 13, no. 5, pp. 989–1000, Sep. 2019.

[41] N. Samuel, T. Diskin, and A. Wiesel, "Deep MIMO detection," *IEEE Workshop on Signal Processing Advances in Wireless Communications, SPAWC*, vol. 2017-July, pp. 1–5, 2017.

[42] N. Farsad and A. Goldsmith, "Detection algorithms for communication systems using deep learning," *CoRR*, vol. abs/1705.0, 2017. [Online]. Available: http://arxiv.org/abs/1705.08044

[43] T. Wang, C. K. Wen, S. Jin, and G. Y. Li, "Deep learning-based CSI feedback approach for time-varying massive MIMO channels," *IEEE Wireless Communications Letters*, vol. 8, no. 2, pp. 416–419, 2019.

[44] F. Rusek, D. Persson, B. K. Lau, E. G. Larsson, T. L. Marzetta, O. Edfors, and F. Tufvesson, "Scaling up MIMO: Opportunities and challenges with very large arrays," *IEEE Signal Processing Magazine*, vol. 30, no. 1, pp. 40–60, 2013.

[45] E. Björnson, E. G. Larsson, and T. L. Marzetta, "Massive MIMO: Ten myths and one critical question," *IEEE Communications Magazine*, vol. 54, no. 2, pp. 114–123, Feb. 2016.

[46] H. Hojatian, J. Nadal, J.-F. Frigon, and F. Leduc-Primeau, "Unsupervised deep learning for massive MIMO hybrid beamforming," *IEEE Transactions on Wireless Communications*, vol. 20, no. 11, pp. 7086–7099, 2021.

[47] ——, "Decentralized beamforming for cell-free massive MIMO with unsupervised learning," *IEEE Communications Letters*, vol. 26, no. 5, pp. 1042–1046, 2022.

[48] H. Hojatian, Z. Mlika, J. Nadal, J.-F. Frigon, and F. Leduc-Primeau, "Learning energy-efficient hardware configurations for massive MIMO beamforming," *Submitted in IEEE Transactions on Machine Learning in Communications and Networking, arXiv preprint arXiv:2308.06376*, 2023.

[49] H. Hojatian, F. Leduc-Primeau, J. Nadal, J.-F. Frigon, and Z. Mlika, "Learning energy-efficient massive MIMO beamforming," U.S Patent PCT/IB2023/053 214, Feb., 2023, filed by Ericsson.

[50] H. Q. Ngo, E. G. Larsson, and T. L. Marzetta, "Energy and spectral efficiency of very large multiuser MIMO systems," *IEEE Transactions on Communications*, vol. 61, no. 4, pp. 1436–1449, 2013.

[51] H. Yang and T. L. Marzetta, "Performance of conjugate and zero-forcing beamforming in large-scale antenna systems," *IEEE Journal on Selected Areas in Communications*, vol. 31, no. 2, pp. 172–179, 2013.

[52] E. Björnson, M. Bengtsson, and B. Ottersten, "Optimal multiuser transmit beamforming: A difficult problem with a simple solution structure," *IEEE Signal Processing Magazine*, vol. 31, no. 4, pp. 142–148, 2014.

[53] X. Li, Y. Zhu, and P. Xia, "Enhanced analog beamforming for single carrier millimeter wave MIMO systems," *IEEE Transactions on Wireless Communications*, vol. 16, no. 7, pp. 4261–4274, 2017.

[54] J. Choi, "Analog beamforming for low-complexity multiuser detection in mm-wave systems," *IEEE Transactions on Vehicular Technology*, vol. 65, no. 8, pp. 6747–6752, 2016.

[55] A. Alkhateeb, O. El Ayach, G. Leus, and R. W. Heath, "Hybrid precoding for millimeter wave cellular systems with partial channel knowledge," in *2013 Information Theory and Applications Workshop (ITA)*, 2013, pp. 1–5.

[56] A. Alkhateeb, J. Mo, N. Gonzalez-Prelcic, and R. W. Heath, "MIMO precoding and combining solutions for millimeter-wave systems," *IEEE Communications Magazine*, vol. 52, no. 12, pp. 122–131, 2014.

[57] X. Gao, L. Dai, S. Han, I. Chih-Lin, and R. W. Heath, "Energy-efficient hybrid analog and digital precoding for mmwave MIMO systems with large antenna arrays," *IEEE Journal on Selected Areas in Communications*, vol. 34, no. 4, pp. 998–1009, 2016.

[58] I. Ahmed, H. Khammari, A. Shahid, A. Musa, K. S. Kim, E. De Poorter, and I. Moerman, "A survey on hybrid beamforming techniques in 5G: Architecture and system model perspectives," *IEEE Communications Surveys & Tutorials*, vol. 20, no. 4, pp. 3060–3097, 2018.

[59] S. Han, C. L. I, Z. Xu, and C. Rowell, "Large-scale antenna systems with hybrid analog and digital beamforming for millimeter Wave 5G," *IEEE Communications Magazine*, vol. 53, no. 1, pp. 186–194, Jan. 2015.

[60] A. Alkhateeb, G. Leus, and R. W. Heath, "Limited feedback hybrid precoding for multi-user millimeter wave systems," *IEEE Transactions on Wireless Communications*, vol. 14, no. 11, pp. 6481–6494, 2015.

[61] L. Wei, R. Hu, Y. Qian, and G. Wu, "Key elements to enable millimeter wave communications for 5G wireless systems," *IEEE Wireless Communications*, vol. 21, no. 6, pp. 136–143, 2014.

[62] S. Payami, M. Ghoraishi, and M. Dianati, "Hybrid beamforming for large antenna arrays with phase shifter selection," *IEEE Transactions on Wireless Communications*, vol. 15, no. 11, pp. 7258–7271, 2016.

[63] A. Alkhateeb, O. El Ayach, G. Leus, and R. W. Heath, "Channel estimation and hybrid precoding for millimeter wave cellular systems," *IEEE Journal on Selected Topics in Signal Processing*, vol. 8, no. 5, pp. 831–846, Oct. 2014.

[64] X. Yu, J.-C. Shen, J. Zhang, and K. B. Letaief, "Alternating minimization algorithms for hybrid precoding in millimeter wave MIMO systems," *IEEE Journal of Selected Topics in Signal Processing*, vol. 10, no. 3, pp. 485–500, 2016.

[65] S. Park, A. Alkhateeb, and R. W. Heath, "Dynamic subarrays for hybrid precoding in wideband mmWave MIMO systems," *IEEE Transactions on Wireless Communications*, vol. 16, no. 5, pp. 2907–2920, 2017.

[66] F. Sohrabi and W. Yu, "Hybrid Digital and Analog Beamforming Design for Large-Scale Antenna Arrays," *IEEE Journal on Selected Topics in Signal Processing*, vol. 10, no. 3, pp. 501–513, Apr. 2016.

[67] ——, "Hybrid analog and digital beamforming for mmWave OFDM large-scale antenna arrays," *IEEE Journal on Selected Areas in Communications*, vol. 35, no. 7, pp. 1432–1443, Jul. 2017.

[68] A. Alkhateeb and R. W. Heath, "Frequency selective hybrid precoding for limited feedback millimeter Wave systems," *IEEE Transactions on Communications*, vol. 64, no. 5, pp. 1801–1818, 2016.

[69] M. N. Kulkarni, A. Ghosh, and J. G. Andrews, "A comparison of MIMO techniques in downlink millimeter wave cellular networks with hybrid beamforming," *IEEE Transactions on Communications*, vol. 64, no. 5, pp. 1952–1967, 2016.

[70] C.-H. Chen, C.-R. Tsai, Y.-H. Liu, W.-L. Hung, and A.-Y. Wu, "Compressive sensing (CS) assisted low-complexity beamspace hybrid precoding for millimeter-wave MIMO systems," *IEEE Transactions on Signal Processing*, vol. 65, no. 6, pp. 1412–1424, 2017.

[71] J. Singh and S. Ramakrishna, "On the feasibility of beamforming in millimeter wave communication systems with multiple antenna arrays," in *2014 IEEE Global Communications Conference*, 2014, pp. 3802–3808.

[72] S. He, C. Qi, Y. Wu, and Y. Huang, "Energy-efficient transceiver design for hybrid sub-array architecture MIMO systems," *IEEE Access*, vol. 4, pp. 9895–9905, 2016.

[73] J. A. Zhang, X. Huang, V. Dyadyuk, and Y. J. Guo, "Massive hybrid antenna array for millimeter-wave cellular communications," *IEEE Wireless Communications*, vol. 22, no. 1, pp. 79–87, 2015.

[74] J. Jiang, Y. Yuan, and L. Zhen, "Multi-user hybrid precoding for dynamic subarrays in mmwave massive MIMO systems," *IEEE Access*, vol. 7, pp. 101 718–101 728, 2019.

[75] L. Yan, C. Han, N. Yang, and J. Yuan, "Dynamic-subarray with fixed phase shifters for energy-efficient terahertz hybrid beamforming under partial CSI," *IEEE Transactions on Wireless Communications*, vol. 22, no. 5, pp. 3231–3245, 2023.

[76] G. Nigam, P. Minero, and M. Haenggi, "Coordinated multipoint joint transmission in heterogeneous networks," *IEEE Transactions on Communications*, vol. 62, no. 11, pp. 4134–4146, 2014.

[77] S. Schwarz and M. Rupp, "Exploring coordinated multipoint beamforming strategies for 5G cellular," *IEEE Access*, vol. 2, pp. 930–946, 2014.

[78] D. Lee, H. Seo, B. Clerckx, E. Hardouin, D. Mazzarese, S. Nagata, and K. Sayana, "Coordinated multipoint transmission and reception in LTE-advanced: deployment scenarios and operational challenges," *IEEE Communications Magazine*, vol. 50, no. 2, pp. 148–155, 2012.

[79] N. Song, H. Sun, and T. Yang, "Coordinated hybrid beamforming for millimeter wave multi-user massive MIMO systems," *2016 IEEE Global Communications Conference, GLOBECOM 2016 - Proceedings*, 2016.

[80] E. Björnson and L. Sanguinetti, "Making cell-free massive MIMO competitive with MMSE processing and centralized implementation," *IEEE Transactions on Wireless Communications*, vol. 19, no. 1, pp. 77–90, 2020.

[81] M. Attarifar, A. Abbasfar, and A. Lozano, "Modified conjugate beamforming for cell-free massive MIMO," *IEEE Wireless Communications Letters*, vol. 8, no. 2, pp. 616–619, 2019.

[82] E. Nayebi, A. Ashikhmin, T. L. Marzetta, H. Yang, and B. D. Rao, "Precoding and power optimization in cell-free massive MIMO systems," *IEEE Transactions on Wireless Communications*, vol. 16, no. 7, pp. 4445–4459, 2017.

[83] G. Femenias and F. Riera-Palou, "Wideband cell-free mmwave massive MIMO-OFDM: Beam squint-aware channel covariance-based hybrid beamforming," *IEEE Transactions on Wireless Communications*, vol. 21, no. 7, pp. 4695–4710, 2022.

[84] E. Björnson and L. Sanguinetti, "Scalable cell-free massive MIMO systems," *IEEE Transactions on Communications*, vol. 68, no. 7, pp. 4247–4261, 2020.

[85] G. Interdonato, M. Karlsson, E. Björnson, and E. G. Larsson, "Local partial zero-forcing precoding for cell-free massive MIMO," *IEEE Transactions on Wireless Communications*, vol. 19, no. 7, pp. 4758–4774, 2020.

[86] P. K. Gkonis, "A survey on machine learning techniques for massive MIMO configurations: Application areas, performance limitations and future challenges," *IEEE Access*, pp. 1–1, 2022.

[87] J. Shi, A.-A. Lu, W. Zhong, X. Gao, and G. Y. Li, "Robust WMMSE precoder with deep learning design for massive MIMO," *IEEE Transactions on Communications*, vol. 71, no. 7, pp. 3963–3976, 2023.

[88] J. Shi, W. Wang, X. Yi, J. Wang, X. Gao, Q. Liu, and G. Y. Li, "Learning to compute ergodic rate for multi-cell scheduling in massive MIMO," *IEEE Transactions on Wireless Communications*, vol. 20, no. 2, pp. 785–797, 2021.

[89] J. Shi, W. Wang, X. Yi, X. Gao, and G. Y. Li, "Deep learning-based robust precoding for massive MIMO," *IEEE Transactions on Communications*, vol. 69, no. 11, pp. 7429–7443, 2021.

[90] J. Kim, H. Lee, and S.-H. Park, "Learning robust beamforming for MISO downlink systems," *IEEE Communications Letters*, vol. 25, no. 6, pp. 1916–1920, 2021.

[91] W. Xia, G. Zheng, Y. Zhu, J. Zhang, J. Wang, and A. P. Petropulu, "A deep learning framework for optimization of MISO downlink beamforming," *IEEE Transactions on Communications*, vol. 68, no. 3, pp. 1866–1880, Mar. 2020.

[92] Q. Hu, Y. Cai, Q. Shi, K. Xu, G. Yu, and Z. Ding, "Iterative algorithm induced deep-unfolding neural networks: Precoding design for multiuser MIMO systems," *IEEE Transactions on Wireless Communications*, vol. 20, no. 2, pp. 1394–1410, 2021.

[93] H. Huang, W. Xia, J. Xiong, J. Yang, G. Zheng, and X. Zhu, "Unsupervised learning-based fast beamforming design for downlink MIMO," *IEEE Access*, vol. 7, pp. 7599–7605, 2019.

[94] J. Kim, H. Lee, S.-E. Hong, and S.-H. Park, "Deep learning methods for universal MISO beamforming," *IEEE Wireless Communications Letters*, vol. 9, no. 11, pp. 1894–1898, 2020.

[95] S. Joung, C. Jeong, and S. Choi, "Deep learning based beam selection for wide beam sweeping system," in *2022 International Conference on Electronics, Information, and Communication (ICEIC)*, 2022, pp. 1–3.

[96] H. Echigo, Y. Cao, M. Bouazizi, and T. Ohtsuki, "A deep learning-based low overhead beam selection in mmwave communications," *IEEE Transactions on Vehicular Technology*, vol. 70, no. 1, pp. 682–691, 2021.

[97] S. K. Vankayala, S. Kumar, T. D, A. Mathur, S. Yoon, and I. Kommineni, "Deep-learning based beam selection technique for 6G millimeter wave communication," in *2022 IEEE 33rd Annual International Symposium on Personal, Indoor and Mobile Radio Communications (PIMRC)*, 2022, pp. 1380–1385.

[98] Y. Long, Z. Chen, J. Fang, and C. Tellambura, "Data-driven-based analog beam selection for hybrid beamforming under mm-Wave channels," *IEEE Journal on Selected Topics in Signal Processing*, vol. 12, no. 2, pp. 340–352, 2018.

[99] T. X. Vu, S. Chatzinotas, V.-D. Nguyen, D. T. Hoang, D. N. Nguyen, M. D. Renzo, and B. Ottersten, "Machine learning-enabled joint antenna selection and precoding design: From offline complexity to online performance," *IEEE Transactions on Wireless Communications*, vol. 20, no. 6, pp. 3710–3722, 2021.

[100] H. Huang, G. Gui, H. Sari, and F. Adachi, "Deep learning for super-resolution DOA estimation in massive MIMO systems," in *IEEE Vehicular Technology Conference*, ser. 2018 IEEE 88th Vehicular Technology Conference (VTC-Fall), vol. 2018-Augus, 2018, pp. 1–5.

[101] A. Alkhateeb, S. Alex, P. Varkey, Y. Li, Q. Qu, and D. Tujkovic, "Deep learning coordinated beamforming for Highly-Mobile millimeter wave systems," *IEEE Access*, vol. 6, pp. 37 328–37 348, 2018.

[102] X. Gao, L. Dai, Y. Sun, S. Han, and I. Chih-Lin, "Machine learning inspired energy-efficient hybrid precoding for mmWave massive MIMO systems," in *IEEE International Conference on Communications*, ser. 2017 IEEE International Conference on Communications (ICC), 2017, pp. 1–6.

[103] M. S. Ibrahim, A. S. Zamzam, X. Fu, and N. D. Sidiropoulos, "Learning-based antenna selection for multicasting," in *2018 IEEE 19th International Workshop on Signal Processing Advances in Wireless Communications (SPAWC)*, 2018, pp. 1–5.

[104] H. Huang, Y. Song, J. Yang, G. Gui, and F. Adachi, "Deep-learning-based millimeter-wave massive MIMO for hybrid precoding," *IEEE Transactions on Vehicular Technology*, vol. 68, no. 3, pp. 3027–3032, Mar. 2019.

[105] A. M. Elbir, "CNN-based precoder and combiner design in mmWave MIMO Systems," *IEEE Communications Letters*, vol. 23, no. 7, pp. 1240–1243, Jul. 2019.

[106] H. Huang, Y. Peng, J. Yang, W. Xia, and G. Gui, "Fast beamforming design via deep learning," *IEEE Transactions on Vehicular Technology*, vol. 69, no. 1, pp. 1065–1069, 2020.

[107] A. M. Elbir and A. K. Papazafeiropoulos, "Hybrid Precoding for Multiuser Millimeter Wave Massive MIMO Systems: A Deep Learning Approach," *IEEE Transactions on Vehicular Technology*, vol. 69, no. 1, pp. 552–563, Jan. 2020.

[108] A. M. Elbir and K. V. Mishra, "Joint antenna selection and hybrid beamformer design using unquantized and quantized deep learning networks," *IEEE Transactions on Wireless Communications*, vol. 19, no. 3, pp. 1677–1688, 2020.

[109] K. Chen, J. Yang, Q. Li, and X. Ge, "Sub-array hybrid precoding for massive MIMO systems: A CNN-based approach," *IEEE Communications Letters*, vol. 25, no. 1, pp. 191–195, 2021.

[110] Z. Liu, Y. Yang, F. Gao, T. Zhou, and H. Ma, "Deep unsupervised learning for joint antenna selection and hybrid beamforming," *IEEE Transactions on Communications*, vol. 70, no. 3, pp. 1697–1710, 2022.

[111] A. Morsali, A. Haghighat, and B. Champagne, "Deep learning-based hybrid analog-digital signal processing in mmWave massive-MIMO systems," *IEEE Access*, vol. 10, pp. 72 348–72 362, 2022.

[112] N. T. Nguyen, M. Ma, N. Shlezinger, Y. C. Eldar, A. Swindlehurst, and M. Juntti, "Deep unfolding hybrid beamforming designs for THz massive MIMO systems," *arXiv preprint arXiv:2302.12041*, 2023.

[113] Y. Zhao, I. G. Niemegeers, and S. H. De Groot, "Power allocation in cell-free massive MIMO: A deep learning method," *IEEE Access*, vol. 8, pp. 87 185–87 200, 2020.

[114] N. Rajapaksha, K. B. Shashika Manosha, N. Rajatheva, and M. Latva-Aho, "Deep learning-based power control for cell-free massive MIMO networks," in *ICC 2021 - IEEE International Conference on Communications*, 2021, pp. 1–7.

[115] R. Wang, W. Dai, and Y. Jiang, "Distributed learning for uplink cell-free massive MIMO networks," *IEEE Transactions on Communications*, pp. 1–1, 2023.

[116] W. Li, W. Ni, H. Tian, and M. Hua, "Deep reinforcement learning for energy-efficient beamforming design in cell-free networks," in *2021 IEEE Wireless Communications and Networking Conference Workshops (WCNCW)*, 2021, pp. 1–6.

[117] R. Nikbakht, A. Jonsson, and A. Lozano, "Unsupervised-learning power allocation for the cell-free downlink," in *2020 IEEE International Conference on Communications Workshops (ICC Workshops)*, 2020, pp. 1–5.

[118] Q. Wang, K. Feng, X. Li, and S. Jin, "PrecoderNet: Hybrid beamforming for millimeter wave systems with deep reinforcement learning," *IEEE Wireless Communications Letters*, vol. 9, no. 10, pp. 1677–1681, 2020.

[119] F. B. Mismar, B. L. Evans, and A. Alkhateeb, "Deep reinforcement learning for 5G networks: Joint beamforming, power control, and interference coordination," *IEEE Transactions on Communications*, vol. 68, no. 3, pp. 1581–1592, 2020.

[120] J. Ge, Y.-C. Liang, J. Joung, and S. Sun, "Deep reinforcement learning for distributed dynamic MISO downlink-beamforming coordination," *IEEE Transactions on Communications*, vol. 68, no. 10, pp. 6070–6085, 2020.

[121] J. Lin, Y. Zout, X. Dong, S. Gong, D. T. Hoang, and D. Niyato, "Deep reinforcement learning for robust beamforming in IRS-assisted wireless communications," in *GLOBECOM 2020 - 2020 IEEE Global Communications Conference*, 2020, pp. 1–6.

[122] T. P. Lillicrap, J. J. Hunt, A. Pritzel, N. Heess, T. Erez, Y. Tassa, D. Silver, and D. Wierstra, "Continuous control with deep reinforcement learning," *arXiv preprint arXiv:1509.02971*, 2015.

[123] G. Matheron, N. Perrin, and O. Sigaud, "Understanding failures of deterministic actor-critic with continuous action spaces and sparse rewards," in *Artificial Neural Networks and Machine Learning – ICANN 2020*, I. Farkaš, P. Masulli, and S. Wermter, Eds. Cham: Springer International Publishing, 2020, pp. 308–320.

[124] T. T. Nguyen, N. D. Nguyen, and S. Nahavandi, "Deep reinforcement learning for multi-agent systems: A review of challenges, solutions, and applications," *IEEE Transactions on Cybernetics*, vol. 50, no. 9, pp. 3826–3839, 2020.

[125] Z. Ding and H. Dong, *Challenges of Reinforcement Learning*. Singapore: Springer Singapore, 2020, pp. 249–272. [Online]. Available: https://doi.org/10.1007/978-981-15-4095-0_7

[126] G. Dulac-Arnold, N. Levine, D. J. Mankowitz, J. Li, C. Paduraru, S. Gowal, and T. Hester, "Challenges of real-world reinforcement learning: definitions, benchmarks and analysis," *Machine Learning*, vol. 110, no. 9, pp. 2419–2468, 2021. [Online]. Available: https://doi.org/10.1007/s10994-021-05961-4

[127] O. E. Ayach, S. Rajagopal, S. Abu-Surra, Z. Pi, and R. W. Heath, "Spatially sparse precoding in millimeter wave MIMO systems," *IEEE Transactions on Wireless Communications*, vol. 13, no. 3, pp. 1499–1513, 2014.

[128] V. W. Wong, *Key technologies for 5G wireless systems*. Cambridge university press, Mar. 2017.

[129] C. Huang, A. Zappone, G. C. Alexandropoulos, M. Debbah, and C. Yuen, "Reconfigurable intelligent surfaces for energy efficiency in wireless communication," *IEEE Transactions on Wireless Communications*, vol. 18, no. 8, pp. 4157–4170, Aug. 2019.

[130] C. Huang, Z. Yang, G. C. Alexandropoulos, K. Xiong, L. Wei, C. Yuen, Z. Zhang, and M. Debbah, "Multi-hop RIS-empowered terahertz communications: A DRL-based hybrid beamforming design," *IEEE Journal on Selected Areas in Communications*, pp. 1–1, Jun. 2021.

[131] L. Zhao, D. W. K. Ng, and J. Yuan, "Multi-user precoding and channel estimation for hybrid millimeter wave systems," *IEEE Journal on Selected Areas in Communications*, vol. 35, no. 7, pp. 1576–1590, Jul. 2017.

[132] C. Huang, L. Liu, C. Yuen, and S. Sun, "Iterative channel estimation using LSE and sparse message passing for mmWave MIMO systems," *IEEE Transactions on Signal Processing*, vol. 67, no. 1, pp. 245–259, Jan. 2019.

[133] K. Venugopal, A. Alkhateeb, N. Gonzalez Prelcic, and R. W. Heath, "Channel sstimation for hybrid architecture-based wideband millimeter wave systems," *IEEE Journal on Selected Areas in Communications*, vol. 35, no. 9, pp. 1996–2009, Sep. 2017.

[134] D. Zhu, B. Li, and P. Liang, "A novel hybrid beamforming algorithm with unified analog beamforming by subspace construction based on partial CSI for massive MIMO-OFDM systems," *IEEE Transactions on Communications*, vol. 65, no. 2, pp. 594–607, Feb. 2017.

[135] L. Liang, W. Xu, and X. Dong, "Low-complexity hybrid precoding in massive multiuser MIMO systems," *IEEE Wireless Communications Letters*, vol. 3, no. 6, pp. 653–656, Dec. 2014.

[136] T. Wang, C. K. Wen, H. Wang, F. Gao, T. Jiang, and S. Jin, "Deep learning for wireless physical layer: opportunities and challenges," *China Communications*, vol. 14, no. 11, pp. 92–111, Nov. 2017.

[137] T. O'Shea and J. Hoydis, "An introduction to deep learning for the physical layer," *IEEE Transactions on Cognitive Communications and Networking*, vol. 3, no. 4, pp. 563–575, 2017.

[138] C. B. Ha and H. K. Song, "Signal detection scheme based on adaptive ensemble deep learning model," *IEEE Access*, vol. 6, pp. 21 342–21 349, Apr. 2018.

[139] X. Li and A. Alkhateeb, "Deep learning for direct hybrid precoding in millimeter wave massive MIMO systems," *Asilomar Conference on Signals, Systems and Computers*, pp. 800–805, Nov. 2019.

[140] H. Hojatian, V. N. Ha, J. Nadal, J. Frigon, and F. Leduc-Primeau, "RSSI-based hybrid beamforming design with deep learning," in *2020 IEEE International Conference on Communications (ICC)*, Jun. 2020, pp. 1–6.

[141] A. Alkhateeb, "DeepMIMO: A generic deep learning dataset for millimeter wave and massive MIMO applications," in *Proc. of Inform. Theory and App. Workshop (ITA)*, San Diego, CA, Feb. 2019, pp. 1–8.

[142] S. Abeywickrama, T. Samarasinghe, C. K. Ho, and C. Yuen, "Wireless energy beamforming using received signal strength indicator feedback," *IEEE Transactions on Signal Processing*, vol. 66, no. 1, pp. 224–235, Jan. 2018.

[143] C. Lin and Q. Feng, "The standard particle swarm optimization algorithm convergence analysis and parameter selection," *Proceedings - Third International Conference on Natural Computation, ICNC 2007*, vol. 3, no. 6, pp. 823–826, Aug. 2007.

[144] E. Telatar, "Capacity of multi-antenna Gaussian channels," *European Transactions on Telecommunications*, vol. 10, no. 6, pp. 585–595, Dec. 1999.

[145] D. Whitley, "A genetic algorithm tutorial," *Statistics and Computing*, vol. 4, no. 2, pp. 65–85, 1994.

[146] S. Ruder, "An overview of multi-task learning in deep neural networks," *CoRR*, vol. abs/1706.0, Jun. 2017.

[147] S. Ioffe and C. Szegedy, "Batch normalization: Accelerating deep network training by reducing internal covariate shift," *32nd International Conference on Machine Learning, ICML 2015*, vol. 1, pp. 448–456, Mar. 2015.

[148] N. Srivastava, G. Hinton, A. Krizhevsky, I. Sutskever, and R. Salakhutdinov, "Dropout: A simple way to prevent neural networks from overfitting," *Journal of Machine Learning Research*, vol. 15, no. 1, pp. 1929–1958, Jun. 2014.

[149] L. Lu, "Dying ReLU and Initialization: Theory and Numerical Examples," *Communications in Computational Physics*, vol. 28, no. 5, p. 1671–1706, Jun. 2020.

[150] D. P. Kingma and J. L. Ba, "Adam: A method for stochastic optimization," *3rd International Conference on Learning Representations, ICLR 2015 - Conference Track Proceedings*, Jan. 2015.

[151] L. Tornheim, "Inversion of a complex matrix," *Communications of the ACM*, vol. 4, no. 9, p. 398, 1961.

[152] D. Dereniowski and M. Kubale, "Cholesky factorization of matrices in parallel and ranking of graphs," in *Parallel Processing and Applied Mathematics*. Springer Berlin Heidelberg, 2004, pp. 985–992.

[153] B. Lee, J. Choi, J.-Y. Seol, D. J. Love, and B. Shim, "Antenna grouping based feedback compression for FDD-based massive MIMO systems," *IEEE Transactions on Communications*, vol. 63, no. 9, pp. 3261–3274, 2015.

[154] V. L. Golub, *Matrix Computations*. J. Hopkins University Press, 1996.

[155] L. You, J. Xiong, A. Zappone, W. Wang, and X. Gao, "Spectral efficiency and energy efficiency tradeoff in massive MIMO downlink transmission with statistical CSIT," *IEEE Transactions on Signal Processing*, vol. 68, pp. 2645–2659, 2020.

[156] C. Lin and G. Y. Li, "Energy-efficient design of indoor mmwave and sub-THz systems with antenna arrays," *IEEE Transactions on Wireless Communications*, vol. 15, no. 7, pp. 4660–4672, 2016.

[157] R. Méndez-Rial, C. Rusu, N. González-Prelcic, A. Alkhateeb, and R. W. Heath, "Hybrid MIMO architectures for millimeter wave communications: Phase shifters or switches?" *IEEE Access*, vol. 4, pp. 247–267, 2016.

[158] J. Joung, "Machine learning-based antenna selection in wireless communications," *IEEE Communications Letters*, vol. 20, no. 11, pp. 2241–2244, 2016.

[159] B. Lin, F. Gao, S. Zhang, T. Zhou, and A. Alkhateeb, "Deep learning-based antenna selection and CSI extrapolation in massive MIMO systems," *IEEE Transactions on Wireless Communications*, vol. 20, no. 11, pp. 7669–7681, 2021.

[160] H. Hojatian, J. Nadal, J. Frigon, and F. Leduc–Primeau, "Flexible unsupervised learning for massive MIMO subarray hybrid beamforming," in *2022 IEEE Global Communications Conference*, 2022, pp. 3833–3838.

[161] E. Björnson, L. Sanguinetti, J. Hoydis, and M. Debbah, "Optimal design of energy-efficient multi-user MIMO systems: Is massive MIMO the answer?" *IEEE Transactions on Wireless Communications*, vol. 14, no. 6, pp. 3059–3075, 2015.

[162] Z.-H. Wang, C.-N. Chen, T.-W. Huang, and H. Wang, "A 28-GHz high linearity up-conversion mixer using second-harmonic injection technique in 28-nm CMOS technology," *IEEE Microwave and Wireless Components Letters*, vol. 31, no. 3, pp. 276–279, 2021.

[163] *8 Ways Stripline DC Pass Power Splitter, 18000 - 40000 MHz, 50*Ω.

[164] G. Shen, W. Che, H. Zhu, F. Xu, and Q. Xue, "Analytical design of millimeter-wave 100-nm GaN-on-Si MMIC switches using FET-based resonators and coupling matrix method," *IEEE Transactions on Microwave Theory and Techniques*, vol. 69, no. 7, pp. 3307–3318, 2021.

[165] M. L. Carneiro, M. Le Roy, A. Pérennec, R. Lababidi, P. Ferrari, and V. Puyal, "Compact analog all-pass phase-shifter in 65-nm CMOS for 24/28 GHz on-Chip- and in-Package phased-array antenna," in *2019 IEEE 23rd Workshop on Signal and Power Integrity (SPI)*, 2019, pp. 1–4.

[166] R. Ben Yishay and D. Elad, "Low loss 28 GHz digital phase shifter for 5G phased array transceivers," in *2018 Asia-Pacific Microwave Conference (APMC)*, 2018, pp. 711–713.

[167] M. Elkholy, S. Shakib, J. Dunworth, V. Aparin, and K. Entesari, "Low-loss highly linear integrated passive phase shifters for 5G front ends on bulk CMOS," *IEEE Transactions on Microwave Theory and Techniques*, vol. 66, no. 10, pp. 4563–4575, 2018.

[168] J. Pang, R. Kubozoe, Z. Li, M. Kawabuchi, and K. Okada, "A 28GHz CMOS phase shifter supporting 11.2Gb/s in 256QAM with an RMS gain error of 0.13dB for 5G mobile network," in *2018 48th European Microwave Conference (EuMC)*, 2018, pp. 807–810.

[169] Y.-W. Chang, T.-C. Tsai, J.-Y. Zhong, J.-H. Tsai, and T.-W. Huang, "A 28 GHz linear and efficient power amplifier supporting wideband OFDM for 5G in 28nm CMOS," in *2020 IEEE/MTT-S International Microwave Symposium (IMS)*, 2020, pp. 1093–1096.

[170] X. Xu, S. Li, L. Szilagyi, C. Matthus, W. Finger, C. Carta, and F. Ellinger, "A 28 GHz and 38 GHz high-gain dual-band power amplifier for 5G wireless systems in 22 nm FD-SOI CMOS," in *2020 50th European Microwave Conference (EuMC)*, 2021, pp. 174–177.

[171] M. Bao, D. Gustafsson, R. Hou, Z. Ouarch, C. Chang, and K. Andersson, "A 24–28-GHz doherty power amplifier with 4-W output power and 32% PAE at 6-dB OPBO in 150-nm GaN technology," *IEEE Microwave and Wireless Components Letters*, vol. 31, no. 6, pp. 752–755, 2021.

[172] S. Dutta, C. N. Barati, D. Ramirez, A. Dhananjay, J. F. Buckwalter, and S. Rangan, "A case for digital beamforming at mmWave," *IEEE Transactions on Wireless Communications*, vol. 19, no. 2, pp. 756–770, 2020.

[173] P. Caragiulo, O. E. Mattia, A. Arbabian, and B. Murmann, "A 2x time-interleaved 28-GS/s 8-Bit 0.03-mm2 switched-capacitor DAC in 16-nm FinFET CMOS," *IEEE Journal of Solid-State Circuits*, vol. 56, no. 8, pp. 2335–2346, 2021.

[174] Y. Chen, P.-I. Mak, S. D'Amico, L. Zhang, H. Qian, and Y. Wang, "A single-branch third-order pole–zero low-pass filter with 0.014-mm^2 die size and 0.8-kHz (1.25-nW) to 0.94-GHz (3.99-mW) bandwidth–power scalability," *IEEE Transactions on Circuits and Systems II: Express Briefs*, vol. 60, no. 11, pp. 761–765, 2013.

[175] A. K. Gupta and J. F. Buckwalter, "Linearity considerations for Low-EVM, millimeter-wave direct-conversion modulators," *IEEE Transactions on Microwave Theory and Techniques*, vol. 60, no. 10, pp. 3272–3285, 2012.

[176] E. Jang, S. Gu, and B. Poole, "Categorical reparameterization with gumbel-softmax," in *ICLR*, 2017.

[177] A. Camuto, M. Willetts, U. Simsekli, S. J. Roberts, and C. C. Holmes, "Explicit regularisation in gaussian noise injections," *Advances in Neural Information Processing Systems*, vol. 33, pp. 16 603–16 614, 2020.